GALAXY FORMATION AND MERGERS WITH STARS AND MASSIVE BLACK HOLES

A DISSERTATION
SUBMITTED TO THE DEPARTMENT OF PHYSICS
AND THE COMMITTEE ON GRADUATE STUDIES
OF STANFORD UNIVERSITY
IN PARTIAL FULFILLMENT OF THE REQUIREMENTS
FOR THE DEGREE OF
DOCTOR OF PHILOSOPHY

Ji-hoon Kim
May 2011

I certify that I have read this dissertation and that, in my opinion, it is fully adequate in scope and quality as a dissertation for the degree of Doctor of Philosophy.

(Tom Abel) Principal Adviser

I certify that I have read this dissertation and that, in my opinion, it is fully adequate in scope and quality as a dissertation for the degree of Doctor of Philosophy.

(Steve Allen)

I certify that I have read this dissertation and that, in my opinion, it is fully adequate in scope and quality as a dissertation for the degree of Doctor of Philosophy.

(Risa Wechsler)

Approved for the Stanford University Committee on Graduate Studies

Abstract

While mounting observational evidence suggests the coevolution of galaxies and their embedded massive black holes (MBHs), a comprehensive astrophysical understanding which incorporates both galaxies and MBHs has been missing. To tackle the nonlinear processes of galaxy formation, we develop a state-of-the-art numerical framework which self-consistently models the interplay between galactic components: dark matter, gas, stars, and MBHs. Utilizing this physically motivated tool, we present an investigation of a massive star-forming galaxy hosting a slowly growing MBH in a cosmological ΛCDM simulation. The MBH feedback heats the surrounding gas and locally suppresses star formation in the galactic inner core. In simulations of merging galaxies, the high-resolution adaptive mesh allows us to observe widespread starbursts via shock-induced star formation, and the interplay between the galaxies and their embedding medium. Fast growing MBHs in merging galaxies drive more frequent and powerful jets creating sizable bubbles at the galactic centers. We conclude that the interaction between the interstellar gas, stars and MBHs is critical in understanding the star formation history, black hole accretion history, and cosmological evolution of galaxies. Expanding upon our extensive experience in galactic simulations, we are well poised to apply this tool to other challenging, yet highly rewarding tasks in contemporary astrophysics, such as high-redshift quasar formation.

keyword: galaxies: formation – galaxies: interaction – galaxies: active – galaxies: nuclei – galaxies: starburst – stars: formation

Preface

The Universe is built from the bottom up: small things form first and large things later. Initially stars form in associations out of the gravitationally collapsing gas clouds. Galaxies, harmonious collections of billions to trillions of stars, are then shaped as stars dynamically congregates. Groups and clusters of galaxies later emerge, and finally, large scale structures of more than millions of lightyears in size slowly materializes. In this process of so-called bottom-up *hierarchical* structure formation, galaxy formation sits right in the middle of the distance scales ranging from stars ($\sim$ lightyears) to large scale structures ($\sim$ up to hundreds of mega-lightyears). Indeed galaxy formation is the basic building block of structure formation in our Universe. Therefore, a reliable theory of *galaxy formation* has been persistently asked for, not only to explain the spectacular beauty and dynamics of the galaxies themselves, but to connect these wildly different scales.

Moreover, surprisingly tight relationships have been recently discovered between galaxies and their embedded massive black holes (MBHs) at the galactic centers. While these observations strongly imply the coevolution of galaxies and their MBHs, a comprehensive astrophysical understanding which incorporates both galaxies and MBHs has not been perfected. How does the interstellar gas accrete onto the MBH? And how does the MBH of such small size regulate the growth of the entire galaxy of much larger size? These mechanisms are not only poorly understood, but also inadequately modeled in contemporary numerical studies. For example, most of the previous computer simulations of galaxy formation have only approximated stellar and MBH physics with parametrized sub-resolution recipes, leaving out many critical physical processes. As recent observations yield excellent constraints on galactic evolution, the need for a refined numerical simulation has never been greater.

The purpose of this thesis will be to demonstrate that a comprehensive theory of galaxy formation can be perfected through unabridged, self-consistent numerical simulations. We will describe a state-of-the-art numerical framework which self-consistently models the interplay between galactic components: dark matter, gas, stars, and massive black holes. Then, we will utilize this tool in different contexts of galaxy formation and mergers, with and without massive black holes. We will show that interactions between galactic components need to be adequately considered in simulations in order to fully comprehend the star formation history, black hole accretion history, and cosmological evolution of galaxies.

Chapter 1, "Introduction", describes the fundamental principles of modern astrophysics and cosmology which provide the theoretical basis of the work presented in this thesis. We list the major players in the act of galaxy formation, and discuss how important those factors are. These are the important physics elements which need to be carefully investigated to construct a realistic galaxy formation theory.

In Chapter 2, "Physics for Forming Galaxies on Computers", we detail our numerical framework which models the interplay between all galactic components: dark matter, gas, stars, and MBHs. The high-resolution adaptive mesh refinement (AMR) code *Enzo* is modified to model the formation and feedback of molecular clouds at 15 pc and the accretion of gas onto a MBH. Two major channels of MBH feedback are also discussed: radiative feedback (X-ray photons followed through full 3D ray tracing) and mechanical feedback (bipolar jets resolved in high-resolution AMR). This chapter is a part of the publication submitted to *The Astrophysical Journal* which is coauthored by John Wise, Marcelo Alvarez, and Tom Abel.

In Chapter 3, "Galaxy Formation with Stars and Massive Black Holes", we present an investigation on the coevolution of a $9.2 \times 10^{11} M_{\odot}$ galaxy and its $10^5 M_{\odot}$ embedded MBH in a cosmological ΛCDM simulation. The MBH feedback heats the surrounding interstellar medium (ISM) up to 10^6 K and locally suppresses star formation in the galactic inner core. The MBH also self-regulates its growth by keeping the surrounding ISM hot for an extended period of time. This chapter is a part of the publication submitted to *The Astrophysical Journal* which is coauthored by John Wise, Marcelo

Alvarez, and Tom Abel. A rendering of the simulation data produced in this work is provided to the Hayden Planetarium at the American Museum of Natural History, New York, for the program of "*Big Bang*" in October 2010.

Chapter 4, "Merging of Galaxies on Adaptive Mesh Refinement", presents the first AMR simulation of two merging, low mass, initially gas-rich galaxies, $1.8 \times 10^{10} M_\odot$ each, including star formation and feedback. We achieve unprecedented resolution of the multiphase interstellar medium, finding a widespread starburst in the merging galaxies via shock-induced star formation. The high dynamic range of AMR also allows us to follow the interplay between the galaxies and their embedding medium depicting how galactic outflows and a hot metal-rich halo form. The results are published in *The Astrophysical Journal Letters*, 2009, Volume 694, L123, and in First Stars III Conference AIP Conference Proceedings, Volume 990, pp. 429-431 (2008). These articles are coauthored by John Wise and Tom Abel.

In Chapter 5, "Galaxy Mergers with Stars and Massive Black Holes", we carry out a simulation of two merging galaxies, $2.1 \times 10^{11} M_\odot$ each, with their $10^5 M_\odot$ embedded MBHs. We find that the feedback from the fast growing MBHs helps to reduce the global star formation on the disk. When compared with the feedback by a slowly growing MBH, these MBHs drive more frequent jets creating sizable bubbles at the galactic centers. This chapter is included in the publication which will be submitted to *The Astrophysical Journal*. This paper is coauthored by John Wise, Marcelo Alvarez, and Tom Abel.

Chapter 6, "Conclusions and Future Works", lists the original findings of the work presented in this thesis, and describes some of the most important future directions and applications of the method developed by the candidate. A portion of this chapter is included in the publication submitted to *The Astrophysical Journal*, coauthored by John Wise, Marcelo Alvarez, and Tom Abel. A more detailed synopsis of the thesis is given in $ 1.5.

Acknowledgements

First and foremost, I would like to express my genuine gratitude to my adviser, Prof. Tom Abel, for his advice and guidance throughout my career at Stanford. His brilliant ideas and continuous assistance have been vital for me to continue to pursue my research. It is also my pleasure to thank Prof. Risa Wechsler for her always encouraging words and support through many group meetings and individual meetings. In addition, I thank my other thesis committee members, Profs. Steve Allen, Thomas Cover, and Vehe Petrosian for their invaluable help and services.

I have been benefited from the insightful comments and advice provided by numerous academic peers including Marcelo Alvarez, Elliott Bloom, Frederic Bournaud, Renyue Cen, Sarah Church, Thomas J. Cox, Andrés Escala, Kristian Finlator, Nick Gnedin, Oliver Hahn, Elizabeth Harper-Clark, Patrik Jonsson, Dušan Kereš, Ralf Klessen, Andrey Kravtsov, Mark Krumholz, Hee-won Lee, Yuexing Li, Yu Lu, Chung-pei Ma, Michael Norman, Greg Novak, Peng Oh, Jeff Oishi, Brian O'Shea, Jeremiah Ostriker, Chang-bom Park, Joel Primack, Cecilia Scannapieco, Paul Shapiro, Volker Springel, Hiro Tajima, Elizabeth Tasker, Romain Teyssier, Matthew Turk, Hsiang-Hsu Wang, Peng Wang, John Wise, Ed Wu, and Fen Zhao. I was especially honored to receive a generous support from the William R. and Sara Hart Kimball Stanford Graduate Fellowship from 2005 to 2009.

I am particularly thankful to John Wise for being the major source of information on *Enzo* code and being very patient when I first began to work on it. I am also grateful to Matthew Turk for providing an *Enzo* analysis toolkit *YT*, and to Ralf Kaehler for rendering many beautiful images in this thesis, and numerous stunning movies out of my galactic simulations. I gratefully acknowledge the endless aid of

Stuart Marshall, Ken Zhou, and the entire SLAC scientific computing service team.

I would like to thank all the people who helped me endure the hardships throughout my graduate career including Shizuka Akiyama, Mustafa Amin, Peter Behroozi, Bijan Berenji, Aurelien Bouvier, Michael Busha, Heon-young Chang, Teddy Cheung, Lixin Dai, Yvonne Edmonds, Steve Healey, Fabio Iocco, Dong-hui Jeong, Young-hwan Kim (1979-2008), Naoko Kurahashi, Joshua Lande, Ziba Mahdavi, Eric Morganson, Yoo-kyung Noh, You-sin Park, David Rapetti, Rachel Reddick, Kevin Schlaufman, Paul Simeon, Lance Simms, John Skinner, Lukasz Stawarz, Takaaki Tanaka, Keith Thompson, and Hao-Yi Wu. Most notably, Becky Spitzer and her family have been instrumental in helping me to adjust to the life in the United States, and to improve my English. Here I would like to express my heartfelt gratitude to Becky, to her husband Bob, and to her entire extended family. I also would like to show my sincere appreciation to Martha Siegel for her help and assistance along the way. She so kindly took care of me every time I badly needed help.

I am deeply indebted to my parents, Hyun-suk Kim and Ran-suk Mun, and my brother Sin-hoon who all have graciously supported my choice of studying (1) astrophysics *and* (2) abroad. I could not have reached here without their endless help and sacrifice. I sincerely hope to give back what I have received from them thus far, so they can at some point finally understand why I chose both (1) *and* (2). Lastly but most importantly I thank Jinhee Park for making me smile and happy all the time, for being the best I have ever encountered in my life, and hopefully the best I will ever cherish for the rest of my life.

Contents

List of Tables

List of Figures

Chapter 1

Introduction

> *"One thing I have learned in a long life: that all our science, measured against reality, is primitive and childlike and yet it is the most precious thing we have."*
> — Albert Einstein (1879-1955)

For a long time human beings had known nothing more about the Universe than any other animals do. It would be fair to say that mankind had long been blind to the laws of the spectacular performance of Mother Nature. And still in the twenty first century so little is known to mankind about how the Universe works, after humans have lived in it for millions of years. We barely understand what is happening on the Earth and inside the Solar system. We only recently realized that we belong to the Milky Way galaxy, a local collection of hundreds of billions of stars. We are just starting to grasp the idea of even larger scale structures, and the immense spatial and temporal extension of the Universe.

Described below is the elementary picture of modern astrophysics and cosmology that mankind has developed and assembled for the past decades, focusing on the theory of *galaxy formation*. While still crude and stained with many unknowns, it will provide the basis of the original work presented by the candidate in this thesis. Schemes of the numerical approach to astrophysical problems are also discussed in order to introduce the computational technique developed by the candidate for simulating galaxies and massive black holes on computers.

1.1 Universe As A Mixture of Many Unknowns

In so-called ΛCDM cosmology – the contemporary understanding of the dynamics of the Universe – it is now well established that the Universe is made up of 73% of dark energy (often represented as the cosmological constant Λ), 23% of cold dark matter (CDM), and 4% of baryonic matter (Kowalski et al., 2008; Komatsu et al., 2011).

$$\frac{H^2}{H_0^2} = \Omega_{\rm r} a^{-4} + \Omega_{\rm m} a^{-3} + \Omega_{\rm k} a^{-2} + \Omega_\Lambda \tag{1.1}$$

Here a is the scale factor of the Universe, $H = \dot{a}/a$ the fractional expansion rate, and H_0 the Hubble constant today. Each of $\Omega_{\rm r}$, $\Omega_{\rm m}$, $\Omega_{\rm k}$, and Ω_Λ represents the radiation, matter, curvature, and dark energy density today, respectively. The adjective "dark" in dark energy and dark matter means that there is no electromagnetic interaction with them which could be observed. It also metaphorically reflects the level of our poor understanding on these components. However, critical information about these dominating dark components is known, just enough to trace back the course of structure formation since the beginning of the Universe.

(1) Dark energy acts as a negative pressure which caused the later acceleration of the expansion of the Universe.

(2) Because dark energy started to dominate the large scale dynamics only recently, i.e. redshift < 0.8, dark matter and baryonic matter were the main drivers of structure formation during most of the history of the Universe.

(3) Only the gravitational pull commands the behavior of dark matter by definition. Its gravitational collapse was seeded by the small density perturbations shown in the cosmic microwave background (redshift ~ 1100), and are well-understood by linear perturbation theory.

(4) The perturbations soon became nonlinear and grew increasingly faster. The dark matter *halos* were thus formed, while baryonic matter was pulled by the gravity of the dark matter deep into the gravitational potential wells. The

physics of baryonic matter started to direct the formation and evolution of luminous objects at the centers of these halos.

(5) Small halos and luminous objects formed first, and then merged to shape increasingly larger structures such as galaxies and galaxy clusters. This picture of bottom-up *hierarchical* structure formation (White and Rees, 1978) is consistent with many observations, has become the standard paradigm of physical cosmology.

With this cosmological model and the brief history of our Universe in mind, we now discuss the theory of galaxy formation. Hundreds of billions of galaxies are presumed to exist in the observable Universe alone, and they are the atoms of cosmological structures. Below we describe in detail our understandings of how galaxies have formed in the ΛCDM framework.

1.2 Basis of Modern Galaxy Formation Theory

One of the most fundamental challenges in any modern cosmological model is to give an explanation of the *formation and evolution of galaxies*. Galaxy formation acts as a building block of structure formation in the ΛCDM paradigm, and as a bridge to connect different scales from star forming regions (pc scales) to large scale structures (Mpc to hundreds of Mpc scales). The endeavor towards the modern galaxy formation theory is initiated by the groundbreaking work of pioneering scholars in 1970s and 1980s (Eggen et al., 1962; Rees and Ostriker, 1977; White and Rees, 1978; Fall and Efstathiou, 1980; White and Frenk, 1991). More recently, powered by analytic (Mo et al., 1998; Somerville and Primack, 1999; Cole et al., 2000) and numerical studies (Barnes and Hernquist, 1996; Steinmetz and Navarro, 1999; Springel and Hernquist, 2003b) in the ΛCDM framework, researchers have now begun to unearth the beauty as well as the complexity of the galaxy formation process. In the following sections, we discuss the important physics elements which need to be incorporated to construct a realistic galaxy formation theory.

1.2.1 Dark Matter Dynamics

The dynamics of dark matter is purely governed by Newtonian gravity. The minuscule matter density fluctuations generated by inflation grow as the self-gravity within the density peaks slowly decouple them from the ever expanding Hubble flow. Starting from simple Gaussian random fields as seen in the cosmic microwave background observations, and assuming a linear growth of perturbations, Press and Schechter (1974) derived the distribution function of dark matter halo masses as

$$\frac{dn}{dM}(M,z) = \left(\frac{2}{\pi}\right)^{1/2} \frac{\rho_0}{M^2} \frac{\delta_c(z)}{\sigma(M)} \left|\frac{d\ln\sigma(M)}{d\ln M}\right| \exp\left[-\frac{\delta_c^2(z)}{2\sigma^2(M)}\right] \tag{1.2}$$

which laid out the basis of structure formation by hierarchical clustering (Eke et al., 1996; Longair, 2008). It is followed by numerous improvements and modifications to better match simulations at all epochs (Sheth and Tormen, 1999; Reed et al., 2003, 2007). Here, ρ_0 is the mean density of the Universe, $\delta_c(z) = 1.686(1+z)$ is the critical overdensity for a collapsing spherical top-hat mass. The probability distribution of the overdensity, $\Delta\rho/\bar{\rho}$, associated with the perturbation of mass M is proportional to the Gaussian

$$\frac{1}{\sigma(M)} \exp\left[-\frac{(\Delta\rho/\bar{\rho})^2}{2\sigma^2(M)}\right] \tag{1.3}$$

with a standard deviation of $\sigma(M)$. Expressed in a different way, $\sigma(M)$ can also be written as

$$\sigma^2(M) = \frac{1}{2\pi^2}\int_0^\infty P(k)\hat{W}^2(M,k)k^2dk \tag{1.4}$$

$$= \frac{1}{2\pi^2}\int_0^\infty P_0(k)T^2(k)\hat{W}^2(M,k)k^2dk \tag{1.5}$$

where $P_0(k)$ is the primordial matter power spectrum, $T(k)$ is the transfer function, and $\hat{W}(M,k)$ is the Fourier transform of a top-hat window function enclosing mass M. The halo mass function, Eq. 1.2, can be further employed to generate the halo merger tree or the mass accretion history of an individual halo (Lacey and Cole, 1993;

Cole et al., 2000; Parkinson et al., 2008).

Although analytic and semi-analytic approaches are rewarding, numerical N-body simulations are also required to better comprehend the dynamics of dark matter, especially their spatial distribution or the mass loss due to three-body interactions (Benson, 2010). Dark matter only N-body simulations consider only the gravitational interaction among dark matter, assuming that baryonic physics is less important in the initial phase of the gravitational collapse. From such simulations, it is verified that the total kinetic energy and gravitational energy reach a *virialized* equilibrium:

$$2\langle E_{\mathrm{kin}}\rangle + \langle E_{\mathrm{grav}}\rangle = 0. \tag{1.6}$$

Here $\langle\,\rangle$ represents the time average. The random motion of dark matter essentially provides the *pressure* which prohibits the halo from collapsing further in. An approximately universal form of dark matter profiles is also found with ranging masses from galaxies to galaxy clusters (Navarro et al., 1996, 1997). This universal form of the dark matter halo structure can be written as

$$\rho(r) = \frac{\rho_{\mathrm{s}}}{(r/r_{\mathrm{s}})[1+(r/r_{\mathrm{s}})]^2} \tag{1.7}$$

where r_{s} is the characteristic scale radius.

In addition, dark matter simulations have demonstrated that the halos can acquire rotational angular momentum via cosmological tidal interactions with neighboring clumps (Peebles, 1969; Barnes and Efstathiou, 1987; Bullock et al., 2001). The rotation of the halo can be characterized by the dimensionless *spin parameter* λ defined as

$$\lambda = \frac{\omega}{\omega_{\mathrm{circ}}} = \frac{J}{MR^2} \Big/ \sqrt{\frac{GM}{R^3}} = \frac{J|E|^{1/2}}{GM^{5/2}} \tag{1.8}$$

where M, J, and $E = -GM^2/R$ are the mass, total angular momentum, and total energy of the halo, respectively. λ is measured to peak between 0.01 and 0.1 for dark matter. Combined with the pressure of random motions, the rotation helps withstand the further shrinkage of the dark matter halo.

1.2.2 Baryonic Physics: Gravity versus Gas Pressure

Dark matter stops its infall towards the gravitational center of the halo due to the pressure and rotational support of its own. However, baryonic matter, i.e. gas, continues to plunge into the center of the halo as it thermally radiates away its kinetic energy. To qualitatively discuss the competition between the kinetic motion and the thermal radiation of the collapsing gas cloud, we define two characteristic time scales. First, the dynamical time is the time scale for a test body to free fall under self-gravity. Assuming a degenerate ellipse with a semi-major axis $0.5R$,

$$t_{\rm dyn} = \frac{t_{\rm orbit}}{2} = \frac{\pi}{\sqrt{GM}}\left(\frac{R}{2}\right)^{3/2} \sim \frac{1}{n^{1/2}} \tag{1.9}$$

where M, R and n are the mass, radius, and number density of the gas cloud, respectively. Second, the cooling time is the time scale for the thermal energy of the gas to radiate away, as

$$t_{\rm cool} = \frac{E}{dE/dt} = \frac{3nk_{\rm B}T}{2n_{\rm p}n_{\rm e}\Lambda(T)} \sim \frac{1}{n} \tag{1.10}$$

where $(3/2)k_{\rm B}T$ is the specific gas energy, and $\Lambda(T)$ is the cooling function by electron free-free radiation (Bremsstrahlung). Hence, depending on the gas density, the cooling time of the collapsing gas cloud at galactic scales can be much shorter than the dynamical time. As a consequence, the collapse of baryonic matter could lead to a runaway *cooling catastrophe* until the collapsing clump is finally supported by other energetic feedback such as stellar radiation or supernova explosions.[1] Understanding the dissipative cooling mechanisms of the gas is therefore crucial to predict the behavior of the galactic gas content.

The main coolants above 10^4 K are hydrogen and helium. The microphysics and reactions between the *primordial* species (H, H^+, He, He^+, He^{++}, e^-) give rise to collisional excitation cooling, collisional ionization cooling, recombination cooling,

[1] Note, however, that depending on the density of the infalling gas and the virial temperature of the halo, the gas can either almost freely contract under self-gravity (cold mode accretion), or adiabatically heat itself and form virial shocks at the outskirts of the halo (hot mode accretion). See Birnboim and Dekel (2003) and Dekel and Birnboim (2006) for more discussions.

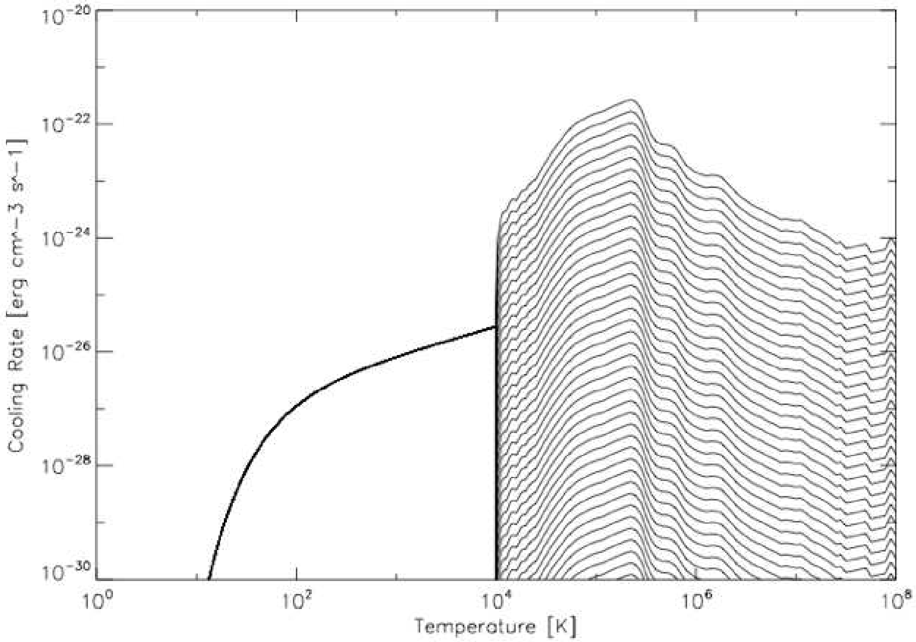

Fig. 1.1.— Metal cooling rates. Shown above 10^4 K is $\Delta\Lambda(Z) = \Lambda_{\rm net}(Z) - \Lambda_{\rm net}(0)$, where $\Lambda_{\rm net}$ is the net cooling rate from Sutherland and Dopita (1993). Different curves covers the range of electron fraction from $\sim 10^{-4}$ to 1. Cooling below 10^4 K is from the analytic fit of Eq. 2 of Vázquez-Semadeni et al. (2010). The rates are normalized at $Z = 0.1Z_{\odot}$; the metallicity linearly scales this plot up and down. Note that these rates are added to the primordial cooling by hydrogen and helium. Compare with Figure 2.2.

Bremsstrahlung cooling, and Compton cooling or heating by the cosmic microwave background (Anninos et al., 1997). Additionally, in the present-day galaxy formation (as opposed to the *primordial* galaxy formation), coolings by metals and molecular hydrogen, H_2, are important. As an example, a non-primordial contribution to the total cooling rate (on top of the primordial cooling rate) is plotted in Figure 1.1. Here the metal contribution above 10^4 K, $\Delta\Lambda(Z) = \Lambda_{\rm net}(Z) - \Lambda_{\rm net}(0)$, is calculated from Sutherland and Dopita (1993), whereas below 10^4 K "atomic line cooling from C II, O I, Fe II, and Si II, ro-vibrational line cooling from H_2 and CO, and atomic and molecular collisions with grain" are modeled by Koyama and Inutsuka (2002)[2].

[2]Note the typo in their equations as mentioned by Vázquez-Semadeni et al. (2010).

As a result of these various channels of cooling, gas condensates into a smaller space than dark matter does. What ultimately decides the fate of the gas cloud is the tug-of-war between self-gravity and gas pressure, encapsulated in the so-called Jeans instability criterion. That is, only when the self-gravity of the cloud overcomes the thermal pressure of the gas within, the cloud starts to collapse onto itself (Jeans, 1902; Sparke and Gallagher, 2006).

$$-\langle \epsilon_{\rm grav} \rangle = \frac{3GM\mu m_{\rm p}}{5R} \quad > \quad 2\langle \epsilon_{\rm kin} \rangle = 3k_{\rm B}T \tag{1.11}$$

Here M, R, and T are the enclosed mass, radius, and temperature of the cloud, respectively. $m_{\rm p}$ is the proton mass, and μ is the mean molecular weight. Replacing $M = \frac{4}{3}\pi\rho R^3$ gives the critical length scale named the *Jeans length*, $\lambda_{\rm Jeans}$, the minimum size of the gas cloud before the self-gravitational collapse occurs:

$$\lambda_{\rm Jeans} = \sqrt{\frac{15k_{\rm B}T}{4\pi G\mu m_{\rm p}\rho}} \tag{1.12}$$

where ρ is the mean mass density of the cloud. All scales larger than the Jeans length are subject to the Jeans instability, while all scales smaller than the Jeans length are stable. Note that the Jeans length and the corresponding Jeans mass decrease as the density grows, causing dense clumps to further fragment into even smaller structures. The Jeans argument is crucial in understanding the formation of small scale structures, such as the galaxies in dense peaks of the matter distribution, or the star clusters in molecular clouds.

1.2.3 Star Formation

Once a gas cloud collapses catastrophically and condenses into an increasingly smaller space, the process will continue until the gas is dense enough to form a protostellar core and ignite the nuclear fusion chains. The birth of stars, and various modes of ensuing stellar feedback complicate the problem of galaxy formation which otherwise would have been a simple gas dynamics phenomenon.

While star formation is a giant branch of observational and theoretical studies by itself and can not possibly be detailed in this short review, we only focus on two recent findings, especially noteworthy in the context of galaxy formation. For comprehensive reviews on the physics of star formation, see McKee and Ostriker (2007) and Krumholz (2011).

Star Formation Rate Surface Density

The idea that the star formation rate density, $\rho_{\rm SFR}$, is proportional to a certain power of the gas density, $\rho_{\rm gas}$, is first proposed by Schmidt (1959). Naively one could say that star formation rate density should be proportional to the gas density divided by the characteristic dynamical time, $t_{\rm dyn}$, as

$$\rho_{\rm SFR} \sim \frac{\rho_{\rm gas}}{t_{\rm dyn}} \sim \rho_{\rm gas}^{1.5}. \tag{1.13}$$

Since then, it has been observationally found that the surface density of star formation rate of a galaxy, $\Sigma_{\rm SFR}$, depends on the gas surface density, $\Sigma_{\rm gas}$, to the power of 1.4 (Kennicutt, 1989, 1998). More recently, using high-resolution galactic scale simulations Robertson and Kravtsov (2008) demonstrated the molecular gas surface density Kennicutt-Schmidt relation of the form

$$\Sigma_{\rm SFR} \sim \Sigma_{\rm H_2}^{1.4}. \tag{1.14}$$

The Kennicutt-Schmidt relationship has also been the basis of an *empirical* star formation recipe used in many galactic scale numerical studies.

Slow Star Formation in Molecular Clouds

There is a set of convincing arguments that the star formation may not have proceeded with one hundred percent efficiency (Larson, 1974; White and Rees, 1978; Benson, 2010). Most notably, Cole et al. (2001) found that the total mass fraction in stars in the Universe, $\Omega_{\rm star} h \sim 2 \times 10^{-3}$, is an order of magnitude smaller than the total baryonic density, $\Omega_{\rm b}$, of the Universe. Recent observations and numerical experiments

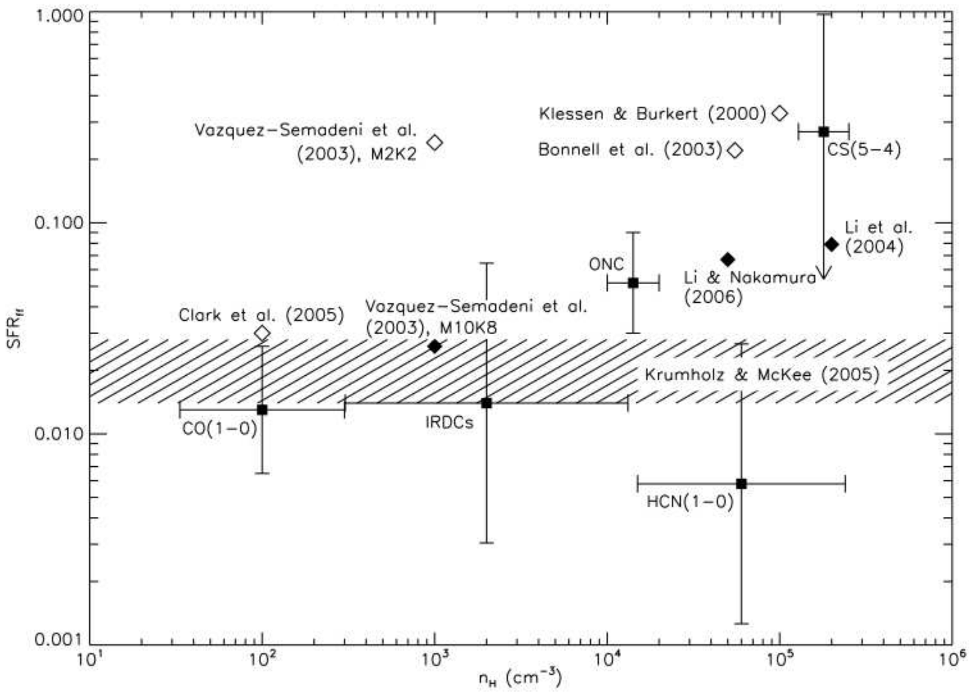

Fig. 1.2.— The specific star formation rate, SFR$_{\rm ff}$, defined as the fractional mass of molecular clouds turned into stars in a dynamical time, adapted from Figure 5 of Krumholz and Tan (2007). Squares with error bars show the observational values, while open and filled diamonds represent the simulation results. The shaded region is the analytic prediction by Krumholz and McKee (2005).

have also found that only about $\sim$ 2% of the gaseous mass in a molecular cloud is converted into stars per dynamical time (see Figure 1.2; Krumholz and McKee, 2005; Krumholz and Tan, 2007, and references therein). This is because turbulence, magnetic fields, and/or radiation pressure all slow down the collapse of the gas, and thus the star formation process. The slow consumption rate of the gas is tightly associated with the negative stellar feedback which is discussed in the next section.

1.2.4 Stellar Feedback

During its lifetime a star acts as an energy *source* in its host galaxy. And the energy input by various modes (stages) of stellar feedback – protostellar outflows, photoionization, radiation pressure, stellar winds, and supernova explosions – is postulated to regulate the next generation of star formation. In this section, we describe two channels of such energy inputs which need to be investigated in order to formulate a successful galaxy formation model.

Protostellar Outflows

A newly formed star routinely suffers from a bipolar mass loss, which could be energetically important in the formation of a star cluster. Massive protostellar outflows from Young Stellar Objects (YSOs) are frequently observed in CO emission lines (Richer et al., 2000). Moreover, the jets found around Herbig-Haro Objects (HHOs) reach a speed of more than 100 $\mathrm{km\,s^{-1}}$ and often last for $\sim$ 1000 years. These jets inject outward momentum into the collapsing star-forming clump and replenish the dissipating turbulence. As a consequence, simulators have shown that protostellar outflow feedback in star-forming clumps suppresses further star formation which otherwise would have been unchecked (e.g. Li and Nakamura, 2006; Nakamura and Li, 2008; Wang et al., 2010).

Supernova Explosions

When the mass of the Ni-Fe core of a very massive star ($> 9M_\odot$, $<$ 100 Myrs of age) exceeds the Chandrasekhar limit, 1.38 $M_\odot$, the *electron* degenerate pressure no longer supports the inward gravitational pressure of the star itself. Then the inner part of the core implodes until it is eventually supported by the *neutron* degenerate pressure. The infalling material suddenly bounces back from the neutron core to create a shock wave, which later gets reinvigorated by absorbing neutrinos escaping from the core. This whole process, a *Type II* supernova or *core collapse* supernova explosion, radiates $\sim 10^{51}$ ergs of thermal energy per explosion, and is known to release mainly lighter elements (e.g. O) while sucking up heaver elements (e.g. Fe).

Another type of the stellar explosion is triggered when a white dwarf slowly accretes materials from a companion star to exceed the Chandrasekhar limit in the end. This *Type Ia* supernova also discharges $\sim 10^{51}$ ergs of total energy, enough to unbind every layer of the star. It is thought to be responsible for enriching the interstellar medium (ISM) with relatively heavier elements. Because the whole process – from the birth of a white dwarf to the final explosion – takes longer time (~ 1 Gyrs) than Type II, the supernovae found in red elliptical galaxies are mostly Type Ia.

These two kinds of supernova explosions are the dominant energy sources in a galactic system (Ceverino and Klypin, 2009; Benson, 2010). They not only self-regulate the global star formation rate, but also heat up the interstellar medium to maintain the overall *multiphase* structure (McKee and Ostriker, 1977; Spitzer, 1990). Supernova explosions have been the most obvious energy inputs considered in numerical simulations of galaxies, successfully reproducing observational trends such as the Kennicutt-Schmidt relation (e.g. Tasker and Bryan, 2008; Robertson and Kravtsov, 2008; Ceverino and Klypin, 2009; Agertz et al., 2011).

1.2.5 Massive Black Hole Growth and Feedback

There is now ample evidence that most galaxies – if not all – including the Milky Way harbor supermassive black holes (SMBHs) at their centers (Antonucci, 1993; Kormendy and Richstone, 1995; Ferrarese and Ford, 2005). In terms of its mass, a supermassive black hole at a galactic center is very different from a stellar mass black hole. The mass of a massive black hole ranges from $3.7 \times 10^6 M_\odot$ at the center of the Milky Way (Sgr A*; Schödel et al., 2002) to $1.8 \times 10^{10} M_\odot$ in OJ 287 (Valtonen et al., 2008). Moreover, surprisingly tight correlations exist between the black hole masses and bulge masses (Magorrian et al., 1998; Häring and Rix, 2004),[3]

$$\log\left(\frac{M_{\rm BH}}{M_\odot}\right) = (8.20 \pm 0.10) + (1.12 \pm 0.06) \cdot \log\left(\frac{M_{\rm bulge}}{10^{11} M_\odot}\right), \qquad (1.15)$$

[3]From this, the median black hole mass at $M_{\rm bulge} = 5 \times 10^{10} M_\odot$ is $M_{\rm BH} \sim 0.0014\ M_{\rm bulge}$.

between the black hole masses and bulge velocity dispersions (Ferrarese and Merritt, 2000; Gebhardt et al., 2000; Gültekin et al., 2009),

$$\log\left(\frac{M_{\rm BH}}{M_\odot}\right) = (8.12 \pm 0.08) + (4.24 \pm 0.41) \cdot \log\left(\frac{\sigma_{\rm bulge}}{200 \ {\rm km\,s^{-1}}}\right), \tag{1.16}$$

and even between the black hole masses and the numbers of galactic globular clusters (Burkert and Tremaine, 2010),

$$\frac{M_{\rm BH}}{M_\odot} = (1.7 \times 10^5) \cdot N_{\rm GC}^{1.08 \pm 0.04}. \tag{1.17}$$

These observations have led to a scientific consensus that the host galaxy and its embedded massive black hole (MBH) have grown together under each other's influence (Silk and Rees, 1998; Kauffmann and Haehnelt, 2000; Wyithe and Loeb, 2003). The interaction between the galaxy and the MBH is not just by the gravitational force, but by the accretion of the interstellar gas onto the MBH and by the energetic feedback of the MBH into the galactic medium.

Massive Black Hole Growth

The most plausible scenario to explain the existence and the growth of supermassive black holes begins with *seed* black holes with relatively small masses ($\sim 10^2 M_\odot$ each) formed from the remnants of high-redshift Population III stars (Heger and Woosley, 2002). Some of these seed black holes could then plausibly accumulate their masses by accretion or mergers, as rapidly as approaching up to $10^9 M_\odot$ at redshift ~ 6.5 (Haiman and Loeb, 2001; Fan et al., 2006).[4]

In galaxy formation simulations in which the accretion disk around the MBH is usually unresolved – i.e., the numerical resolution is much bigger than the radius of the innermost stable circular orbit (ISCO) or the Schwarzschild radius of the MBH –, the gas *accretion* onto the MBH is often approximated with the Eddington-limited

[4] However, see Alvarez et al. (2009) for potential problems with this scenario for the formation of seed black holes.

Bondi-Hoyle formula (Bondi and Hoyle, 1944; Bondi, 1952; Springel et al., 2005b):

$$\dot{M}_{\rm BH} = \texttt{min}(\dot{M}_{\rm B}\,,\, \dot{M}_{\rm Edd}) \tag{1.18}$$

$$= \texttt{min}\left(\frac{4\pi G^2 M_{\rm BH}^2 \rho_{\rm B}}{c_{\rm s}^3}\,,\, \frac{4\pi G M_{\rm BH} m_{\rm p}}{\epsilon_{\rm r}\sigma_{\rm T} c}\right) \tag{1.19}$$

where $\rho_{\rm B}$ and $c_{\rm s}$ are the density and sound speed of the accreting gas, $M_{\rm BH}$ is the mass of the MBH, $m_{\rm p}$ is the mass of a proton, $\epsilon_{\rm r}$ is the radiative efficiency of the black hole, and $\sigma_{\rm T}$ is the Thomson scattering cross-section. This estimate models a gravitational capture by a dominating black hole in a pressurized, spherically symmetric gas sphere.

Likewise, *merging* of two massive black holes is equally difficult to exactly model in galactic scale simulations. During the final coalescence phase of galaxy mergers, the massive black holes at the galactic centers also become one via (1) the in-spiral, (2) the ring-down, and then (3) the final merger.[5] However, these processes all occur below the typical resolution of galactic scale simulations. As long as the numerical resolution is far from entering the regime of the general relativity and the gravitational wave generation, black holes are often merged simply when they are gravitationally bound (e.g. Li et al., 2007b; Sijacki et al., 2009).

Massive Black Hole Feedback

Intriguingly enough, supermassive black holes are not just mass *sinks*, but also extremely powerful energy *sources*. Accretion disks around the high-redshift SMBHs are believed to power the brightest extragalactic sources in the Universe known as *quasi-stellar objects* or *quasars* (Blandford and Znajek, 1977; Blandford and Payne, 1982). The prominent relativistic jets at the center of a giant elliptical galaxy M87 provide direct evidence of the energy and duration its MBH can yield (Biretta et al., 1999; Junor et al., 1999; Kovalev et al., 2007; McKinney and Blandford, 2009). The energy coming from an active massive black hole, $\sim \epsilon_{\rm r} M_{\rm BH} c^2$, could sometimes be orders of magnitude larger than the total gravitational binding energy of the galactic gas, $\sim M_{\rm gal}\sigma_{\rm gal}^2$ (Loeb, 2006). Although still unclear, the MBH energy can be

[5] For thorough reviews on merging of comparable-mass black holes and its contemporary treatments using numerical relativity, see Centrella et al. (2010).

dumped into the interstellar medium via multiple channels including (Sazonov et al., 2004; Ciotti and Ostriker, 2007; Ciotti et al., 2009; Benson, 2010):

(1) *Radiative channel:* Radiation from the MBH heats up the cooling flow via photoionization and Compton scattering, exert radiation pressure on dusts, and/or drive powerful winds from the broad line region surrounding the MBH.

(2) *Mechanical channel:* Highly collimated jets from the MBH itself pierce the galactic disk, sometimes reaching the galactic halo.

As a powerful energy outlet, therefore, the MBH plays a significant role in altering the color and morphology of its host galaxy (e.g. Hopkins et al., 2008; Cattaneo et al., 2009). As such, the feedback from the MBH is starting to be considered as one of the most important energy sources in numerical galaxy formation (Springel et al., 2005b; Di Matteo et al., 2005; Johansson et al., 2009; Booth and Schaye, 2009).

1.2.6 Interactions Between Galaxies

By reason of Newtonian gravity, galaxies are born to interact with one another. Various facets of galactic interactions include major mergers, minor mergers, harassment, tidal destruction, strangulation (starvation), ram pressure stripping, cannibalism, and so forth (Baugh, 2006; Benson, 2010). Discussed below are some of these interactions which are the most relevant to this thesis work.

Mergers: Major and Minor, Wet and Dry

The peculiar morphology of merging galaxies have captured the attention of pioneering researchers as early as in 1950s and 1960s (Holmberg, 1941; Zwicky, 1956; Alladin, 1965; Arp, 1966). Indeed, galaxy mergers are among the most energetic and spectacular phenomenon in the Universe. The shear mechanical energy involved in collisions, $\sim M_{\rm gal} v_{\rm col}^2$ with $v_{\rm col} \sim 300\ {\rm km\,s^{-1}}$, is already comparable to or in excess of the total binding energy of the galaxies (Struck, 1999). Consequently, merging of galaxies has played an essential role in shaping galactic morphology (merger hypothesis; Toomre, 1977; Barnes and Hernquist, 1992a) and in constructing large scale structures from the bottom up (White and Rees, 1978).

Dynamical friction of collisionless components (Chandrasekhar, 1943) and dissipative gas dynamics reduce the angular momentum of interacting galaxies to terminate frequently in a gravitationally bound orbit. When the two merging galaxies have comparable masses (i.e. mass ratio $> 1/3$) it is called a *major* merger; otherwise, it is called a *minor* merger. When the participating galaxies have enough fresh fuel for a new generation of star formation it is called a *wet* (gas-rich) merger, as opposed to a *dry* (gas-poor) merger. The most impactful change is driven by wet major mergers. A direct collision between the galactic gas content briefly enhances star formation (*starburst*, $\sim$ 100 Myrs), and triggers quasar activities (Hopkins et al., 2008). The morphology and content of merging galaxies are drastically altered by direct mechanical agitation, violent relaxation, and induced star formation. Once the two galaxies finally coalesce, the remnant is often devoid of the star-forming gas; this is because the fuel has been violently exhausted in the merger-driven starburst, and because the triggered quasar often prompts massive gas expulsion. Hence, such major mergers are responsible for creating giant red ellipticals in a relatively short time period.

Inherently nonlinear nature of violent galaxy mergers has forced researchers to use computational techniques to study them. Groundbreaking studies have opened the door for studying interacting galaxies with computers in 1970s and 1980s (Toomre and Toomre, 1972; Toomre, 1978; Negroponte and White, 1983; Barnes and Hut, 1986; Barnes, 1988). Since then, numerical simulations have successfully reproduced (1) the change of galactic morphology at various stages of mergers, (2) the merger-induced starbursts at close encounters, and (3) the sudden gas inflow towards the galactic center triggering the growth and feedback of massive black holes (Barnes and Hernquist, 1991, 1992b; Mihos and Hernquist, 1994a; Barnes and Hernquist, 1996; Mihos and Hernquist, 1996; Springel et al., 2005a,b; Di Matteo et al., 2005; Cox et al., 2006a,b; Mayer et al., 2007; Li et al., 2007a; Saitoh et al., 2008; Governato et al., 2009; Karl et al., 2010; Teyssier et al., 2010a; Bournaud et al., 2011).[6]

[6]Note that these previous studies are either pure N-body simulations or smoothed particle hydrodynamics (SPH) simulations, with the exception of Teyssier et al. (2010a) and Bournaud et al.

Strangulation and Ram Pressure Stripping

When a small satellite galaxy penetrates the hot atmosphere of a larger host, the hydrodynamic interaction between the satellite gas and the intracluster medium (ICM) can be very important. The ram pressure of the ambient medium,

$$P_{\rm ram} = \rho_{\rm ICM} \cdot v_{\rm gal}^2, \tag{1.20}$$

could sometimes exceed the gravitational binding energy of the baryonic content of the galaxy, either of the hot halo or of the cold disk. A sufficient level of ram pressure leads to a phenomenon called *strangulation* or *starvation* in which the fuel for long-term star formation – infalling gas in the galactic halo – is slowly removed from the galaxy. As a result, this *environmental* effect causes a gradual change in the colors of galaxies in a few Gyrs, but is not necessarily accompanied by a severe morphological transformation (Larson et al., 1980). A stronger version of such interaction is dubbed *ram pressure stripping* where even the cold gas in the galactic disk is stripped away by the ram pressure of the dense ICM (Gunn and Gott, 1972). This pure hydrodynamic interaction between ISM and ICM has been considered in semi-analytic and numerical investigations to explain the color change from blue star-forming galaxies to red sequence galaxies (Tonnesen et al., 2007; Roediger and Brüggen, 2007, 2008; Font et al., 2008; Tonnesen and Bryan, 2009).

1.2.7 Additional Known Unknowns

After many years of development, an abundance of *known* unknowns still linger in the theory of galaxy formation: magnetic fields, cosmic ray diffusion, stellar ultraviolet radiation, dust re-emission, thermal conduction, et cetera. Some of these processes may not be as energetically important as others, so their omission in theoretical or numerical formulations could probably be justified. However, many such unknowns are not fully investigated only because it is nontrivial to adequately incorporate them in the contemporary framework, numerical or analytic.

(2011). We will get back to this issue in Chapter 4.

The most obvious ones among such unknowns are magnetic fields and cosmic rays. According to the *equipartition principle* galactic magnetic fields may provide additional nonthermal pressure, further suppressing star formation and regulating the ISM structure. However, integrating hydrodynamics, magnetic fields, and star formation and feedback in one framework is only in its infancy stage (Piontek and Ostriker, 2007; Wang and Abel, 2009; Dubois and Teyssier, 2010; Kotarba et al., 2010). Because cosmic ray particles get accelerated in supernova remnant shocks and propagates through the magnetic fields (Fermi, 1954), cosmic ray physics can be appropriately modeled only in an all-inclusive magnetohydrodynamic (MHD) simulation of galaxies (Strong et al., 2007; Enßlin et al., 2007; Sharma et al., 2009). Another unknown which is now actively being scrutinized is the stellar ultraviolet radiation and dust re-emission. The diffuse photoelectric heating by UV-irradiated dust grains has been argued to be a dominant heating source for cold and warm neutral medium (CNM/WNM) in galactic disks (Bakes and Tielens, 1994; Wolfire et al., 1995). Such heating with a uniform rate of

$$\Gamma_{\rm pe} = 8.5 \times 10^{-26} \text{ ergs cm}^{-3} \text{ s}^{-1} \tag{1.21}$$

has been considered in galactic scale simulations (e.g. Joung and Mac Low, 2006).

1.3 Numerical Approaches To Galaxy Formation

Astrophysics is distinctively different from most other branches of natural science in view of the fact that a hands-on experiment is often impractical. Moreover, the dynamical times of most astrophysical systems are much longer time than the human lifespan, making temporal observations of such systems only occasionally meaningful. Therefore computer simulations are often the last resort for astronomers who wish to observe the full dynamical evolution of astrophysical systems at close range. While analytic or semi-analytic understandings of galaxy formation are very informative (White and Frenk, 1991; Mo et al., 1998; Somerville and Primack, 1999; Cole et al., 2000; Baugh, 2006; Stringer and Benson, 2007; De Lucia and Helmi, 2008), a

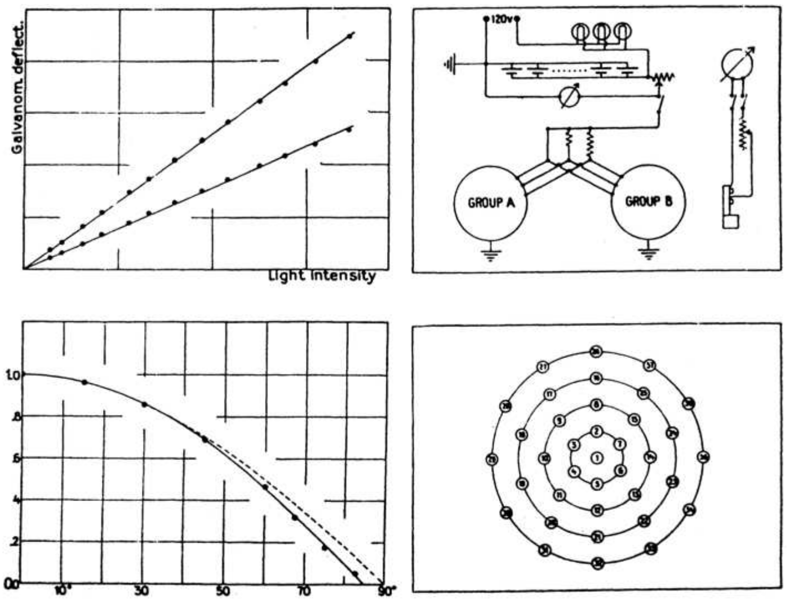

Fig. 1.3.— Holmberg's experiment adapted from Figures 2 and 3 of Holmberg (1941). Each galaxy is composed of 37 lightbulbs and photoelectric cells.

reasonable theory of galaxy formation must also pass numerical experiments.

Modeling galactic evolution on computers requires high numerical resolution as it consists of numerous processes occurring on a wide range of distance scales: from pc (star forming regions) to Mpc (distance between galaxies at which tidal interactions occur). In other words, simulations must cover a large *dynamic range*. Further, one also needs to integrate the physics at small scales (e.g. star formation and feedback) and the correct understanding of large scale structure evolution. These requirements have made the galaxy formation simulation a uniquely challenging task. In the following sections, we first describe the history and the state of the numerical astrophysics focusing on the evolution of gravity solvers, and then on two different numerical approaches for the numerical hydrodynamics.

1.3.1 History and State of the Field

The first-of-its-kind numerical calculation of an astrophysical system was performed by Holmberg (1941) with 74 light bulbs and photoelectric cells (Figure 1.3). It was a pure gravitational force calculation using the fact that the gravitational attraction at each location is proportional to the light intensity measured by a galvanometer. It is remarkable that Holmberg did "all the work in person, including the rebuilding of the laboratory room and making all electrical installations", and yet reproduced a largely correct morphological change of merging galaxies (Rood, 1987). His ingenious attempt inspired subsequent numerical investigations of the astrophysical objects using computers (Pfleiderer and Siedentopf, 1961; Toomre and Toomre, 1972).

Towards the Better and the Faster

Ever since, numerical investigations of the physics of galaxy formation have obviously been benefited from the expeditious developments of both numerical techniques and computer hardwares. As an example, we discuss the numerical solvers of *gravitational* dynamics, a key problem that needs to be tackled in numerical astrophysics.

$$\frac{d\mathbf{r}_i}{dt} = \mathbf{u}_i \tag{1.22}$$

$$\frac{d\mathbf{u}_i}{dt} = -\nabla\phi(\mathbf{r}_i) \tag{1.23}$$

$$\nabla^2\phi(\mathbf{r}_i) = 4\pi G[\rho(\mathbf{r}_i) - \bar{\rho}] \tag{1.24}$$

Here, ϕ is the gravitational potential.[7] The technique to follow the gravitational interaction between many bodies has evolved from a direct particle-particle summation (PP; von Hoerner, 1960; Peebles, 1970; Aarseth et al., 1979), to a particle-mesh algorithm (PM; Klypin and Shandarin, 1983), to a particle-particle particle-mesh algorithm (P^3M; Hockney and Eastwood, 1981, 1988; Efstathiou and Eastwood, 1981)[8], and then to an adaptive P^3M algorithm (AP^3M; Couchman, 1991; Couchman et al., 1995). Another branch of evolution of the gravity solver was to a Tree algorithm

[7] For cosmological simulations, these equations are written in comoving coordinates in which the Hubble expansion is subtracted out (Bertschinger, 1998):

$$\frac{d\mathbf{r}_i}{dt} = \frac{1}{a}\mathbf{u}_i, \quad \frac{d\mathbf{u}_i}{dt} + H\mathbf{u}_i = -\nabla\phi(\mathbf{r}_i), \quad \nabla^2\phi(\mathbf{r}_i) = 4\pi Ga[\rho(\mathbf{r}_i) - \bar{\rho}].$$

[8] PP at short distance, PM at long distance

(Barnes and Hut, 1986; Hernquist, 1987), and to a Tree code PM algorithm (TPM; Xu, 1995; Bode et al., 2000), in which particles are recursively bisected (*kD-tree*) or octsected (*oct-tree*) to speed up the gravity solver.[9] Such clever techniques, combined with the rapid increase in computing power[10] and the success of massively parallelized computing, have allowed simulators to use more and more particles (Springel et al., 2005c; Diemand et al., 2007, 2008; Springel et al., 2008; Klypin et al., 2010). Increasingly larger and more accurate simulations are feasible at cheaper costs to achieve better numerical resolution.

State of the Field: Galaxy Formation Simulations

Taking the full advantage of the numerical techniques available, a growing number of galaxy formation simulations have demonstrated promising results both in a *cosmological* set-up (e.g. Steinmetz and Navarro, 1999, 2002; Springel and Hernquist, 2003b; Abadi et al., 2003; Robertson et al., 2004; Oppenheimer and Davé, 2008; Ocvirk et al., 2008) and in an *isolated* set-up (e.g. Springel and Hernquist, 2003a; Scannapieco et al., 2005, 2006; Brook et al., 2006; Stinson et al., 2006; Kaufmann et al., 2007a,b; Governato et al., 2007; Rocha et al., 2008; Robertson and Kravtsov, 2008; Dubois and Teyssier, 2008; Foyle et al., 2008; Robertson and Kravtsov, 2008; Christensen et al., 2010).[11] Some authors have used a hybrid *zoom-in* approach: (1) first run a simulation with a cosmological initial condition, and (2) identify a small Lagrangian volume that eventually ends up as a galactic halo, and finally (3) rerun a simulation on the extracted subset with higher resolution. This way one can achieve high resolution at small scales, while maintaining large scale powers in structure formation (e.g. Kravtsov and Gnedin, 2005; Tassis et al., 2008; Scannapieco et al., 2008; Ceverino and Klypin, 2009; Kereš and Hernquist, 2009; Agertz et al., 2011). Others have focused only on the galactic ISM structure with high resolution by simulating the evolution of an exponential disk embedded in a static dark matter halo (e.g. de Avillez, 1999; Li et al., 2005; Wada and Norman, 2007; Tasker and Bryan, 2006,

[9]Likewise, advancement has been made in hydrodynamics solvers; see §1.3.3 and §1.3.4.
[10]Moore's law, 1965, *Electronics*
[11]For details on cosmological and isolated initial conditions, see §1.4.1 and §1.4.2.

Table 1.1 Selected Previous Studies - Galaxy Formation Simulations Since 2000

	Author(s)	Code	Setup	Resolution	Typical M_{vir}	SF	Fbck
SPH	Abadi et al. (2003)	*GrapeSPH*	cosmological	500 pc	$5.6 \times 10^{11} M_{\odot}/h$	◯	◯
	Springel and Hernquist (2003a)	*Gadget*	isolated	30 pc/h	$10^{10} M_{\odot}/h$	◯	◯
	Springel and Hernquist (2003b)	*Gadget*	cosmological	≥190 pc/h	$10^{8} - 10^{15} M_{\odot}$	◯	◯
	Robertson et al. (2004)	*Gadget2*	cosmological	650 pc/h	$2.2 \times 10^{11} M_{\odot}/h$	◯	◯
	Bailin et al. (2005)	*GCD+*	cosmological	570 pc	$10^{12} M_{\odot}$	◯	◯
	Scannapieco et al. (2005)	*Gadget2*	isolated	400 pc/h	$10^{12} M_{\odot}/h$	◯	×
	Governato et al. (2007)	*Gasoline*	isolated	325 pc	Milky Way	◯	◯
	Kaufmann et al. (2007b)	*Gasoline*	isolated	∼100 pc	$10^{10} - 10^{12} M_{\odot}$	◯	◯
	Robertson and Kravtsov (2008)	*Gadget2*	isolated	100 pc	$\sim 10^{9} - 10^{12} M_{\odot}$	◯	◯
	Kereš and Hernquist (2009)	*Gadget2*	zoom-in	400 pc/h	Milky Way	◯	◯
	Christensen et al. (2010)	*Gasoline*	isolated	≥21 pc	$10^{9} - 10^{13} M_{\odot}$	◯	◯
AMR	Kravtsov and Gnedin (2005)	*ART*	zoom-in	45 pc/h	$\sim 10^{12} M_{\odot}/h$	◯	◯
	Gibson et al. (2008)	*Ramses*	zoom-in	435 pc	$5 - 8 \times 10^{11} M_{\odot}$	◯	◯
	Tassis et al. (2008)	*ART*	zoom-in	52 pc	$2 \times 10^{11} M_{\odot}/h$	◯	◯
	Ceverino and Klypin (2009)	*ART*	zoom-in	35 pc	$\sim 10^{12} M_{\odot}/h$	◯	◯
	Agertz et al. (2011)	*Ramses*	zoom-in	170 pc	$\sim 10^{12} M_{\odot}$	◯	◯

Table 1.2 Selected Previous Studies - Galactic Disk Formation Simulations Since 2000

	Author(s)	Code	Setup	Resolution	Typical M_{vir}	SF	Fbck
SPH	Li et al. (2005)	*Gadget*	disk	40 pc	$10^{10} - 10^{12} M_{\odot}/h$	◯	×
	Dalla Vecchia and Schaye (2008)	*Gadget*	disk	17 pc	$10^{10}, 10^{12} M_{\odot}$	◯	◯
	Bush et al. (2008)	*Gadget2*	disk	280 pc	$10^{12} M_{\odot}$	◯	×
AMR	Tasker and Bryan (2008)	*Enzo*	disk	25 pc	Milky Way	◯	◯
	Tasker (2011)	*Enzo*	disk	7.8 pc	Milky Way	◯	◯
Unigrid	Wada and Norman (2007)	*AUSM*	axisym.	5 pc	only disk	◯	◯

2008; Schaye and Dalla Vecchia, 2008; Dalla Vecchia and Schaye, 2008; Bush et al., 2008; Tasker, 2011). Selected previous studies in numerical galaxy formation are put together in Tables 1.1 and 1.2.

What is equally important – if not more – as the gravity in galactic astrophysics is the *hydrodynamic* interaction of the baryonic content. Therefore a lot of effort has been made to secure an accurate, yet fast hydrodynamics solver. We now discuss such solvers adopted for the studies in Tables 1.1 and 1.2.

1.3.2 Hydrodynamics Modules

Hydrodynamics calculation poses an entirely different challenge to simulators. While long range tidal interactions are important in gravity solvers, hydrodynamics – the conservation and fluidic transport of mass, momentum, and energy (Euler equations) – is concerned with the local interactions between neighboring elements:

$$\frac{\partial \rho}{\partial t} + \nabla \cdot (\rho \mathbf{u}) = 0 \tag{1.25}$$

$$\frac{\partial (\rho \mathbf{u})}{\partial t} + \nabla \cdot (\rho \mathbf{u}\mathbf{u}^{\mathrm{T}}) + \nabla P = \rho \mathbf{g} \tag{1.26}$$

$$\frac{\partial (\rho E)}{\partial t} + \nabla \cdot [(\rho E + P)\mathbf{u}] = \Gamma - \Lambda \tag{1.27}$$

where $\rho, \mathbf{u}, \epsilon, E = \epsilon + \frac{1}{2}|\mathbf{u}|^2$ and $P = \rho(\gamma - 1)\epsilon$ are the density, velocity, internal energy, total energy, and pressure, respectively. γ is the adiabatic index, $\mathbf{g} = -\nabla\phi$ is the gravitational field, and Γ and Λ are heating and cooling rates per unit volume, respectively.[12] Thus resolving the local contact between different streams (e.g. shearing flows, discontinuities at shocks) is the main challenge for any hydrodynamics solver. For future reference, without the external gravity, source, and sink terms, Eqs. 1.25

[12] In comoving coordinates the Euler equations are written as:

$$\frac{\partial \rho}{\partial t} + \frac{1}{a}\nabla \cdot (\rho \mathbf{u}) = 0, \quad \frac{\partial (\rho \mathbf{u})}{\partial t} + \frac{1}{a}\nabla \cdot (\rho \mathbf{u}\mathbf{u}^{\mathrm{T}}) + H\mathbf{u} + \frac{1}{a}\nabla P = \rho \mathbf{g}, \quad \frac{\partial (\rho E)}{\partial t} + \frac{1}{a}\nabla \cdot [(\rho E + P)\mathbf{u}] = \Gamma - \Lambda.$$

to 1.27 can be written as the continuity equation in a vector form of

$$\frac{\partial \mathbf{U}}{\partial t} + \nabla \cdot (\mathbf{F}(\mathbf{U})) = 0 \tag{1.28}$$

where

$$\mathbf{U} = \begin{pmatrix} \rho \\ \rho \mathbf{u} \\ \rho E \end{pmatrix} \quad \text{and} \quad \mathbf{F}(\mathbf{U}) = \begin{pmatrix} \rho \mathbf{u} \\ \rho \mathbf{u}\mathbf{u}^{\mathrm{T}} + P \\ (\rho E + P)\mathbf{u} \end{pmatrix}. \tag{1.29}$$

In the next two sections, we discuss the pros and cons of two varying attempts to tackle hydrodynamics, widely adopted in astrophysics: smoothed particle hydrodynamics (SPH) and adaptive mesh refinement (AMR). We again caution that either of these two approaches has *both* strengths and drawbacks. It is very rare for a reasonable simulator to become self-assured enough to claim that one approach is better than the other in *all* astrophysical applications. Rather, what is much more important for simulators is to decide: (1) which approach can be employed to best fit their needs, and (2) to what extent the results can be trusted given the shortcomings of the approach. Until a breakthrough is made combining only the virtues of these two approaches (for example, see the attempt by Springel (2010)), simulators should always keep these two rules in mind.

1.3.3 Smoothed Particle Hydrodynamics

As was shown in §1.3.1, gravitational dynamics of *collisionless* particles has been dealt with on a particle-based scheme.[13] In the smoothed particle hydrodynamics, the *collisional* fluid element of the astrophysical systems is simply rendered as another type of a Lagrangian particle which is under the hydrodynamic interaction as well (i.e. the repelling force representing the gas pressure; Gingold and Monaghan, 1977; Lucy, 1977; Monaghan, 1992). This *tracer* particle, unlike stars or dark matter, samples and carries the gas properties such as thermal energy (or entropy), pressure, and

[13] as opposed to solving the collisionless Boltzmann equations in a phase space

metallicity. However, quite obviously, one cannot populate the entire domain with such discrete blobs; therefore, in order to estimate the baryonic quantities at a certain location, $\mathbf{r}_i$, the averaged values of N neighboring SPH particles is calculated.[14] For example, the gas density estimate ρ_i at $\mathbf{r}_i$ is

$$\rho_i = \sum_{j=1}^{N} m_j \; W(|\mathbf{r}_j - \mathbf{r}_i|, h_i) \tag{1.30}$$

where m_j is the mass of each tracer particle, and the possible choices of the smoothing kernel $W(r,h)$ could be the spline kernel (Monaghan and Lattanzio, 1985; Monaghan, 1992; Springel, 2005),

$$W_1(r,h) = \frac{8}{\pi h^3} \begin{cases} 1 - 6\left(\frac{r}{h}\right)^2 + 6\left(\frac{r}{h}\right)^3 & \text{if } 0 \le \frac{r}{h} \le \frac{1}{2} \\ 2\left(1-\frac{r}{h}\right)^3 & \text{if } \frac{1}{2} < \frac{r}{h} \le 1 \\ 0 & \text{if } 1 < \frac{r}{h} \end{cases}, \tag{1.31}$$

or the Gaussian form of

$$W_2(r,h) = \frac{1}{h\sqrt{\pi}} \exp\left(-\frac{r^2}{h^2}\right). \tag{1.32}$$

Inherently Galilean invariant, this Lagrangian scheme has been widely employed in many astrophysical simulations where particles collapse to form clumps, or dynamically interact with one another with high speeds. Of great importance in this method is that the numerical resolution is automatically increased in the regions where the mass is concentrated as a result of the gravitational collapse (e.g. collapsing filaments, galactic gas disks, star forming regions). Therefore one does not need to explicitly implement cumbersome adaptive refinement machineries in order to manually increase the resolution in the regions of interest. However, significant concerns continue to exist in the SPH methods as well. Although simulations using SPH methods have tried to duplicate complex hydrodynamic phenomena, many of the results reveal less than ideal agreement. It is mainly because the SPH method

[14]The default value of N in *Gadget-2* – one of the most popular SPH codes – is 64.

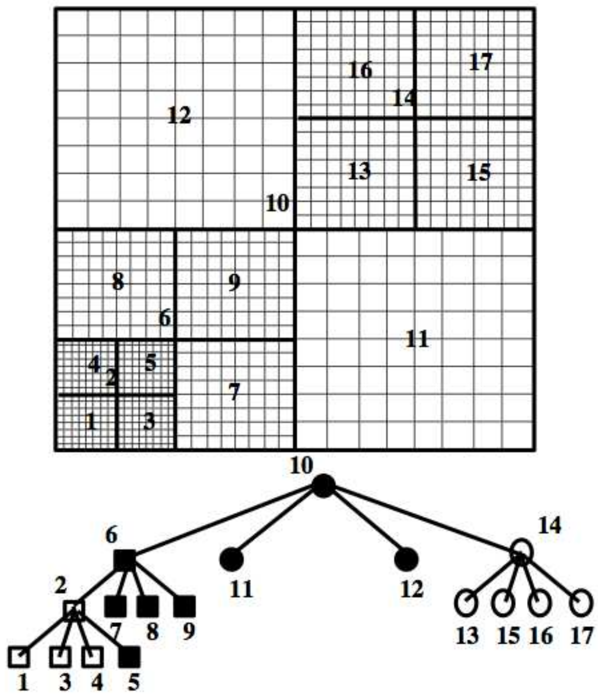

Fig. 1.4.— Block-structured adaptive mesh of the astrophysical hydrodynamics code *FLASH*, adapted from Figure 2 of Fryxell et al. (2000). Each block has the identical dimension regardless of its refinement level. The different symbols in the tree indicates which processor the block is located on.

poorly resolves shocks, instabilities, and contact discontinuities due to the spurious surface tension and numerical diffusivity (Agertz et al., 2007; Tasker et al., 2008; Abel, 2011). Combined with insufficient numerical resolution, the numerical viscosity could sometimes lead to a so-called angular momentum catastrophe in which too small disks with unrealistically high rotational velocities form in cosmological simulations (van den Bosch, 2001). Furthermore, due to the limit in computational resources, it is often challenging to populate less dense regions (e.g. diffuse galactic halos, voids between filaments) with an enough number of SPH tracer particles. This makes it very difficult to investigate certain physics, such as the interplay between the galactic disk and embedding halo, or the galactic superwind driven by supernova explosions.

1.3.4 Adaptive Mesh Refinement

A more traditional way to solve the continuity equations (Eqs. 1.25 to 1.27, or Eq. 1.28) is to discretize the flows using fixed Eulerian grids and directional splitting as

$$U_i^{n+1} - U_i^n = \frac{\Delta t}{\Delta x}(F_{x,\,i-1/2} - F_{x,\,i+1/2}) \tag{1.33}$$

where the index i represents the spatial ordering of the grid points, $i \pm 1/2$ the left and right cell interfaces, and n the temporal ordering. Several different methods to solve this partial differential equation have been developed including a first-order accurate Godunov method, a second-order accurate piecewise linear monotonic spatial interpolation (PLM; van Leer, 1979), a third-order accurate piecewise parabolic monotonic interpolation (PPM; Colella and Woodward, 1984), and so forth. Among these, PPM is particularly powerful in capturing shocks and following the instabilities at contact discontinuities (Agertz et al., 2007; Tasker et al., 2008). While the Godunov methods try to find the accurate solution to the Riemann boundary problems at cell interfaces, there exist other fast ways to solve the continuity equations. For example, the ZEUS method (Stone and Norman, 1992a,b; Anninos and Norman, 1994) employs an artificial viscosity term to prevent infinitely large gradients at shocks. Although this scheme is known to dissipate shock fronts and introduce spurious effects, it is widely used in many astrophysical applications because of the stability of its solutions, excellent performance, and acceptable errors when combined with sufficient resolution.

As the gas cloud gravitationally collapses, the Jeans length (Eq. 1.12) and the Jeans mass decrease and the gas starts to fragment into even smaller clumps. In order to resolve these clumps in numerical simulations, typically four cells or more need to be placed across the Jeans length (Truelove criterion; Truelove et al., 1997). Hence the mesh is desired to be adaptively refined according to the local Jeans length, the densities of individual cells, or any other equivalent criterion (see Figure 1.4). With this technique (AMR; Berger and Oliger, 1984; Berger and Colella, 1989) one can adaptively focus computational power on the regions of interest rather than having to refine everywhere uniformly. When the targeted problem covers a large dynamic range (of up to 10^{15} in recent applications), this could mean a substantial saving in computation. Another benefit of the AMR approach is that the low dense regions are naturally populated by coarse cells, allowing simulators to simultaneously follow those regions without any special treatment. However, several problems are identified with the Eulerian AMR approach as well. Many have noted the lack of Galilean invariance in Eulerian methods when combined with the inadequate spatial and temporal resolutions (Tasker et al., 2008). Others have claimed that the discontinuous jumps in resolution may cause a suppression of the growth of small halos (Springel, 2010).

1.4 Generating A Piece of The Universe

With the simulation tools in hand (i.e. the physics to evolve *things*), we now need a piece of the fake Universe on which we can run our tools (i.e. the initial positions and velocities of the *things*). Initial conditions of astrophysical simulations are typically generated in two ways: *cosmological* initial condition and *isolated* initial condition.

1.4.1 Cosmological Initial Condition

First a three dimensional domain is set up with a uniform Galilean lattice, $\mathbf{q}$, of equal-mass particles. Inflation predicts small Gaussian random fluctuations at redshift $\sim$ 1100 when recombination occurs and photons and baryons decouple from each other. The density fluctuations, $\delta(\mathbf{q}) = \Delta\rho(\mathbf{q})/\bar{\rho}$, are determined at a particular redshift by the matter power spectrum, $P(k) = P_0(k)T^2(k)$, as

$$\langle \delta(\mathbf{k})\delta^*(\mathbf{k}') \rangle = \frac{2\pi^2}{k^3} P(k) \cdot \delta_{\rm Dirac}(\mathbf{k} - \mathbf{k}'), \tag{1.34}$$

and assumed to grow linearly at later times (Zel'dovich approximation; Zel'Dovich, 1970). A standard way to realize these density fluctuations is to sample the density and corresponding velocity fields on the lattice by perturbing the particles from the uniform lattice point $\mathbf{q}$ (Efstathiou et al., 1985; Bertschinger, 1998):

$$\mathbf{r} = \mathbf{q} + D(t)\nabla\phi(\mathbf{q}) \tag{1.35}$$

$$\mathbf{u} = a\frac{dD(t)}{dt}\nabla\phi(\mathbf{q}). \tag{1.36}$$

Here $D(t)$ is the growth factor, and the displacement field, $\nabla\phi(\mathbf{q})$, is evaluated by solving the Poisson equation,

$$\nabla^2\phi(\mathbf{q}) = -\frac{\delta(\mathbf{q})}{D(t)}, \tag{1.37}$$

via the numerical fast Fourier transform (Bertschinger, 1995). Because the density field is sampled onto a lattice of finite number of particles, the mass resolution of the initial condition severely limits the power at small scales. To address this issue, the Gaussian random fields are generated typically with multiple levels of resolution adaptively focused on the regions of interest (e.g. *GRAFIC-2*; Bertschinger, 2001).[15]

1.4.2 Isolated Initial Condition

While cosmological simulations are very rewarding, one may want to focus on a much smaller scale system, the evolution of which has already long been decoupled from the Hubble expansion or the linear growth. A fully evolved galaxy where the stars and dark matter have been dynamically well mixed for a long time could be one such example. This galaxy model can be used to study the instabilities in the galactic disks or to simulate merging galaxies. Consequently, generating a dynamically stable astrophysical system has been a topic of great interest (e.g. Barnes, 1988; Hernquist, 1993; Springel et al., 2005b; Widrow and Dubinski, 2005).

A case in point is *GalactICS*, a galactic initial condition generator which sets up a self-consistent bulge-disk-halo model (Kuijken and Dubinski, 1995). First an analytic form of the *distribution function* for each galactic component is written in terms of integrals of motion. As an example, the distribution function for the bulge (King,

[15]See also the recent effort by Hahn and Abel (2011).

1962) can be written as

$$f_{\rm bulge}(E) = \begin{cases} \frac{\rho_{\rm b}}{(2\pi\sigma_{\rm b})^{3/2}} \exp\left(\frac{\Psi_0 - \Psi_{\rm c}}{\sigma_{\rm b}^2}\right) \left[\exp\left(-\frac{E-\Psi_c}{\sigma_{\rm b}^2}\right) - 1\right] & \text{if } E < \Psi_{\rm c} \\ 0 & \text{if } E > \Psi_{\rm c} \end{cases} \tag{1.38}$$

where $\rho_{\rm b}$ is approximately the central density, $\sigma_{\rm b}$ the velocity dispersion, Ψ_0 the potential at the center, and $\Psi_{\rm c}$ the cutoff potential. The distribution function not only provides the exact spatial density, but yields a steady-state solution of the collisionless Boltzmann equation (Jeans theorem). An iterative scheme is used to numerically generate a self-consistent N-body realization to the Poisson equation and the collisionless Boltzmann equation.

Thanks to the tremendous improvement in the numerical techniques and parallel computing, we are now well poised to run ambitious massive numerical simulations of galaxy formation. In the last section of this Chapter, we preview the organization and contents of the rest of this thesis.

1.5 Thesis Overview

Galaxy formation is the building block of hierarchical structure formation in ΛCDM paradigm. Unmistakably, galaxy formation consists of vibrant interactions between gas, stars, and central massive black holes (MBHs). How do collapsing gas clumps give birth to stars? How does stellar feedback then change the interstellar medium? How does gas accrete onto a MBH, and how does MBH feedback in turn affect the galaxys growth? Therefore, for galaxy formation studies it is imperative to numerically follow these highly nonlinear interactions with physically motivated modelings.

Nevertheless, a comprehensive numerical simulation which self-consistently incorporates gas, stars, and MBHs has been absent. Most galactic simulations so far have modeled stars and MBHs with phenomenologically parametrized sub-resolution recipes: for example, the stopping of cooling to mimic stellar feedback, or thermal energy injection to depict MBH feedback (e.g. Springel et al., 2005b). While pioneering in some applications (e.g. Di Matteo et al., 2005; Sijacki et al., 2009), previous approaches with *ad hoc* recipes often lack the physics and resolution required to reproduce even the obvious aspects of observed galaxies (e.g. Guo et al., 2010). Especially when recent observations yield excellent constraints on galactic evolution (e.g. Zheng et al., 2009), the need for an unabridged, self-consistent galaxy formation simulation has never been greater.

1.5.1 Building A Self-consistent Numerical Framework for Galaxy Formation

To circumvent the limitations of previous studies and follow the actual physical processes between gas, stars, and MBHs, we developed a fully self-consistent galaxy formation simulation integrating these components in one comprehensive framework (Kim et al. (2010); Chapter 2). The high-resolution adaptive mesh refinement (AMR) code *Enzo* (Norman et al., 2007) is modified to model the formation and feedback of molecular clouds at its characteristic scale of 15.2 pc, and the accretion of gas onto a MBH. Two major channels of MBH feedback, radiative and mechanical, are considered. Our unique framework harbors five novel features:

1. *Molecular cloud formation*: Unlike previous star formation recipes based on the simple scaling of $\rho_{\rm SFR} \sim \rho_{\rm gas}^{1.5}$ (Schmidt, 1959), we self-consistently deposit a particle when a gas cell of a molecular cloud size actually becomes Jeans unstable.

2. *Stellar feedback*: The molecular cloud particle then gradually produces stellar mass while returning a large fraction of mass back to the gas with thermal feedback energy. It models the observed slow star formation in a molecular cloud (Krumholz and Tan, 2007).

3. *MBH accretion*: Gas accretion rate onto a MBH is estimated assuming a pressurized spherical collapse (Bondi-Hoyle estimates; Bondi, 1952) but without any empirical boost factor (e.g. as in Springel et al., 2005b), since high-resolution AMR resolves the high densities near the MBH.

4. *MBH radiative feedback*: Monochromatic X-ray photons from the MBH is followed through full 3D adaptive ray tracing (Wise and Abel, 2010) rendering the radiative feedback of the MBH. Here photons ionize and heat the gas, and exert momentum onto the gas (Figure 2.4A).

5. *MBH mechanical feedback*: Bipolar jets with velocities of $\sim 10^3\ \mathrm{km\,s^{-1}}$ are launched from the vicinity of the MBH, well resolved in high-resolution adaptive mesh (Figure 2.4B).

This machinery is then applied to the various contexts of galaxy formation described in next Chapters.

1.5.2 Galaxy Formation with Stars and MBHs

One of the outstanding problems which can be better addressed by our comprehensive numerical approach is the coevolution of galaxies and their MBHs. The growth of the MBH is limited by the gas inflow to the galactic center while, in turn, the radiation and outflows released by the accreting MBH limits the galaxys growth. Though many observations have detailed the interwoven destiny of galaxies and MBHs (e.g. Ferrarese and Merritt, 2000), it is still unclear how the small scale physics of a MBH can be such tightly linked with the overall galactic evolution at a much larger scale.

With a much improved numerical tool in hand, we investigated the coevolution of a $9.2 \times 10^{11} M_\odot$ galaxy and its $10^5 M_\odot$ embedded MBH at redshift 3 in a ΛCDM simulation (Kim et al. (2010); Chapter 3). By employing advanced treatment of MBH physics, we find that MBH feedback heats its surrounding interstellar medium (ISM) up to 10^6 K through photoionization and Compton heating, and deprives the galactic inner core of cold star-forming gas. Locally suppressed star formation then significantly changes the stellar distribution and the stellar to gas mass ratio at the galactic center. This feedback channel is particularly interesting because it is only locally dominant and, unlike stellar feedback, does not require the heating of the gas globally on the disk. Besides, without having to unbind all of its surrounding gas, the MBH self-regulates its growth by keeping the surrounding ISM hot for an extended period of time. These results depict an analogue of "radio-mode" feedback by a slowly growing MBH for which the accretion rate is usually $< 5\%$ of the Eddington limit (Croton et al., 2006).

Our novel framework renders a completely different, yet physically more accurate picture of how a galaxy and its embedded MBH evolve under each others influence. For example, our results strongly suggest one of many viable routes to terminate the growth of massive secular bulges often found at the centers of simulated galaxies (e.g. Piontek and Steinmetz, 2009a). The bulge-dominated disks made by migrations of dense clumps in numerical simulations can be avoided if the radiation from the MBH keeps the inner core devoid of star-forming gas. Our results also undoubtedly demonstrate that we can finally build an unabridged, self-consistent numerical framework for both galaxies and MBHs, providing a powerful means to investigate their coevolution. The radiation and outflows from the MBH heat up the surrounding gas, but the thermal couplings of the MBH energy to its environment are all carried out by the radiation hydrodynamics AMR scheme itself, not by any presupposed sub-resolution model.

1.5.3 Merging Galaxies on Adaptive Mesh Refinement

In hierarchical structure formation of ΛCDM cosmology, merging of galaxies is frequent and known to dramatically affect their properties, therefore a key to understand galactic evolution. It is also believed to induce quasar activities (Hopkins et al., 2008), and to instigate the rapid growth of black hole masses in the early phase of structure formation (Haiman and Loeb, 2001). Although it is very useful to utilize a high-resolution simulation to study merging galaxies because of the nonlinear coupling between pc and Mpc scales, many such studies have lacked the necessary resolution.

To this end, we performed the very first adaptive mesh refinement (AMR) simulation of two merging galaxies, $1.8 \times 10^{10} M_\odot$ each, including star formation and feedback (Kim et al. (2009); Chapter 4). With galaxies resolved by $\sim 2 \times 10^7$ total computational elements we achieve 3.8 pc resolution in the multiphase ISM, finding a widespread starburst via shock-induced star formation. Having a $\sim$ pc resolution is essential to properly capture the clumpy star formation on disks and spirals, as was later confirmed by Teyssier et al. (2010a) and others. The high dynamic range of AMR also traces the interplay between galaxies and the embedding medium depicting how galactic outflows and a hot metal-rich halo form.

1.5.4 Galaxy Mergers with Stars and MBHs

We also carried out a simulation of two merging galaxies, $2.1 \times 10^{11} M_{\odot}$ each, with their $10^5 M_{\odot}$ embedded MBHs, portraying an analogue of merger-induced "quasar-mode" feedback by fast growing MBHs (Hopkins et al., 2008) for which the accretion rates are $> 5\%$ of the Eddington limit (Kim et al. (2011); Chapter 5). We find that the feedback from the fast growing MBHs helps to reduce the global star formation on the disk. When compared with the feedback by a slowly growing MBH, these MBHs drive more frequent jets creating sizable bubbles at the galactic centers.

In addition, we have been investigating the following questions: Is the feedback from fast growing MBHs strong enough to remove the gas out of the galactic potential? If so, how does it compare with the previous recipes (e.g. Springel et al., 2005b))? What are the relative contributions for the suppression of star formation between radiative and mechanical feedback? What is the dominant channel of feedback? How does the merger remnant look? Does the MBH feedback change the remnant morphology? Answering these questions will bring a new insight to the role of fast growing MBHs during and after the galaxy mergers, potentially shaping red elliptical galaxies with little ongoing star formation activity. The accurate, unabridged descriptions of MBH feedback in our comprehensive framework will help us to understand how galaxies and MBHs interact in mergers of galaxies.

Finally, the original conclusions of this thesis are brought together in Chapter 6. Ideas on how to improve our numerical approach are summarized. Possible future projects, including the formation of high-redshift quasars, are also discussed.

Chapter 2

Building A Self-consistent Numerical Framework for Galaxy Formation

> *"It is unworthy of excellent men to lose hours like slaves in the labor of calculation which could be relegated to anyone else if machines were used."*
> — Gottfried Wilhelm Leibnitz (1646-1716)

There is mounting evidence for the coevolution of galaxies and their embedded massive black holes (MBHs) in a hierarchical structure formation paradigm. To tackle the nonlinear processes of galaxy - MBH interaction, we describe a self-consistent numerical framework which incorporates both galaxies and MBHs. The high-resolution adaptive mesh refinement (AMR) code *Enzo* is modified to model the formation and feedback of molecular clouds at their characteristic scale of 15.2 pc and the accretion of gas onto a MBH. Two major channels of MBH feedback, radiative feedback (X-ray photons followed through full 3D adaptive ray tracing) and mechanical feedback (bipolar jets resolved in high-resolution AMR), are employed.

This chapter is a part of the publication submitted to *The Astrophysical Journal* which is coauthored by John Wise, Marcelo Alvarez, and Tom Abel.

2.1 Introduction and Motivation

2.1.1 Introduction

Ever since the discovery of the ubiquitous existence of supermassive black holes at the centers of massive galaxies (e.g. Kormendy and Richstone, 1995), a plethora of evidence has accumulated to indicate the coevolution of galaxies and their embedded massive black holes (MBHs). The observed tight correlation between MBH masses and bulge velocity dispersions (Ferrarese and Merritt, 2000; Gebhardt et al., 2000) have bolstered the idea that the fates of a host galaxy and its embedded MBH are fundamentally intertwined and heavily affected by each other's influence (Silk and Rees, 1998; Kauffmann and Haehnelt, 2000; Wyithe and Loeb, 2003).

Recent observations provide more solid constraints on the coevolution of galaxies and MBHs. For example, cosmological star formation history and black hole accretion history are measured to be proportional to each other (e.g. Zheng et al., 2009). Merging of galaxies is believed to induce quasar activity (e.g. Hopkins et al., 2008), and the existence of high-redshift quasars (Fan et al., 2006) indicate the rapid growth of black hole masses in the early phase of hierarchical structure formation, most likely by mergers (Haiman and Loeb, 2001). Unmistakably it is a complicated and highly nonlinear process for a galaxy to affect its embedded MBH, and vice versa. Therefore, developing a numerical tool which incorporates both galaxies and MBHs in one self-consistent framework is indispensible to fully comprehend their coevolution.

The seminal work by Springel et al. (2005b) to include accretion and feedback of a MBH in a galactic simulation has been followed by many detailed investigations. These studies have helped extend our understanding of galaxy - MBH interaction in various contexts and scales: (a) Merging of Milky Way sized galaxies was simulated to show that quasar-like MBH feedback drives a massive gas outflow leading to quenched star formation, and to the observed $M_{\rm BH} - \sigma_{\rm bulge}$ relation (Springel et al., 2005a,b; Di Matteo et al., 2005; Johansson et al., 2009). (b) Successive mergers of galaxies and MBHs were performed in a cosmological volume to yield a viable route to form high-redshift quasars (Li et al., 2007b; Sijacki et al., 2009). (c) MBH feedback at the center of a galaxy cluster was demonstrated to release sufficient energy to stop an overly cooled inflow of gas (Sijacki et al., 2007; Booth and Schaye, 2009; Teyssier et al., 2010b; Dubois et al., 2010).

2.1.2 State of the Field and Scientific Motivation

Nonetheless, a comprehensive numerical understanding which incorporates both galaxies and MBHs is still missing, for various reasons. First and foremost, simulated galaxies do not match some of the most obvious aspects of observed galaxies. For example, simulated galaxies are prone to lock baryons into too many stars (Guo et al., 2010, and references therein), or contain bulge-dominated disks that are too centrally concentrated and have a greatly reduced angular momentum relative to those observed (van den Bosch, 2001; Kaufmann et al., 2007a; Piontek and Steinmetz, 2009a). These problems are somewhat alleviated by lowering star formation efficiency and/or increasing stellar feedback (Governato et al., 2007; Piontek and Steinmetz, 2009b; Agertz et al., 2011), or even by introducing a new powerful energy source such as MBH feedback. However, the former fix has not been entirely successful even with varied feedback parameters while the latter almost always powers large-scale gas outflow leaving behind a "red and dead" galaxy devoid of gas for a long time (Borgani et al., 2004; Kravtsov et al., 2005; Springel et al., 2005b; Teyssier et al., 2010b). Obviously numerical simulations are still missing one or more essential ingredients. It could be the ignored physical processes such as stellar UV radiation and magnetic fields. Or it could be the inaccurate descriptions of MBH accretion and feedback.

Second, most numerical studies to date lack necessary resolution and technique to describe how gas falls onto a central MBH and how the energy input of MBH feedback is deposited to its surrounding gas. While the 1 - 100 kpc resolution in large-scale simulations is clearly insufficient to adequately describe the accretion flow onto a MBH, even galactic scale simulations do not generally resolve the Bondi radius (See §2.2.6; Eq.(2.10)), which is required in order to trace how a MBH gravitationally influences its surroundings and how the radiation and outflows from the MBH are thermally coupled to the gas. Indeed, poor resolution has forced simulators to skip the thermalization process below the resolution limit, and to simply thermodynamically deposit MBH feedback energy near the MBH. While crude, it has been an effective approximation characterizing MBH feedback on a resolved scale (Springel et al., 2005b). And it might be a fairly reasonable choice if MBH feedback is powerful enough to drive thermal shock waves (so-called "quasar-mode"; $\dot{M}_{\rm BH} > 0.02\,\dot{M}_{\rm Edd}$). However, it can not adequately describe the energy coupling of the radiation from a weak, quiescent MBH ("radio-mode"; $\dot{M}_{\rm BH} < 0.02\,\dot{M}_{\rm Edd}$; Croton et al., 2006; McNamara and Nulsen, 2007). For this reason injecting thermal energy in a small volume of poorly resolved interstellar medium (ISM) can hardly be an accurate description of MBH feedback (See §2.2.6 for detailed discussion). Modeling how MBH feedback energy is *actually* coupled to the gas is a critical missing piece in contemporary galaxy formation simulations.

Third, partly due to the lack of proper resolution, most numerical calculations to date have modeled stars and MBHs with phenomenologically parametrized *ad hoc* formulations. Most notably, the Eddington-limited Bondi-Hoyle accretion estimate employed by many authors (e.g. Springel et al., 2005b; Di Matteo et al., 2005; Johansson et al., 2009, See §2.2.6 for definitions of variables) has had to be empirically boosted by an efficiency parameter α =10 - 300.

$$\dot{M}_{\rm BH} = \texttt{min}\left(\frac{4\pi\alpha G^2 M_{\rm BH}^2 \rho_{\rm B}}{c_{\rm s}^3}\ ,\ \frac{4\pi G M_{\rm BH} m_{\rm p}}{\epsilon_{\rm r}\sigma_{\rm T} c}\right). \tag{2.1}$$

While this nondimensional boost factor α is to correct the large-scale averaged, and probably underestimated $\rho_{\rm B}$ near the MBH, α is typically fixed after the MBH has grown so the Bondi radius is resolved even with coarse resolution.[1] Another example of introducing tunable parameters based on unknown physics is to use two different implementations of MBH feedback, depending on the estimated accretion rate: quasar-mode feedback and radio-mode feedback (Sijacki et al., 2007; Puchwein et al., 2008). While useful in some applications, these *ad hoc* approaches ironically demonstrate that the physics of MBHs has not yet been adequately described in simulations.

[1]See Johansson et al. (2009) or Booth and Schaye (2009) for more discussion. Attempts have also been made to entirely avoid using Bondi-Hoyle estimation (DeBuhr et al., 2010; Hopkins and Quataert, 2010; Power et al., 2010)

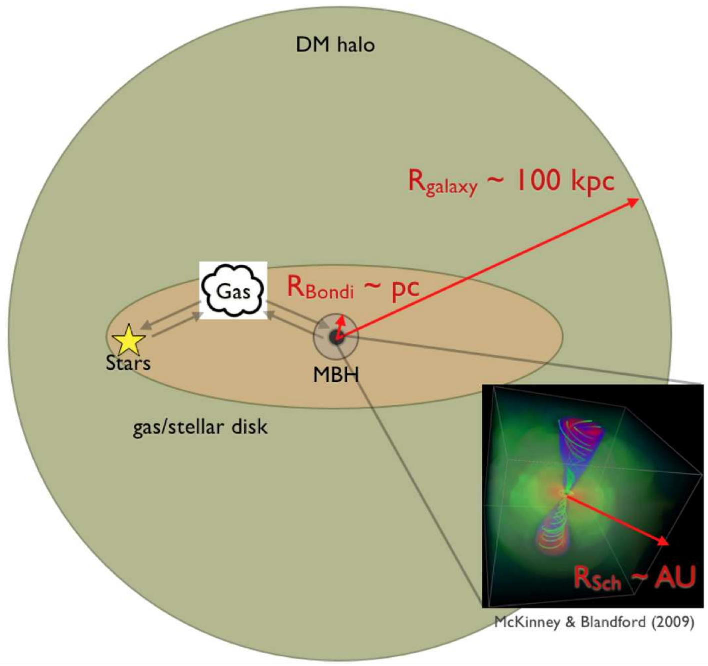

Fig. 2.1.— Schematic illustration of the scales in galaxy - massive black hole (MBH) coevolution picture. While the typical dynamical scale of galaxies is ~ 100 kpc, star cluster formation on the gas disk or Bondi accretion (Bondi, 1952) onto the MBHs must be described at ~ 1 pc scale. Further, the energy of the MBH is extracted via Blandford and Znajek (1977) mechanism at the scale of $\sim$ AU. Massively different dynamic scales involved in this picture makes the computational approach to this problem uniquely challenging. The picture in the inset illustrates the relativistic jets calculated by general relativistic magnetohydrodynamics (GRMHD) simulations. Adapted from Figure 1 of (McKinney and Blandford, 2009).

In order to circumvent the limitations of previous approaches outlined above and to follow the actual physical processes between gas, stars, and MBHs, we develop a *fully self-consistent* galaxy formation simulation integrating the growths of both galaxies and MBHs in one comprehensive framework. We limit the use of *ad hoc* formulation but instead more accurately model the physics in all aspects of galaxy formation, namely: (a) molecular cloud formation, (b) stellar feedback, (c) MBH accretion, and (d) MBH feedback. Our code models the formation and feedback of molecular clouds at their characteristic scale of 15.2 pc (§2.2.4 to 2.2.5) and the accretion of gas onto a MBH (§2.2.6). Two major channels of MBH feedback are also considered: radiative feedback (monochromatic X-ray photons followed through full three dimensional adaptive ray tracing; §2.2.7) and mechanical feedback (bipolar jets resolved in high-resolution adaptive mesh; §2.2.8).

2.2 Modeling the Physics of Galaxy Formation

The high-resolution Eulerian adaptive mesh refinement (AMR) code *Enzo-2.0* (http://enzo.googlecod Bryan and Norman, 1997; Norman and Bryan, 1999; Bryan et al., 2001; O'Shea et al., 2004; Norman et al., 2007) captures the gravitational collapse of turbulent fragmentation with high spatial resolution (Wise and Abel, 2007; Wise et al., 2008; Turk et al., 2009) and attains multiphase gas dynamics in the ISM as it sharply resolves shocks and phase boundaries (Slyz et al., 2005; Agertz et al., 2007; Tasker et al., 2008). Our enhanced version of *Enzo* contains all relevant features previously discussed in simulating galaxy evolution (Tasker and Bryan, 2006, 2008; Kim et al., 2008, 2009) as well as a treatment of several new physical processes discussed in detail in the following sections.

2.2.1 Hydrodynamics and Gravitational Dynamics

The ZEUS astrophysical hydrodynamics module included in *Enzo* is employed to solve the Euler equations for the collisional baryon fluid represented by grids (Stone and Norman, 1992a,b; Anninos and Norman, 1994). While known to introduce spurious effects, this scheme is widely used with AMR because of the stability of its solutions, and the acceptable error when combined with high resolution.

Dark matter, stars, and MBHs are treated as collisionless particles which interact only by the gravitational force. To evolve the particle positions and velocities, the gravitational dynamics are solved by an N-body adaptive particle-mesh solver. After particles are gridded onto the mesh by the cloud-in-cell interpolation, the Poisson equation is solved on the discretized density grids via fast Fourier transform and multigrid solvers (Hockney and Eastwood, 1988; O'Shea et al., 2004).

2.2.2 Adaptive Mesh Refinement Strategy

Enzo decides whether each parent cell needs to be refined into eight child cells based on the mass of the cell in gas or in particles. The timestep is also adaptively determined level by level so that the timestep dt satisfies

$$dt \leq 0.3 \times \frac{\Delta x}{c_{\rm s}} = 0.3 \times (\text{sound crossing time}) \tag{2.2}$$

for all the cells at that level. Here $c_{\rm s}$ is the sound speed of the gas, and we choose the Courant-Friedrichs-Lewy (CFL) safety number of 0.3. As decisions for refinement are made recursively, the resulting dataset is a nested grid-patch structure. In our work, the grids are adaptively refined down to 15.2 pc resolution. This value is in accord with the Jeans length for a dense gas clump of $n = 125$ cm^{-3} at $\sim$200 K, at which point a corresponding Jeans mass of 16000 $M_\odot$ collapses to spawn a molecular cloud particle.

We refine the cells by factors of 2 in each axis, on gas and particle overdensities of 8. The mass thresholds, $M_{\rm ref}$, above which a cell refines are functions of a refinement level l as

$$M^l_{\rm ref,gas} = 2^{-0.378l} M^0_{\rm ref,gas} = 2^{-0.378l} \cdot 0.125 \Omega_{\rm b} \rho_0 \Delta x^3 \tag{2.3}$$
$$M^l_{\rm ref,part} = 2^{-0.105l} M^0_{\rm ref,part} = 2^{-0.105l} \cdot 0.125 \Omega_{\rm m} \rho_0 \Delta x^3 \tag{2.4}$$

where factors $0.125 = 8(1/2^3)^2$ guarantees to refine all the cells of the first two nested levels (§3.1.1). Δx is the cell size at a root grid, and $\rho_0 = 3H^2/8\pi G$ is the critical density. $\Omega_{\rm m} = 0.27$, $\Omega_{\rm b} = 0.044$, and $H = 71\,{\rm km\ s^{-1} Mpc^{-1}}$ are matter density, baryon density, and the Hubble constant, respectively.

For example, at the finest static level, $l = 2$, a cell is refined if it has more mass than $8.9 \times 10^5 M_\odot$ in gas or $6.7 \times 10^6 M_\odot$ in particles. At level $l = 11$ ($\Delta x = 15.2$ pc at $z = 3$) a cell is refined if more than $8.4 \times 10^4\ M_\odot = 5\ M_{\rm Jeans}(125\ {\rm cm^{-3}}, 200\ {\rm K})$ in gas or $3.5 \times 10^6\ M_\odot = 47\ M_{\rm DM,smallest}$ in particles. This way we refine the grids more on small scales, which allows us to focus our computational resources more on the dense star forming regions, making the simulation super-Lagrangian (O'Shea and Norman, 2008).

2.2.3 Chemistry and Radiative Cooling

We use non-equilibrium chemistry model to track six species (H, H^+, He, He^+, He^{++}, e^-) by following six collisional processes among them. At the same time, *Enzo*'s cooling module considers collisional excitation cooling, collisional ionization cooling, recombination cooling, Bremsstrahlung cooling, and CMB Compton cooling to compute the radiative loss of internal gas energy (Anninos et al., 1997; Abel et al., 1997). Added to these primordial cooling rates is the metallicity-dependent metal cooling rate $\Delta\Lambda(Z) = \Lambda_{\rm net}(Z) - \Lambda_{\rm net}(0)$ above 10^4 K, where $\Lambda_{\rm net}$ is the net cooling rate tabulated in Sutherland and Dopita (1993). Cooling below 10^4 K is also enabled with fine structure metal-line cooling by C, O, and Si (Glover and Jappsen, 2007; Wise and Abel, 2008). This treatment ensures that a thin galactic disk forms by being cooled below 10^4 K, the approximate virial temperature of the ISM in a galactic disk.

We further refine our module with photoionization heating at $z < 3$ by the metagalactic background UV of quasars and galaxies (Haardt and Madau, 1996, 2001), which is known to give rise to a warm diffuse ISM and prevent star formation in optically thin gas (Ceverino and Klypin, 2009). An approximate self-shielding factor is applied when the heating term is added (Cen et al., 2005). While not introducing a marked difference in overall results analyzed here, inclusion of this additional heating term results in a more realistic interstellar medium.

2.2.4 Molecular Cloud Formation

Our *molecular cloud* particle formation is based on Cen and Ostriker (1992) formalism with several important modifications. With a fixed formation efficiency of $\epsilon_* = 0.5$, the finest cell of physical size $\Delta x = 15.2$ pc and gas density $\rho_{\rm gas}$ produces a molecular cloud particle of mass

$$M_{\rm MC} = \epsilon_* \rho_{\rm gas} \Delta x^3 \tag{2.5}$$

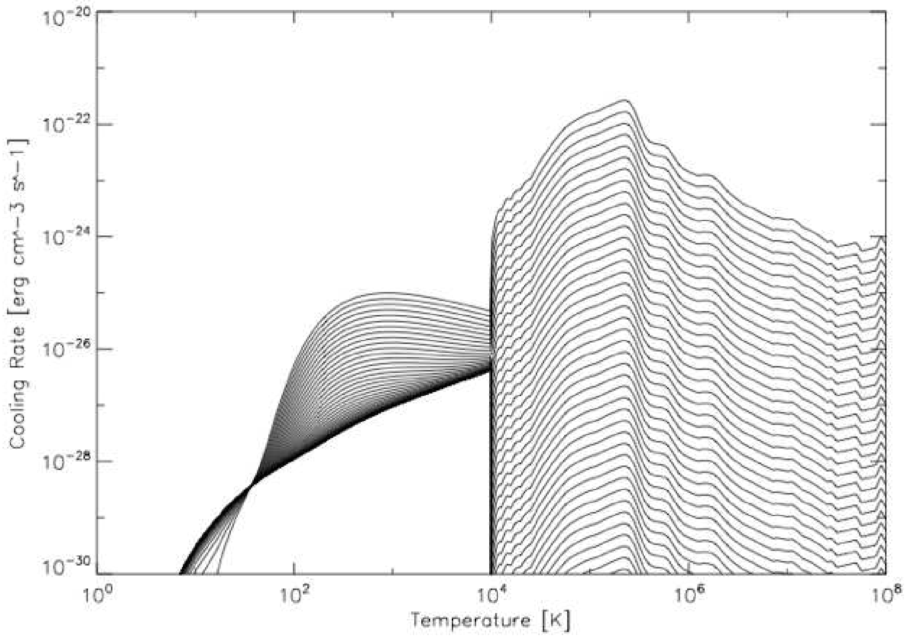

Fig. 2.2.— Metal cooling rates with temperature and electron fraction dependences normalized at $Z = 0.1 Z_\odot$. Shown above 10^4 K is $\Delta\Lambda(Z) = \Lambda_{\rm net}(Z) - \Lambda_{\rm net}(0)$, where $\Lambda_{\rm net}$ is the net cooling rate tabulated in Sutherland and Dopita (1993). Cooling below 10^4 K is by fine structure metal-lines of carbon, oxygen, and silicon (Glover and Jappsen, 2007). Note that this cooling rate is added to the primordial cooling by hydrogen and helium. Compare with Figure 1.1.

when the following four criteria are met:

(a) the proton number density exceeds the threshold $n_{\rm thres} = 125$ cm^{-3},

(b) the velocity flow is converging; i.e. $\nabla \cdot \mathbf{v} < 0$,

(c) the cooling time $t_{\rm cool}$ is shorter than the dynamical time $t_{\rm dyn}$ of the cell: $E_{\rm int}/\dot{E} < [3\pi/(32 G \rho_{\rm gas})]^{1/2}$, and

(d) the particle produced has at least $M_{\rm thres} = 8000\ M_\odot$.

The consequence of our criteria is the following. The gas in the finest cell is converted into a particle as soon as the cell has accumulated more than $M_{\rm thres}/\epsilon_* = 16000\ M_\odot$, the Jeans mass at $n = 125$ cm^{-3} at $\sim$200 K. Because 8000 - 42000 $M_\odot$ is instantly

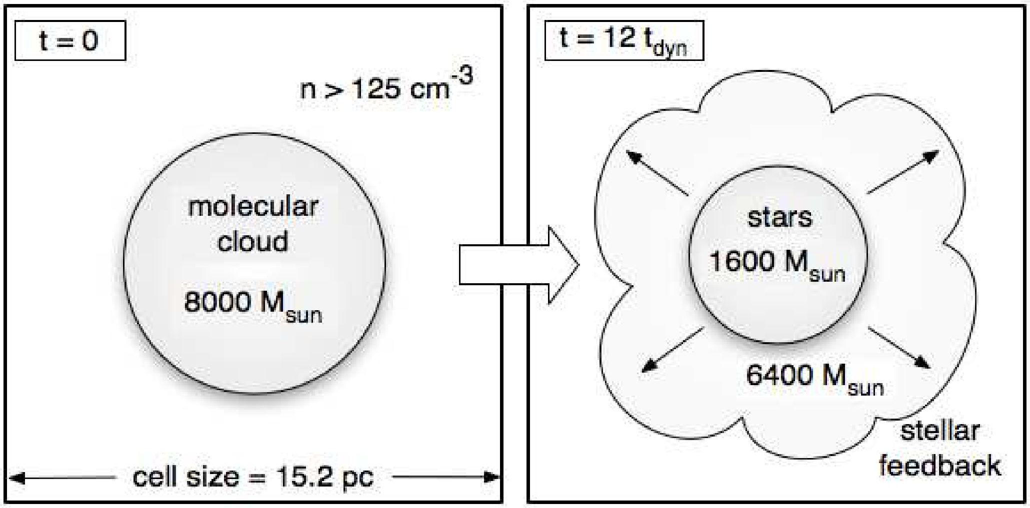

Fig. 2.3.— A schematic view of the molecular cloud formation and the stellar feedback. $12\,t_{\rm dyn}$ after a molecular cloud particle ($M_{\rm MC} \simeq 8000\ M_\odot$) is formed, only 20% of its mass remains as an actual stellar mass $M_{\rm star}(t)$ while the rest 80% has returned to the gas along with thermal feedback energy.

removed from the cell every time a particle is created, the gas mass in the finest cell never reaches the refinement threshold $M^{l=11}_{\rm ref,gas} = 84000\ M_\odot$ described in §2.2.2, ensuring the consistency between the refinement criteria and the particle formation.[2] The values used here are in good agreement with those corresponding to collapsing Giant Molecular Clouds (GMC; McKee and Ostriker, 2007) where star-forming molecular clumps are enshrouded by cold atomic gas.

As an additional note, differences from more traditional star particle formation criteria such as in Tasker and Bryan (2008) include: (a) the Jeans condition $\rho_{\rm gas}\Delta x^3 > M_{\rm Jeans}$ is removed because this condition could have allowed mass greater than $M_{\rm Jeans}$ to accumulate while not being properly resolved until a particle finally forms, (b) the factor $\Delta t/t_{\rm dyn}$ in Eq.(1) of Tasker and Bryan (2008) is removed in order to instantly create a particle and not leave any unresolved mass behind, and (c) stochastic star

[2]Readers should be cautioned that the mass resolution of the reported simulation is $84000\ M_\odot = 5\ M_{\rm Jeans}(125\ {\rm cm}^{-3}, 200\ {\rm K})$. Ideally, if one properly combines the refinement strategy and the molecular formation criteria, the local Jeans mass can be resolved this way without explicitly requiring it.

formation is not imposed.

With these modifications, our criteria guarantee that a particle forms before an unphysically large mass begins to accrete onto any unresolved dense clump. It is worth to emphasize the differences between our molecular cloud formation criteria and prior studies. While many previous studies with particle-based codes (e.g. Mihos et al., 1991; Katz, 1992; Mihos and Hernquist, 1994b; Springel and Hernquist, 2003a; Governato et al., 2007) place a star particle using the Schmidt relation ($\rho_{\rm SFR} \sim \rho_{\rm gas}^{1.5}$; Schmidt, 1959), we deposit a particle when a gas cell of a typical molecular cloud size actually becomes Jeans unstable. For this reason, the particle in our simulation represents a *star-forming molecular cloud* that is self-gravitating, is thus decoupled from the gas on the grid.[3] It is tagged with its mass $M_{\rm MC}$, dynamical time $t_{\rm dyn} = \texttt{max}([3\pi/(32G\rho_{\rm gas})]^{1/2}, 1.0 \text{ Myr})$, creation time $t_{\rm cr}$, and metallicity. Each molecular cloud particle gradually yields an *actual* stellar mass, $M_{\rm star}(t)$, over 12 $t_{\rm dyn}$ which then contributes to stellar feedback (See Figure 2.3 and §2.2.5).

2.2.5 Stellar Feedback

Observational evidence suggests that only $\sim 2\%$ of the gas in GMCs is converted into stars per dynamical time (Krumholz and McKee, 2005; Krumholz and Tan, 2007, and references therein). Numerical studies also indicate that turbulence, magnetic fields, or radiation pressure can make the star formation process surprisingly slow (e.g. Murray et al., 2010; Wang et al., 2010). To reflect these observations in our simulation, only 20% of the molecular cloud particle mass, $M_{\rm MC}$, turns into an actual stellar mass, $M_{\rm star}(t)$, over 12 $t_{\rm dyn}$ by

$$M_{\rm star}(t) = 0.2\, M_{\rm MC} \int_0^{\tau} \tau' e^{-\tau'}\, d\tau' \qquad (2.6)$$

$$= 0.2\, M_{\rm MC} \left[1 - (1+\tau)e^{-\tau}\right], \qquad (2.7)$$

[3] We point out that the usual terminology of *star particle* to represent $10^5 - 10^6 M_\odot$ has been a misnomer. We therefore make each of our particles to be 8000 $M_\odot$, regarding it as a molecular cloud gradually spawning stellar mass in it. These particles are still collisionless and do not fully represent the real nature of molecular clouds. However, we emphasize that our molecular cloud particles harbor a slow star formation rate matching observations.

where $\tau = (t - t_{\rm cr})/t_{\rm dyn}$. In this formulation, the production of the stellar mass peaks at $t_{\rm dyn}$. As 7.5×10^{-7} of the rest mass energy of $M_{\rm star}$ is gradually deposited into the cell in which the particle resides,[4] this thermal stellar feedback replenishes the energy loss to radiative cooling. At the same time, the rest of the molecular cloud particle mass, $0.8\, M_{\rm MC}$, slowly returns to the gas grid. This again reflects the fact that most of the gas in GMCs does not end up locked in stars in a few dynamical time, but is blown out into the ISM to be recycled. Meanwhile, 2% of the ejected mass is counted as metals, contributing to the metal enrichment of the ISM (See Figure 2.3).

Overall, our feedback treatment corresponds to the energy of 10^{51} ergs for every 750 $M_\odot$ of actual stellar mass formed. Although Type II supernovae explosions are its dominant source (Spitzer, 1990; Tasker and Bryan, 2006, 2008), this feedback also models various other types such as protostellar outflows (Li and Nakamura, 2006; Nakamura and Li, 2008), photoionization (McKee, 1989), and stellar winds (Oey et al., 2001). Therefore no explicit time delay is necessary between the formation of a molecular cloud and the start of stellar feedback. This thermal feedback heats the mass of $\sim 10^4 M_\odot$ in a < 30 pc cell up to $\sim 10^7$ K, but a multiphase medium (McKee and Ostriker, 1977) is naturally established without using any sub-resolution model. The so-called overcooling problem (Somerville and Primack, 1999; Balogh et al., 2001) is absent in our simulation since the cooling time of these hot cells is much longer than the sound crossing time (Kim et al., 2009).

2.2.6 Accreting Massive Black Hole (MBH)

A $10^5 M_\odot$ massive black hole (MBH) is put as a seed at the center of each simulated galaxy. It is treated as a collisionless sink particle, but grows in mass by accreting gas

[4] Assuming the Salpeter initial mass function $dn/dM \propto (M/M_\odot)^{-2.3}$ in a star cluster (Salpeter, 1955), the fractional mass which ends as Type II supernova (SNII, $> 9\ M_\odot$) is 1.2%. Thus, fixing the mass of each SNII to be 9 $M_\odot$ we inject 10^{51}ergs per 9 $M_\odot/1.2\% = 750\ M_\odot$ of the stellar mass formed. This ratio 10^{51}ergs / 750 $M_\odot = 1.3 \times 10^{48}$ ergs $M_\odot^{-1}$ equals to 7.5×10^{-7} of the stellar rest mass energy.

from its surroundings. We estimate the rate of accretion by employing the Eddington-limited spherical Bondi-Hoyle formula (Bondi and Hoyle, 1944; Bondi, 1952):

$$\dot{M}_{\rm BH} = \texttt{min}(\dot{M}_{\rm B}\,,\, \dot{M}_{\rm Edd}) \tag{2.8}$$

$$= \texttt{min}\left(\frac{4\pi G^2 M_{\rm BH}^2 \rho_{\rm B}}{c_{\rm s}^3}\,,\, \frac{4\pi G M_{\rm BH} m_{\rm p}}{\epsilon_{\rm r}\sigma_{\rm T} c}\right), \tag{2.9}$$

where $M_{\rm BH}$ is the mass of a MBH, $c_{\rm s}$ is the sound speed of the gas at the cell the MBH resides in, $m_{\rm p}$ is the mass of a proton, and $\sigma_{\rm T}$ is the Thomson scattering cross-section. Note that, when compared with Eq.(2.1) the nondimensional parameter α is absent. $\rho_{\rm B}$ is the density at the Bondi radius

$$R_{\rm B} = \frac{2GM_{\rm BH}}{c_{\rm s}^2} \simeq 8.6 \text{ pc}\left(\frac{M_{\rm BH}}{10^5 M_\odot}\right)\left(\frac{10\,\rm km/s}{c_{\rm s}}\right)^2, \tag{2.10}$$

and is extrapolated from the density $\rho_{\rm gas}$ of the cell of size Δx where the MBH resides by

$$\rho_{\rm B} = \rho_{\rm gas} \cdot \texttt{min}((\Delta x/R_{\rm B})^{1.5}, 1.0) < \rho_{\rm gas}. \tag{2.11}$$

Here an $r^{-3/2}$ density profile is assumed inside the sphere of $R_{\rm B}$ (Wang et al., 2010). Adopting a radiative efficiency $\epsilon_{\rm r} = 0.1$ for a non-rotating Schwarzschild black hole (Shakura and Sunyaev, 1973; Booth and Schaye, 2009), the Eddington rate for a $10^5 M_\odot$ black hole is $\simeq 0.002\ M_\odot\,{\rm yr}^{-1}$.[5] To minimize any numerical artifacts, the gas mass accreting onto the MBH is uniformly subtracted from grid cells within a Bondi

[5] The Bondi accretion rate estimate at the molecular cloud formation threshold $n = n_{\rm thres} = 125\,{\rm cm}^{-3}$ and $c_{\rm s} = 10\ {\rm km\,s}^{-1}$ is

$$\dot{M}_{\rm B} \simeq 0.004\ (M_{\rm BH}/10^5 M_\odot)^2\ M_\odot\,{\rm yr}^{-1}, \tag{2.12}$$

bigger than the Eddington rate,

$$\dot{M}_{\rm Edd} \simeq 0.002\ (M_{\rm BH}/10^5 M_\odot)\ M_\odot\,{\rm yr}^{-1}. \tag{2.13}$$

Therefore the density threshold for molecular cloud formation does not limit the accretion rate at any time. To put it in another way, because the Bondi accretion rate can surpass the Eddington rate in dense clumps of $n \sim n_{\rm thres}$, the Eddington limit should play a crucial role in restricting the accretion.

radius. The MBH also inherits the momentum of the accreting gas.

Most importantly, to probe the gas dynamics accreting onto the MBH and to fully incorporate the MBH in a galactic simulation, it is imperative to always reach the resolution close to the Bondi radius around the MBH. To resolve the gas around the MBH with the best resolution available, eight nearby cells close to the MBH are required to successively refine down to 15.2 pc (proper) at all times. In practice, the MBH naturally sits at the densest region most of the time, surrounded by many finest cells. While our spatial resolution is still slightly too large to resolve the Bondi radius of a $10^5 M_\odot$ black hole, Eq.(2.10), it is enough to resolve the Bondi radii of more massive MBHs such as in nearby X-ray luminous galaxies (e.g. $\sim 120\,\mathrm{pc}$ for SMBH in M87; Allen et al., 2006). This shows that our simulations are beginning to depict the self-consistent coevolution of both galaxies and MBHs in one comprehensive framework. Admittedly, this resolution is still far from the Schwarzschild radius of any black hole

$$R_{\rm Sch} = \frac{2GM_{\rm BH}}{c^2} \;\simeq\; 10^{-8}\,{\rm pc}\left(\frac{M_{\rm BH}}{10^5 M_\odot}\right), \tag{2.14}$$

which is needed to thoroughly describe its accretion disk. Due to our resolution limit, a MBH particle in our framework represents not just the black hole itself, but also includes accreting gas and stars deep within the galactic nucleus; in other words, the Bondi-Hoyle accretion estimate does not accurately model the physics below the resolution limit (See §6.2).

We note that, even without the aid of the boost factor (unlike in Eq.(2.1)), the Bondi estimate in our simulations can surpass the Eddington limit, and averages at 0.2 - 0.6 $\dot{M}_{\rm Edd}$ in the reported simulation (See §3.2.4). In other words, had we used the boost factor the Bondi estimate would have been almost always limited by the Eddington limit. It is partly because the gas density in our simulations reaches up to $n = n_{\rm thres}$ in the finest cells. It also justifies our choice of not employing the boost factor which has been common in the previous work. However, the omission of the usual boost factor does *not* indicate that our calculation can capture the turbulent accreting flow around the MBH accretion disk. No contemporary galactic scale simulation - including the reported simulation - has ever captured the turbulent interstellar medium well below the typical resolution limit. Hence many other models for the accretion estimate are equally applicable in galactic scale simulations, including the Bondi formula with a boost factor parametrized by the gas density (e.g. Booth and Schaye, 2009).

2.2.7 Massive Black Hole Radiative Feedback

We now turn our attention to the feedback of an accreting massive black hole. The gravitational potential energy of the gas accreting onto a black hole is extracted during the gravitational infall. Assuming an infall down to the innermost stable orbit of an accretion disk, the conversion rate from the rest mass energy to feedback energy is 10%, previously defined as the radiative efficiency $\epsilon_{\rm r}$. Hence the bolometric radiation luminosity of a MBH is

$$L_{\rm BH} = \epsilon_{\rm r} \dot{M}_{\rm BH} c^2. \tag{2.15}$$

As was discussed earlier, for a long time a *thermal* energy deposition has been the dominant strategy to treat the feedback of an accreting MBH (Springel et al., 2005b; Di Matteo et al., 2005; Colberg and Di Matteo, 2008; Booth and Schaye, 2009; Callegari et al., 2010; Teyssier et al., 2010b, See Sijacki et al. (2008) or DeBuhr et al. (2010) for other approaches). Without question, it has been an effective approximation characterizing the impact of an accreting MBH on a resolved scale when sufficient resolution or full radiative transfer is inaccessible (See Figure 2.4(C); Springel et al., 2005b). Despite its practical efficiency, however, better feedback models are imperative for high-resolution galaxy formation studies where the Bondi radius is starting to be resolved. In the next two sections, we explain the detailed implementations of two modes of MBH feedback: radiative and mechanical. The thermal feedback model previously used can be regarded as an approximation of these two feedback channels combined.

Although the radiation from the MBH in a galaxy was tested in spherically symmetric or axisymmetric models (Ciotti and Ostriker, 2007; Proga et al., 2008; Ciotti et al., 2009; Kurosawa et al., 2009; Park and Ricotti, 2010), a three dimensional radiative transfer calculation of the impact of a MBH has never been performed in galactic scale simulations. In what follows, we treat the MBH as a point source of radiation and carry out a three dimensional transport computation to evolve the radiation fields (See Figure 2.4(A); note that molecular cloud particles are not treated as radiation

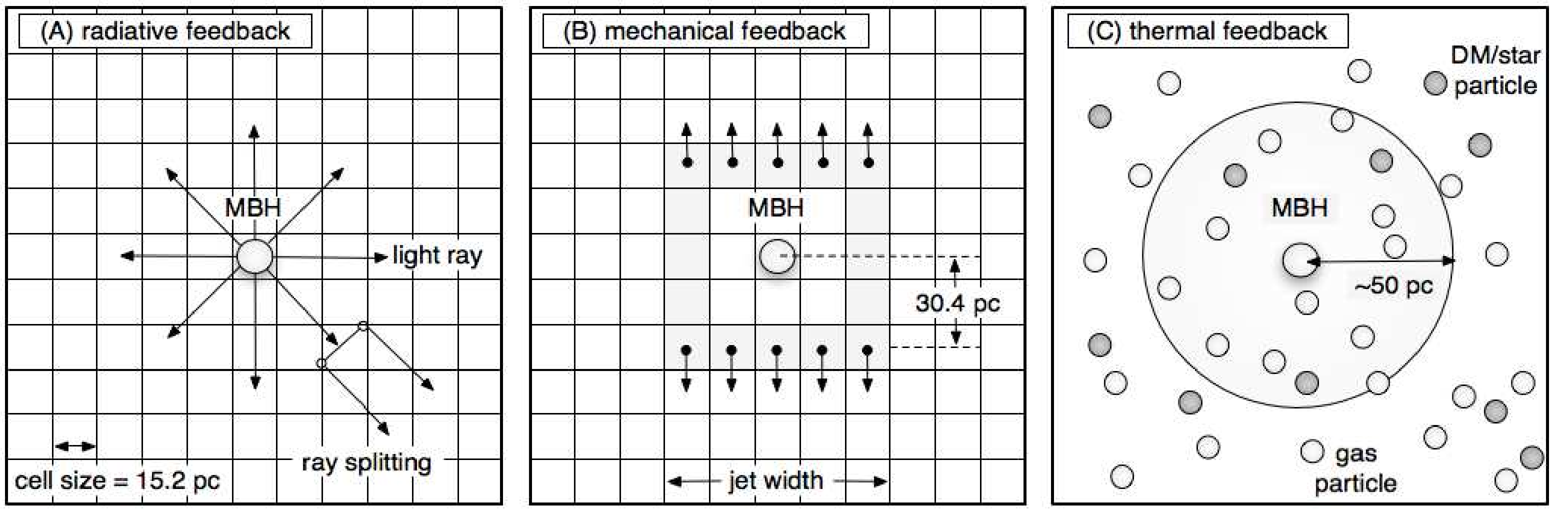

Fig. 2.4.— Two dimensional schematic views of the different modes of massive black hole feedback. (A) radiative feedback model described in §2.2.7: photon rays carrying the energy are adaptively traced via full radiative transfer, (B) mechanical feedback model described in §2.2.8: a momentum is injected to the cells around the MBH along pre-calculated directions, and (C) thermal feedback model predominantly used in particle-based galactic scale simulations: thermal energy is kernel-weighted to the neighboring gas particles around the MBH.

sources). Achieving high resolution around the MBH is critical here because, if otherwise, the optical depth of the radiation could be small even at the smallest resolved distance from the MBH (Omma et al., 2004).

Enzo's radiative transfer module incorporates the adaptive ray tracing technique (Abel and Wandelt, 2002) with the hydrodynamics, energy, and chemistry solvers. It has been applied to problems such as the radiative feedback from Pop III stars (Abel et al., 2007; Wise and Abel, 2008; Wise et al., 2010) and from Pop III black holes (Alvarez et al., 2009). For algorithmic and numerical details of *Enzo* radiative transfer we refer the readers to Wise and Abel (2010)[6]; and, here we briefly describe the machinery relevant to the presented results. First the luminosity of the MBH is assigned by Eq.(2.15). Then 768 ($= 12 \times 4^3$; *Healpix* level 3) rays are isotropically cast with a monochromatic energy of $E_{\rm ph} = 2$ keV, a characteristic temperature of an averaged quasar spectral energy distribution (SED; Sazonov et al., 2004, 2005; Ciotti and Ostriker, 2007).[7] Consequently the number of photons per each initial ray is

$$P_{\rm init} = \frac{L_{\rm BH}\, dt_{\rm ph}}{E_{\rm ph} \cdot 768} = \frac{\epsilon_{\rm r}(\dot{M}_{\rm BH} dt_{\rm ph})c^2}{E_{\rm ph} \cdot 768} \tag{2.16}$$

given the photon timestep $dt_{\rm ph}$ which we set as the the light-crossing time of the entire computational domain. This choice is justified because the photons are in a free streaming regime, and the energy deposited by the radiation per timestep is relatively small. Each ray is traced at speed c until the ray reaches the edge of the computational domain or most of its photons (99.99995%) are absorbed. It is adaptively split into four child rays whenever the area associated with a ray becomes larger than $0.2\,(\Delta x)^2$ of a local cell.

[6]Aimed to be the primary reference for the Enzo radiative transfer module, Wise and Abel (2010) carefully details the Enzo radiative transfer machinery both physically and algorithmically, encompassing the implemented physics relevant to many applications including MBH radiation.

[7] A characteristic temperature of the quasar SED is estimated by equating Compton heating and Compton cooling by the given SED (Sazonov et al., 2004). Therefore it can be considered as the temperature of a Comptonized hot plasma in the vicinity of the MBH, which is represented by our MBH particle resolved only by 15.2 pc. Note, however, that the choice of the monochromatic photon energy, $E_{\rm ph}$, does not change the total luminosity of the MBH, nor does it greatly affect the nonrelativistic Klein-Nishina cross section for Compton scattering, $\sigma_{\rm KN}$, in the regime of $E_{\rm ph} \ll m_{\rm e}c^2$.

Table 2.1 Simulation Suite Description

Physics[a]		Sim-SF	Sim-RF	Sim-MF	Sim-RMF
Molecular cloud formation	(See §2.2.4)	○	○	○	○
Stellar feedback	(See §2.2.5)	○	○	○	○
MBH accretion	(See §2.2.6)	○	○	○	○
MBH radiative feedback	(See §2.2.7)	×	○	×	○
MBH mechanical feedback	(See §2.2.8)	×	×	○	○

[a]For detailed explanation, see the referenced section. ∘ = included, × = not included.
[a]For detailed explanation, see the referenced section. ∘ = included, × = not included.

Photons in the emitted ray then interact with the surrounding gas in three ways: they (1) ionize the gas, (2) heat the gas, and (3) exert momentum onto the gas. First, the ray loses its photons when it photoionizes H, He, and He^+ with the respective *photoionization* rates of

$$k_{\rm ph,H} = \frac{P_{\rm \,in}(1-e^{-\tau_{\rm H}})(E_{\rm ph}Y_{k,{\rm H}}/E_{i,{\rm H}})}{n_{\rm H}(\Delta x)^3 dt_{\rm ph}} \tag{2.17}$$

$$k_{\rm ph,He} = \frac{P_{\rm \,in}(1-e^{-\tau_{\rm He}})(E_{\rm ph}Y_{k,{\rm He}}/E_{i,{\rm He}})}{n_{\rm He}(\Delta x)^3 dt_{\rm ph}} \tag{2.18}$$

$$k_{\rm ph,He^+} = \frac{P_{\rm \,in}(1-e^{-\tau_{\rm He^+}})}{n_{\rm He^+}(\Delta x)^3 dt_{\rm ph}} \tag{2.19}$$

where $P_{\rm \,in}$ is the number of photons coming into the cell, $\tau_{\rm H} = n_{\rm H}\sigma_{\rm H}dl$ is the optical depth, $n_{\rm H}$ is the hydrogen number density, $\sigma_{\rm H}$ is the energy-dependent hydrogen photoionization cross-section (Verner et al., 1996), dl is the path length through the cell, and $E_i = 13.6,\ 24.6,\ 54.4\,{\rm eV}$ are the ionization thresholds for H, He, He^+, respectively. The factors Y_k are the energy fractions used for ionization when secondary ionizations are considered (Shull and van Steenberg, 1985).[8]

Second, the excess energy above the ionization threshold, E_i, heats each of the

[8]$Y_{k,{\rm H}} = 0.3908(1-x^{0.4092})^{1.7592}$ and $Y_{k,{\rm He}} = 0.0554(1-x^{0.4614})^{1.6660}$ are fitted as a function of an ionization fraction $x = n_{\rm H^+}/n_{\rm H,tot} \simeq n_{\rm He^+}/n_{\rm He,tot}$; the effect of secondary ionizations on He^+ can be ignored.

species with the *photoheating* rates of

$$\Gamma_{\rm H} = \frac{P_{\rm in}(1 - e^{-\tau_{\rm H}})E_{\rm ph}Y_{\Gamma}}{n_{\rm H}(\Delta x)^3 dt_{\rm ph}}, \quad \text{etc.} \tag{2.20}$$

where Y_Γ is the fraction of energy deposited as heat when secondary ionizations are taken into account.[9] The 2 keV soft X-ray photon can also scatter off and heat an electron resulting in the *Compton heating* rate of

$$\Gamma_{\rm C} = \frac{P_{\rm in}(1 - e^{-\tau_{\rm e}})\Delta E(T_{\rm e})}{n_{\rm e}(\Delta x)^3 dt_{\rm ph}} \tag{2.21}$$

where $\tau_{\rm e} = n_{\rm e}\sigma_{\rm KN}dl$ is the optical depth, $n_{\rm e}$ is the electron number density, $\sigma_{\rm KN}$ is the nonrelativistic Klein-Nishina cross-section ($\simeq \sigma_{\rm T}$; Rybicki and Lightman, 1979), and $\Delta E(T_{\rm e}) = 4k_{\rm B}T_{\rm e} \cdot (E_{\rm ph}/m_{\rm e}c^2)$ is the nonrelativistically transferred energy to an electron at $T_{\rm e}$ (Ciotti and Ostriker, 2001). It should be noted that, in Compton scattering, a photon loses its energy by a factor of $\Delta E(T_{\rm e})/E_{\rm ph}$, but essentially keeps propagating without being absorbed. However, in order to model this with *monochromatic* photons, we instead subtract $P_{\rm in}(1 - e^{-\tau_{\rm e}})\Delta E(T_{\rm e})/E_{\rm ph}$ photons from the ray. This is another way a ray loses its photons while traveling through a cell. Combined, the total heating rate by absorbed and scattered photons becomes

$$\Upsilon = n_{\rm H}\Gamma_{\rm H} + n_{\rm He}\Gamma_{\rm He} + n_{\rm He^+}\Gamma_{\rm He^+} + n_{\rm e}\Gamma_{\rm C}\,. \tag{2.22}$$

Lastly, photons exert outward momentum to the gas when they are taken out from the ray either by photoionization or by Compton scattering. It was claimed that the *radiation pressure* from the MBH may markedly alter the environment near the MBH, especially within $\sim$ 0.1 kpc in radius (Haehnelt, 1995; DeBuhr et al., 2010). The large-scale galactic wind driven by deposited photon momentum is also considered as a possible explanation for the $M_{\rm BH} - \sigma_{\rm bulge}$ relation (Murray et al.,

[9] Note that $Y_\Gamma = 0.9971[1 - (1 - x^{0.2263})^{1.3163}]$ approaches 0 when the ionization fraction gets close to 0. In other words, when the ionization fraction is low photons are preferentially used to first ionize the gas rather than to heat the gas.

2005). The added acceleration onto the cell by the radiation pressure is calculated by

$$\mathbf{a}_{\rm ph} = \frac{d\mathbf{p}_{\rm ph}}{m_{\rm cell} dt_{\rm ph}} = \frac{P_{\rm lost} E_{\rm ph}}{\rho_{\rm gas} (\Delta x)^3 c dt_{\rm ph}} \hat{\mathbf{r}} \tag{2.23}$$

where $d\mathbf{p}_{\rm ph}$ is the photon momentum exerted onto the cell in $dt_{\rm ph}$, $P_{\rm lost}$ is the number of photons lost in the cell, and $\hat{\mathbf{r}}$ is the directional unit vector of the ray. Neglecting the radiation pressure on dust grains is conservative because its inclusion would further enhance the negative feedback effect (See §6.2).

2.2.8 Massive Black Hole Mechanical Feedback

Observations find that a significant portion of the energy extracted during the accretion onto a MBH is released as mechanical energy, creating bipolar jets (Bridle and Perley, 1984; Pounds et al., 2003) or inflating cavities (Fabian et al., 2002; McNamara et al., 2005) at the sites of active galactic nuclei (AGN). A number of authors have used a numerical approach to explore the effectiveness of jets in heating up a cooling flow (Fabian et al., 1994; Peterson and Fabian, 2006); most of them targeted the gas dynamics in galaxy clusters with $\sim$ kpc resolution excluding detailed galactic scale physics (e.g. Omma et al., 2004; Cattaneo and Teyssier, 2007; Antonuccio-Delogu and Silk, 2008; Dubois et al., 2010). In the meantime, a numerical analysis on stellar winds from nuclear disk or MBH jets has been carried out in a galactic scale, but only in an one dimensional context (Ciotti et al., 2009, 2010; Shin et al., 2010) Here, we construct a mechanical feedback model of a MBH applicable in three dimensional galactic simulations, which creates accretion-rate-dependent subrelativistic bipolar jets launched at the vicinity of the MBH (See Figure 2.4(B)).

Let us assume that all of the bolometric luminosity of the MBH, $L_{\rm BH}$, is converted to the "mechanical" power of jets. Because the ejecta has to climb out of the potential well of the MBH, the "kinetic" power of the jets is less than $L_{\rm BH}$ by

$$L_{\rm BH} = P_{\rm mech} \tag{2.24}$$

$$= P_{\rm kin} + (\text{gravitational potential energy}). \tag{2.25}$$

Therefore the "kinetic" power of the jets, as we introduce at a scale of $R_{\rm jet} = 2\Delta x = 30.4$ pc, can be written as

$$P_{\rm kin} = \epsilon_{\rm kin} L_{\rm BH} = \epsilon_{\rm kin}\epsilon_{\rm r}\dot{M}_{\rm BH}c^2 = \frac{1}{2}\dot{M}_{\rm jet}v_{\rm jet}^2, \tag{2.26}$$

where $\epsilon_{\rm kin} < 1$ is the "kinetic" coupling constant denoting the fractional energy available for the kinetic motion of the jets (See Figure 2.4(B)). $\dot{M}_{\rm jet}$ is the mass ejection rate of the jets, and $v_{\rm jet}$ is the jets velocity when introduced in the simulation. Hence $\epsilon_{\rm kin}$ encapsulates not only the acceleration of the jets powered by the AGN central engine, but also the gravitational "redshift" from the scale of an accretion disk ($\sim R_{\rm Sch}$) to a resolved scale of jets in simulations ($\sim R_{\rm jet}$). Ciotti et al. (2009) provides estimates for a MBH of $l = \dot{M}_{\rm BH}/\dot{M}_{\rm Edd} = 0.005$ as

$$\epsilon_{\rm kin} = \frac{P_{\rm kin}}{\epsilon_{\rm r}\dot{M}_{\rm BH}c^2} = \frac{0.0125}{\epsilon_{\rm r}(1+400l)^4} \simeq 0.0015 \tag{2.27}$$

$$\eta_{\rm jet} \equiv \frac{\dot{M}_{\rm jet}}{\dot{M}_{\rm BH}} = \frac{0.2}{(1+100l)^4} \simeq 0.04, \tag{2.28}$$

based on which we fiducially adopt conservative values of $\epsilon_{\rm kin} = 10^{-4}$ and $\eta_{\rm jet} = 0.05$.

With $\epsilon_{\rm kin}$ and $\eta_{\rm jet}$ now fixed, the kinetic motion of the jets can be fully described. First, as usual, out of a sphere of $R_{\rm B}$ centered on the MBH the accreting mass is taken out at every finest hydrodynamical timestep dt; then 5% of the accreted mass, $\dot{M}_{\rm jet}dt = 0.05\ \dot{M}_{\rm BH}dt$, is set aside as a mass of jets. Now Eq.(2.26) yields the initial jet momentum, $(\dot{M}_{\rm jet}dt)v_{\rm jet}$, with

$$v_{\rm jet} = c\left(\frac{2\epsilon_{\rm kin}\epsilon_{\rm r}}{\eta_{\rm jet}}\right)^{1/2} = 6000\ {\rm km\,s^{-1}} \tag{2.29}$$

for $\epsilon_{\rm r} = 0.1$. This value of $v_{\rm jet}$ is consistent with numerous observational evidence (e.g. Biretta and Junor, 1995; Junor et al., 1999; Homan et al., 2009) and relativistic MHD simulations (e.g. Vlahakis and Königl, 2003, 2004) suggesting the existence of at least mildly relativistic AGN jets on scales of 1 - 10 pc from a central engine. This $v_{\rm jet}$ is also well-matched with the velocity of momentum-driven AGN winds discussed by

King (2009). Finally the launch speed of the surrounding cells is found by averaging the momentum of jets and the preexisting gas in those cells (Wang et al., 2010).

One may want to continuously launch the jets at every finest hydrodynamical timestep. However, if the injected mass of jets is minuscule compared to the preexisting mass in surrounding cells, the jets make little or no dynamical impact on the surrounding cells after being mass-weighted averaged with them. Since it is unfeasible to resolve all gas cells around the MBH down to $\dot{M}_{\rm jet}dt$, an alternative approach is indispensable. Moreover, there is growing observational evidence of double-lobed radio galaxies (or double-double radio galaxies; DDRG) implying that the jets have launched in an episodic fashion with jets interruption timescales of 10^5 -10^8 years (Stawarz, 2004; Saikia et al., 2006). These two considerations lead us to adopt the following method: every time the accumulated jet mass, $\Sigma\, \dot{M}_{\rm jet}dt$, exceeds the threshold of 300 $M_\odot$ it is injected in collimated bipolar jets of a width of five finest cells in the vicinity of the MBH. This approach renders jets intermittent (once every 30 Myr if $\dot{M}_{\rm BH} = 10^{-5} M_\odot {\rm yr}^{-1}$) and dynamically important in our calculation.

The jets are injected parallel and anti-parallel to the total angular momentum $\mathbf{L}$ of the accreted gas up to that point. The angular momentum vector $\mathbf{L}$ changes its direction frequently while it asymptotes to the overall galactic rotation axis. This implementation is motivated by the observations of X-shaped radio galaxies (XRGs) where the radio jets rapidly reorient themselves by the interaction with the surrounding gas or by mergers (Merritt and Ekers, 2002; Gopal-Krishna et al., 2003). Lastly, since the mechanical or the radiative feedback alone may not describe the whole picture, we include hybrid models in which each of these two channels constitutes half of the MBH bolometric luminosity, $L_{\rm BH}$ (Sim-RMF; see Table 2.1).

Note that the mechanical channel has not been a main driver of MBH feedback in the presented calculation because, with highly suppressed mass accretion rate, jets have launched only a few tens of times in 350 Myr (See §3.2.2). We later comment upon its efficiency in §6.2.

Chapter 3

Galaxy Formation with Stars and Massive Black Holes

"Watch the stars, and from them learn. To the Master's honor all must turn, each in its track, without a sound, forever tracing Newton's ground."
— Albert Einstein (1879-1955)

Using the computational techniques described in Chapter 2, we investigate the co-evolution of a $9.2 \times 10^{11} M_\odot$ galactic halo and its $10^5 M_\odot$ embedded MBH at redshift 3 in a cosmological ΛCDM simulation. The MBH feedback heats the surrounding interstellar medium (ISM) up to 10^6 K through photoionization and Compton heating and locally suppresses star formation in the galactic inner core. The feedback considerably changes the stellar distribution there. This new channel of feedback from a slowly growing MBH is particularly interesting because it is only locally dominant, and does not require the heating of gas globally on the disk. The MBH also self-regulates its growth by keeping the surrounding ISM hot for an extended period of time.

This paper will be the first in a series that assembles a number of high-resolution galaxy formation simulations with self-consistently modeled stars and MBHs. This article is organized as follows. The initial condition of our simulation is the topic of §3.1. §3.2 is devoted to the results of our experiments, with an emphasis on the feedback-regulated star formation and black hole growth. Discussed in §3.3 are the summary and conclusions of this work.

This chapter is a part of the publication submitted to *The Astrophysical Journal* which is coauthored by John Wise, Marcelo Alvarez, and Tom Abel.

3.1 The Simulations

The improved physics of galaxy formation are first extensively tested in isolated galaxies. We then apply them to a massive star-forming galactic halo of $9.2 \times 10^{11} M_\odot$ at redshift 3 in a cosmological ΛCDM simulation. We begin by describing how the initial conditions of our simulation are generated.

3.1.1 Setting Up A $\sim 10^{12} M_\odot$ Halo

A three dimensional cubic volume of 16 comoving Mpc on a side is set up at $z = 60$ assuming a flat ΛCDM cosmology with dark energy density $\Omega_\Lambda = 0.73$, matter density $\Omega_{\rm m} = 0.27$, baryon density $\Omega_{\rm b} = 0.044$, and Hubble constant $h = 0.71$ (in the unit of $H_0 = 100\,{\rm km\ s^{-1} Mpc^{-1}}$). A scale-invariant primordial power spectrum (spectral index $n = 1$, Eisenstein and Hu, 1999) is adopted with $\sigma_8 = 0.81$, the rms density fluctuation amplitude in the sphere of 8 h^{-1}Mpc.

We identify a dark matter halo of $\sim 10^{12} M_\odot$ at $z = 3$ by performing a coarse-resolution adiabatic run. Then we recenter the density field around this halo and set up a new initial condition which preserves the same large-scale power yet contains a small-scale power as well, with a 128^3 root grid and a series of two nested child grids of twice finer resolution each (160^3 cells for level $l = 1$, and 200^3 for $l = 2$). Therefore the finest nested grid at level $l = 2$ spans 6.25 comoving Mpc on a side, contains 200^3 dark matter particles of $9.6 \times 10^5 M_\odot$, and manifests the equivalent resolution of a 512^3 unigrid. Initially all the cells throughout $l = 2$ grids are allowed to be further refined; however, the volume in which additional refinement is enabled ($\mathbf{V}_{\rm ref}$; in the shape of a rectangular solid) continually shrinks in size in such a way that it encloses only the smallest dark matter particles.[1] An initial metallicity of $Z = 0.003\, Z_\odot$ is also set up everywhere to track the metallicity evolution and to facilitate cooling below

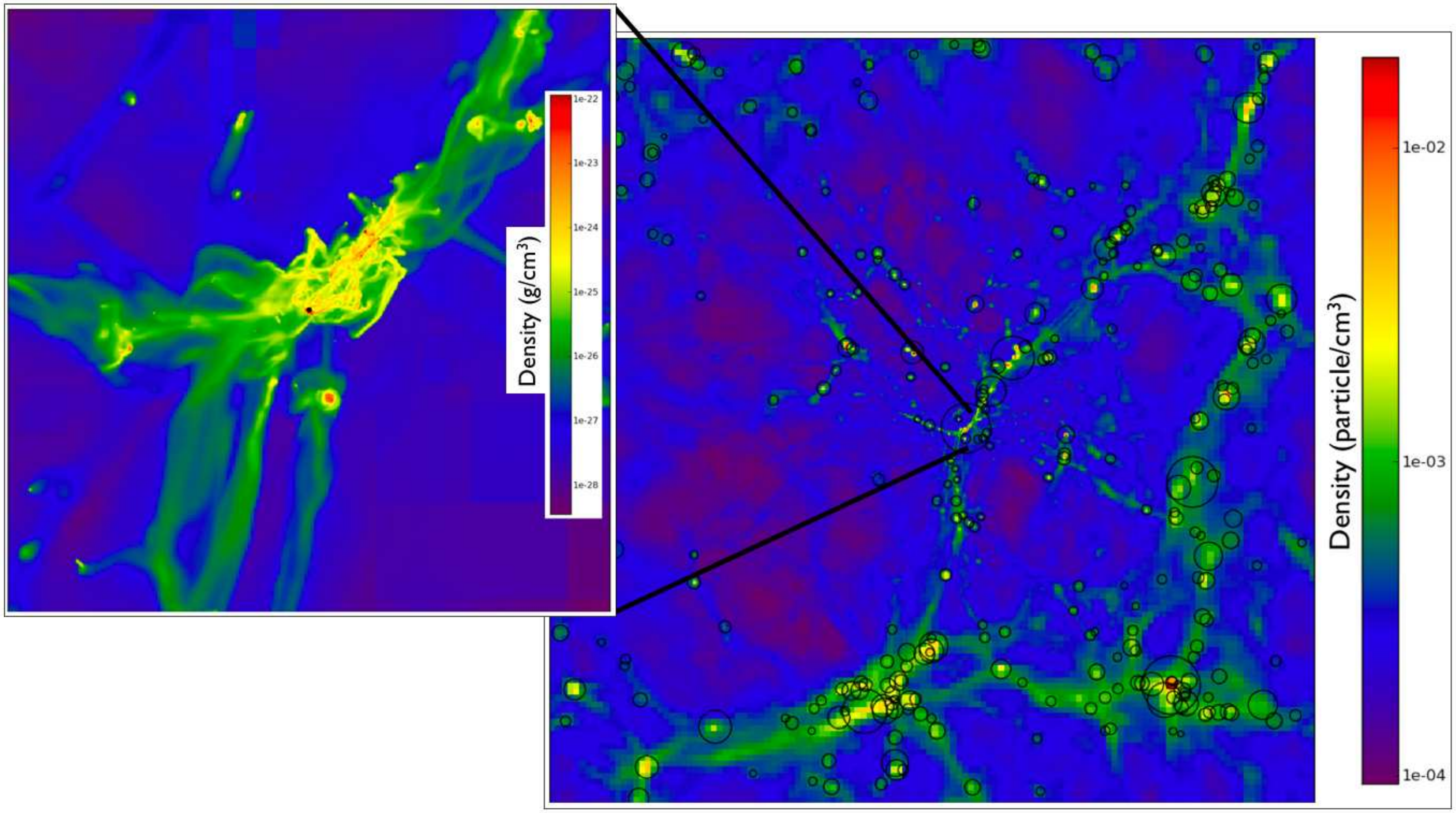

Fig. 3.1.— A projected density of the simulation box (16 comoving Mpc) at $z = 3$ is displayed on the right; circles represent the identified massive halos. On the left a $9.2 \times 10^{11} M_{\odot}$ halo, i.e. the *model galaxy*, is shown in a 200 kpc box (proper). High-resolution images are at http://www.jihoonkim.org/.

10^4 K.

Our initial condition is first evolved to $z = 3$ with a low-resolution (121.6 pc) refinement strategy and a particle formation and feedback recipe, without an accreting MBH. At $z = 3$ we split each dark matter and star particle inside the focused volume ($\mathbf{V}_{\rm foc}$; a rectangular hexahedron of 1.28 comoving Mpc on a side, a subset of $\mathbf{V}_{\rm ref}$) into 13 child particles using the particle refinement technique by Kitsionas and Whitworth (2002). This algorithm places child particles on a hexagonal close packed (HCP) array, and has been applied to many particle-based applications requiring enhanced particle resolution in a resimulated region (e.g. Bromm and Loeb, 2003; Kitsionas and Whitworth, 2007; Yoshida et al., 2008). After the particle splitting procedure, each dark matter particle in $\mathbf{V}_{\rm foc}$ represents a collective mass of 74000 $M_\odot$. Across $\mathbf{V}_{\rm foc}$ cells are now allowed to refine up to 11 additional levels, achieving maximum spatial resolution of 15.2 pc at $z \sim 3$ (See §2.2.2).

3.1.2 Galactic Parameters

Consequently, this process produces our focused object at $z = 3$ dubbed a *model galaxy*, on which a suite of high-resolution simulations is performed (Figure 3.1). The model galaxy has a mass of $M_{\rm vir} \simeq 9.2 \times 10^{11} M_\odot$ at $z = 3$ and a corresponding virial radius of

$$R_{\rm vir} = M_{\rm vir}^{1/3} \left[\frac{H_0^2 h^2 \Omega_{\rm m} \Delta_{\rm c}}{2G} \right]^{-1/3} \simeq 310 \ \ \text{comoving} \ \ \text{kpc} \tag{3.1}$$

given $h = 0.71$, $\Omega_{\rm m} = 0.27$, and $\Delta_{\rm c} = 200$. The dark matter halo represented by $\sim 1.1 \times 10^7$ particles constitutes $\sim 88\%$ of the total mass. About $\sim 1.0 \times 10^7$ particles contain $8.0 \times 10^{10} M_\odot$ of stellar mass, whereas the rest, $3.5 \times 10^{10} M_\odot$, is in gaseous form available for future star formation, either in the ISM or in the embedding halo. There is no shortage of gas supply, as the gas from outside the halo continuously falls inward either by spherical accretion or by cold accretion along one of the multiple

[1]This active adjustment on the size of $\mathbf{V}_{\rm ref}$ prevents heavier dark matter particles of initial $l = 0$ and $l = 1$ grids from penetrating the central region of a simulation box, thereby causing runaway refinement. Typically $\mathbf{V}_{\rm ref}$ becomes $\sim 60\%$ of the entire $l = 2$ region in length at $z = 3$, which is still large enough to encompass the Lagrangian volume of a $\sim 10^{12} M_\odot$ halo at $z = 3$.

filaments (Dekel et al., 2009; Ceverino et al., 2010). The halo has spin parameters of 0.051 for dark matter, and 0.069 for gas. At the center of all lies a $10^5 M_\odot$ MBH we plant as a gravitational seed. This choice of the initial MBH mass lies below the Magorrian et al. (1998) relationship assuming 10% of the stellar mass is in the bulge, which may have resulted in a weaker mode of MBH feedback - possibly a "radio-mode" analogue - and the negligible gas expulsion by the MBH (See §3.2.2 and §3.2.4). Therefore the reported results should not be interpreted as a general picture of MBH feedback. It remains to be seen whether more massive MBHs or fast growing MBHs have different effects. We will come back to this issue in §3.2.4.

3.2 Results

A suite of simulations with optional modes of feedback is performed from $z = 3$ to 2.6 in order to investigate the evolution of a massive star-forming galaxy with its embedded massive black hole. We mostly focus on two simulations, one with and the other without MBH feedback (Sim-SF and Sim-RMF; Table 2.1). Each of the calculations is performed on 16 processors of the Orange cluster[2] at Stanford University. Grids and particles altogether, each simulation is routinely resolved with $\sim 6.5 \times 10^7$ total computational elements ($\sim 4.5 \times 10^7$ particles and $\sim 270^3$ cells). To evolve the system for 350 Myr, each of these runs typically takes $\sim$ 20000 CPU hours.

3.2.1 Star Formation Rates

First we check the validity of our molecular cloud formation criteria (§2.2.4) and stellar feedback (§2.2.5) by comparing star formation rate (SFR) with gas density. Figure 3.2 displays a relation between the SFR surface density and the gas surface density in Sim-SF at $z = 2.75$. In a (20 kpc)^3 box centered on a MBH, each data point is made by taking the mean values in a (1 kpc)^3 bin, the typical aperture size of $\Sigma_{\rm SFR} - \Sigma_{\rm gas}$ studies for spatially-resolved nearby galaxies (e.g. Kennicutt et al.,

[2] Infiniband-connected AMD, 8 cores per node, 4 GB memory per core

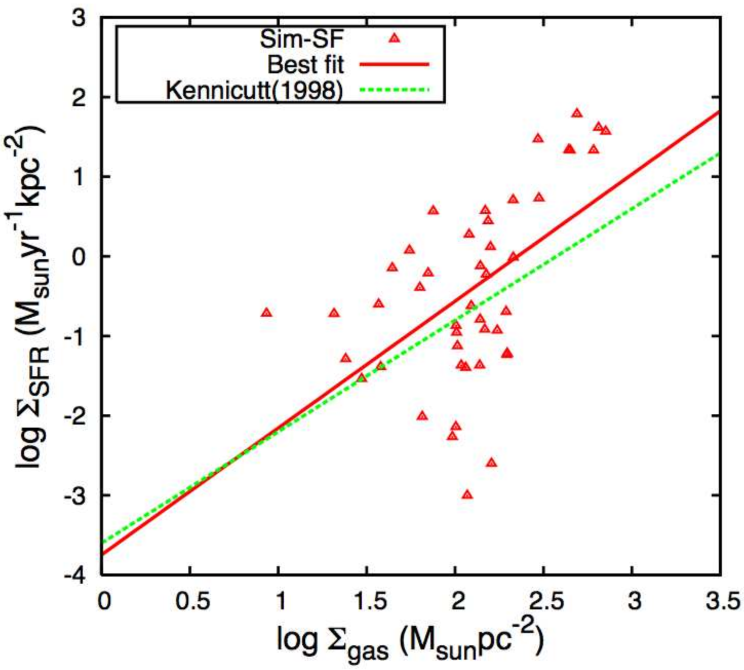

Fig. 3.2.— The relationship between star formation rate (SFR) and gas surface density. The data is from a (20 kpc)^3 box centered on a MBH in Sim-SF at $z = 2.75$. The solid line is the best fit for simulated data while the dashed line is from observations of nearby galaxies ($\Sigma_{\rm SFR} \propto \Sigma_{\rm gas}^{1.4}$; Kennicutt, 1998).

2007). Here Eq.(2.7) is used to calculate the stellar mass newly spawning in each cell, and the data points below the observation limit, $10^{-5} M_{\odot}{\rm yr}^{-1}{\rm kpc}^{-2}$, are discarded.

The molecular cloud formation and stellar feedback, joined with high spatial resolution, work together to self-regulate star formation. However, authors note that our best fit to this particular snapshot of the galaxy is steeper than the observed trend of $z \sim 0$ with larger dispersion.

3.2.2 Lack of Star-forming Gas in the Inner Core

Now we turn to the topic of an accreting massive black hole and its feedback. We focus on how MBH feedback changes its surrounding ISM, and how it locally suppresses molecular cloud formation. For this purpose, we hereafter examine the snapshot of the model galaxy at $z = 2.75$ (or 2410 Myr after the Big Bang), about 220 Myr after

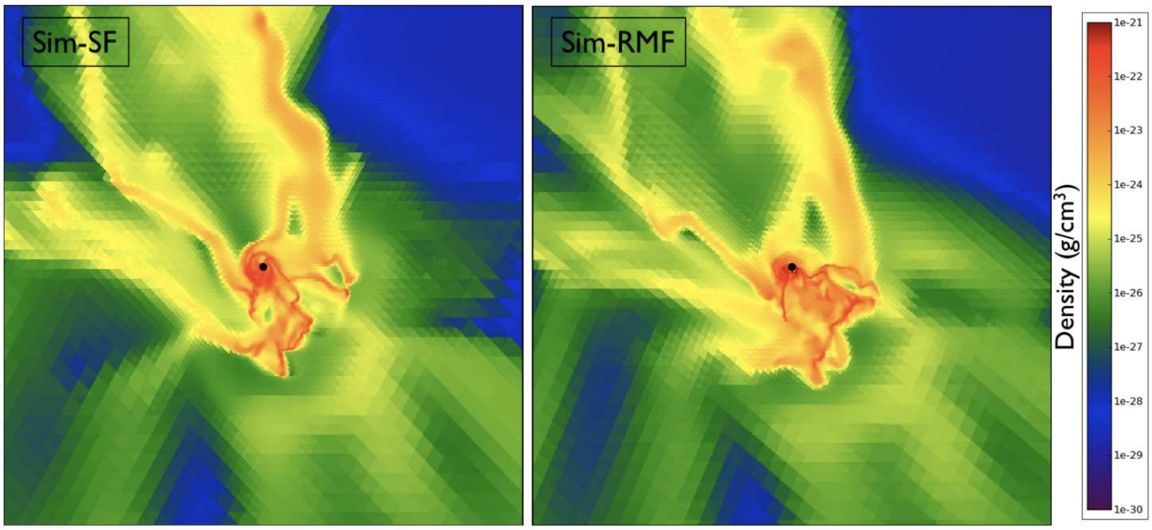

Fig. 3.3.— The face-on views of the disks. Density in the central 20 kpc (proper) sliced through the MBH (black dots at the centers) at $z = 2.75$, about 220 Myr after the MBH is placed. Sim-SF on the left, and Sim-RMF on the right. Compare with Figure 3.4.

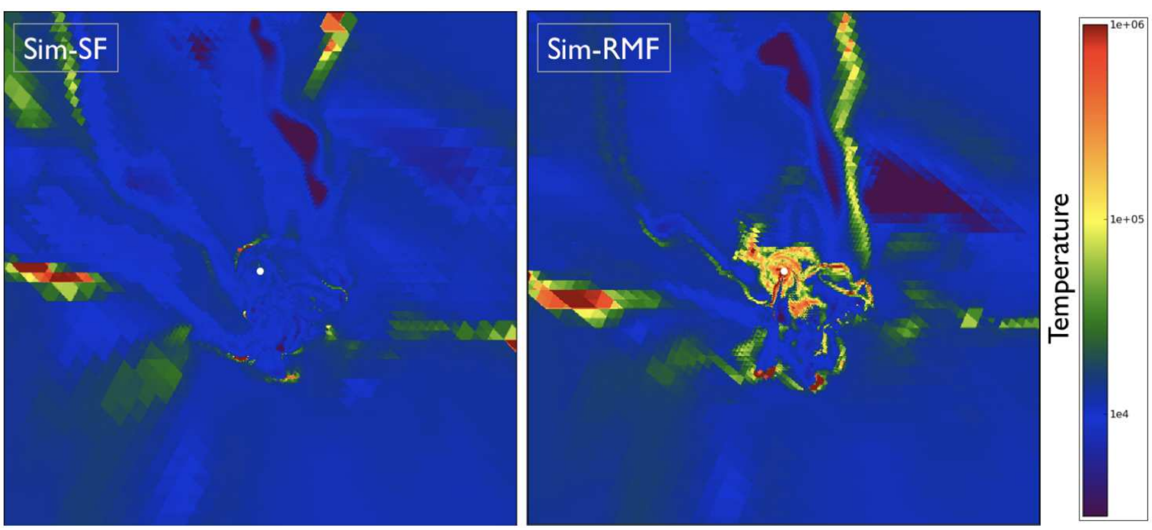

Fig. 3.4.— The face-on views of the disks. Temperature in the central 20 kpc (proper) sliced through the MBH (white dots at the centers) at $z = 2.75$. Sim-SF on the left, and Sim-RMF on the right. A hot region of a size ~ 2 kpc in Sim-RMF heated by MBH feedback is prominent, which remarkably contrasts with a much colder ISM in Sim-SF.

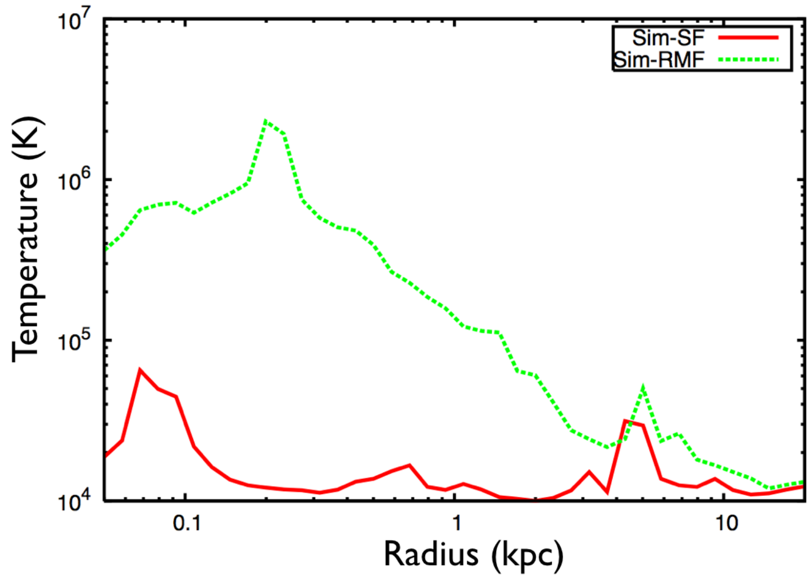

Fig. 3.5.— The mass-weighted radial profile of temperature in a 20 kpc sphere centered on the MBH at $z = 2.75$. The red solid line and the green dashed line represent Sim-SF and Sim-RMF, respectively. The temperature within ~ 2 kpc radius is raised mostly by the radiation from the MBH.

an accreting MBH is placed at the center of the galaxy. The model galaxy now has a mass of $M_{\rm vir} \simeq 9.0 \times 10^{11} M_\odot$ and correspondingly, a virial radius of $R_{\rm vir} \simeq 80$ kpc (proper; radii are hereafter in proper kpc, not comoving, unless marked otherwise).

When a MBH starts to accrete gas, the gravitational potential energy of the accreting gas is released in the form of radiation and jets. Even in the case of a slowly growing MBH, as in our simulations (a possible "radio-mode" analogue; $\dot{M}_{\rm BH} \sim 0.05\,\dot{M}_{\rm Edd}$; see §3.2.4), the feedback from the MBH is known to play a major role in regulating star formation and its own growth (Croton et al., 2006; McNamara and Nulsen, 2007; Sijacki et al., 2007; Puchwein et al., 2008).

The density and temperature structures in the central regions of the galaxies from Sim-SF (left; without MBH feedback) and Sim-RMF (right; with radiative and mechanical MBH feedback) are shown in Figures 3.3 and 3.4. In particular, in Figure 3.4 for Sim-RMF, a hot region of size ~ 2 kpc surrounding the MBH is prominent, which remarkably contrasts with a much colder ISM in Sim-SF. This region is heated up to 10^6 K by ionizing photons heating hydrogen and helium, and scattering off electrons. The latter, i.e. Compton heating, is important especially in a highly ionized region. When the fractions of neutral species (or singly ionized He) are low, the effect of photoheating on H, He, and He^+ is mild; instead, the contribution of Compton heating on electrons is relatively large. The hot temperature at the center of Sim-RMF is also evident in the radially averaged temperature profile of Figure 3.5. Note that the 1-2 kpc distance over which the gas is heated is consistent with the characteristic distance found in an analytic study (Figure 4 of Sazonov et al., 2005) out to which the gas is heated by photoionization and Compton scattering.

A hot temperature in the inner core of the galaxy in Sim-RMF leads to a significant deprivation of cold, dense star-forming gas. Figure 4.10 illustrates how the structure of ISM is changed by MBH feedback, in terms of joint probability distribution functions of gas density and temperature.

- The left figure depicts a typical ISM without MBH feedback but still with stellar feedback (Sim-SF). It features a multiphase ISM that is naturally achieved in adaptively refined mesh, including cold, dense star-forming gas (T $< 10^4$ K, $\rho > 10^{-24}$ g cm^{-3}), and hot diffuse supernovae bubbles. As expected, above the molecular cloud formation threshold ($n_{\rm thres} = 125$ cm^{-3}; denoted by a dashed line), gas cells immediately turn into molecular cloud particles, and thus no cell is left behind unresolved.

- On the right, the gas cells of density $> 10^{-24}$ g cm^{-3} are now heated up to 10^6 - 10^7 K, populating zone "A". These cells are mostly located on the disk in relatively close proximity (< 2 kpc) to the central MBH. These cells are very stable against fragmentation because they are so hot that they can barely cool down to a typical molecular cloud temperature in a dynamical time (i.e. $t_{\rm cool} \gg t_{\rm dyn}$). For that reason, the cells have hard time to fulfill the condition (c) of the molecular cloud formation criteria described in §2.2.4. The heating by the X-ray radiation thus increases the amount of dense gas in the vicinity of the MBH which is incapable of condensing into stars.[3]

[3]Some hot gas cells above the molecular cloud formation threshold still exist on this PDF, not turning into particles (zone "B"). While it is due to the violation of one of the molecular cloud

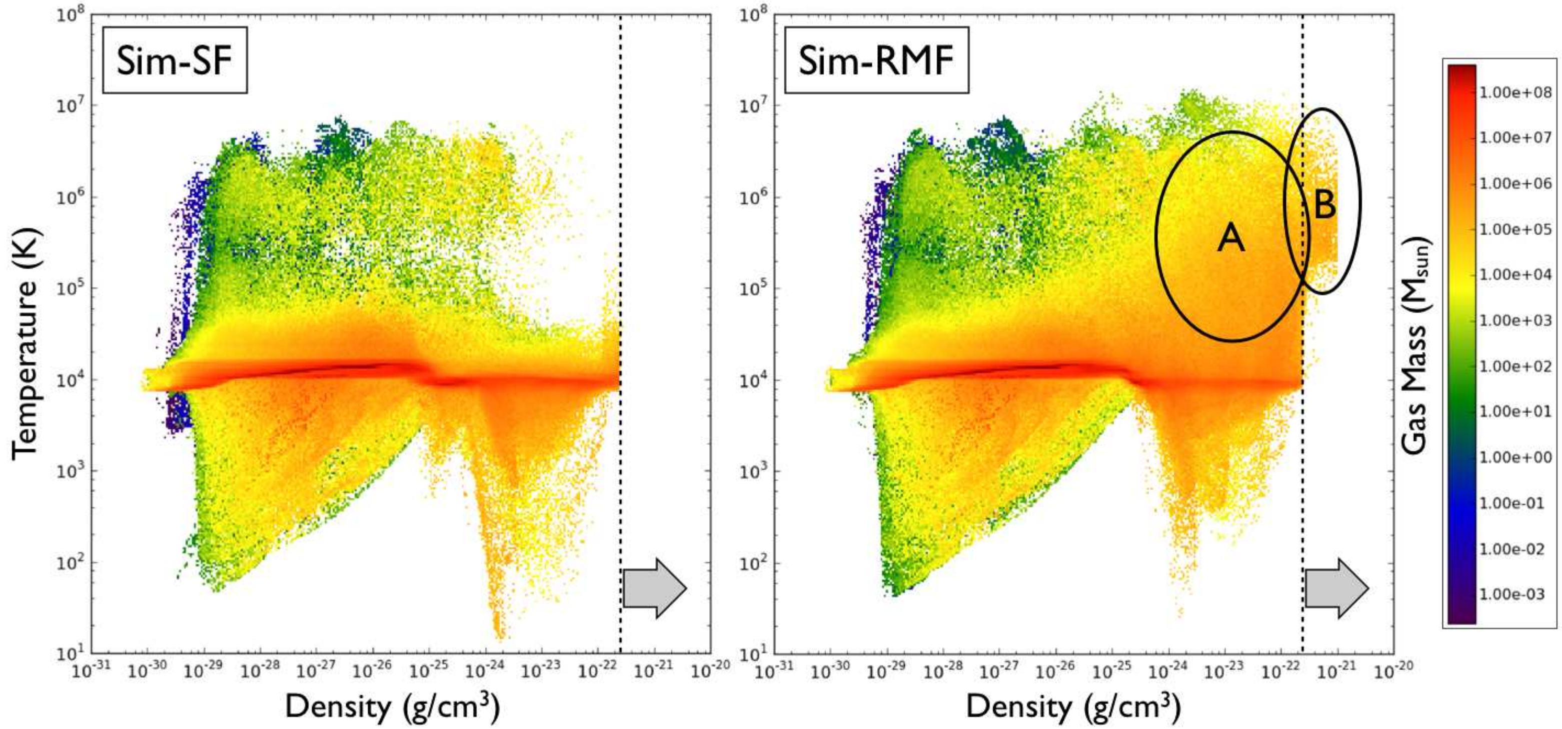

Fig. 3.6.— Joint probability distribution functions (PDFs) of gas density and temperature colored by gas mass in each bin. The data is for a 200 kpc sphere centered on the MBH at $z = 2.75$. Sim-SF on the left, and Sim-RMF on the right. The vertical dashed line in each plot denotes the density threshold for molecular cloud formation $n_{\rm thres}$ (§2.2.4). Note that the MBH feedback in Sim-RMF heats the dense gas up to 10^6-10^7 K increasing the amount of high density gas stable against fragmentation (zone "A").

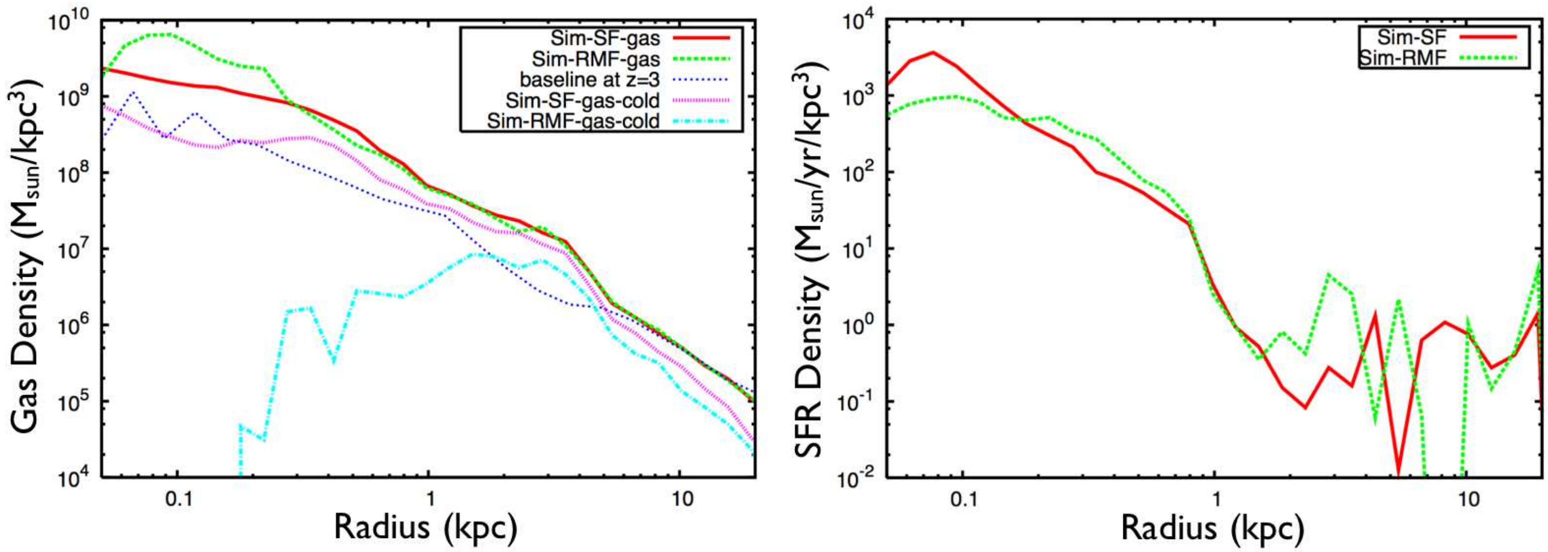

Fig. 3.7.— Spherically-averaged radial gas density profiles centered on the MBH at $z = 2.75$. In each panel, the red solid line and the green dashed line represent Sim-SF and Sim-RMF, respectively. Left: in Sim-RMF the radiation from the MBH keeps a large amount of gas at the galactic center (green dashed line) compared to Sim-SF (red solid line). Only a minimal fraction of the gas within 0.2 kpc radius is below 10^4 K (the cyan dot-dashed line) whereas in Sim-SF, 10 - 30% of the gas in the same region is considered to be cold (the pink dotted line). The blue thin dotted line shows the density profile at $z = 3$. Right: star formation rate (SFR) density shows significantly suppressed star formation activity in the central 0.2 kpc sphere.

Therefore, the feedback from even a slowly growing MBH retains hot dense gas at a galactic center which otherwise could have created strong star formation. Figure 3.7 dramatically demonstrates the distinct changes in radially averaged density profiles when MBH feedback is included.

- The left figure of gas density profiles displays that the radiation from the MBH keeps a substantial amount of gas at the core of the galaxy, and inhibits the gas from all turning into stars. The total gas density of Sim-RMF (the green dashed line) at 0.1 kpc from the MBH is about ~ 5 times as high as that of Sim-SF (the red solid line). The thin blue dotted line represents the initial profile of gas at z=3 when the simulation restarts with 15 pc resolution. However in Sim-RMF, only a minimal fraction of the gas within 0.2 kpc radius is below 10^4 K (the cyan dot-dashed line) whereas in Sim-SF, 10 - 30% of the gas in the same region is considered to be cold, thus potentially star-forming (the pink dotted line).

- The deprivation of cold dense gas in Sim-RMF inevitably prompts the suppression of star formation activity in the inner core of the galaxy. The right figure reveals the star formation rate density (in $M_\odot \mathrm{yr}^{-1} \mathrm{kpc}^{-3}$) as a function of distance from the MBH. Eq.(2.7) is again used to calculate the new stellar mass being generated in each cell. The SFR density of Sim-RMF at 0.1 kpc from the MBH is reduced by more than $\sim 50\%$ when compared with that of Sim-SF.[4] Overall, the X-ray radiation from the MBH severely suppresses the SFR of Sim-RMF inside the 0.2 kpc sphere.

The gas masses enclosed within a radius r, $M_{\mathrm{gas}}(< \mathrm{r})$, are plotted in Figure 3.8, showing the impact of MBH feedback as a powerful energy source to reshape the galactic gas distribution. Sim-RMF harbors ~ 2.5 times more gas ($1.3 \times 10^8 M_\odot$) within 0.2 kpc than what Sim-SF does ($5.1 \times 10^7 M_\odot$), but almost none of this gas is

formation conditions ($t_{\mathrm{cool}} < t_{\mathrm{dyn}}$), we emphasize that the thermodynamical properties here are unreliable as they are above the resolution-dependent molecular cloud formation threshold.

[4] Note that since we used Eq.(2.7) to estimate SFR, each molecular cloud particle will generate stellar mass for 12 t_{dyn}. Therefore the SFR inside the 0.1 kpc sphere would include a number of particles that were formed outside the sphere, but have migrated inward and are now forming stars there. This is why the SFR density is not as suppressed as one would have naively expected from the density profile of cold gas.

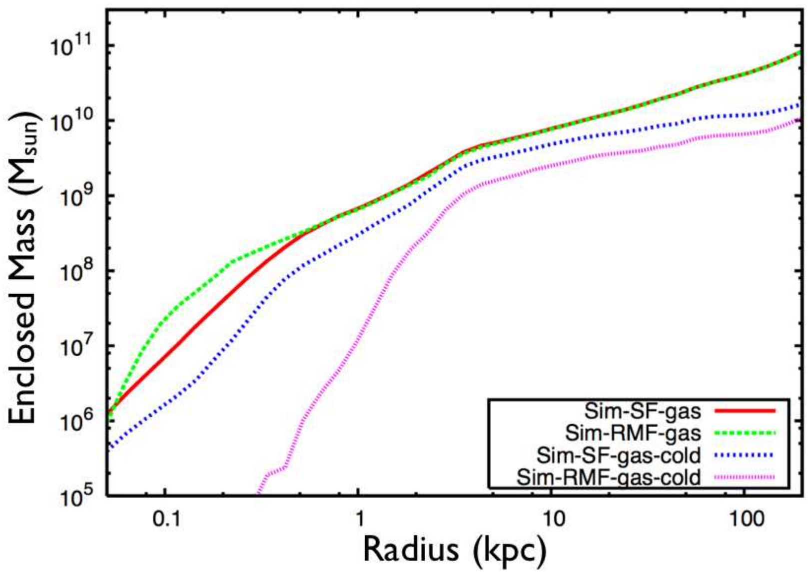

Fig. 3.8.— Enclosed mass profiles of total gas and cold gas (T $< 10^4$ K) centered on the MBH at $z = 2.75$. The red solid line and the green dashed line represent Sim-SF and Sim-RMF, respectively. Sim-RMF harbors more gas within 0.2 kpc than what Sim-SF does, but almost none of this gas is below 10^4 K.

below 10^4 K. This gas in the core is not consumed by star formation, nor is pushed away by any mechanical outflow. Note that in Sim-RMF cold gas mass within 10 kpc is reduced by $\sim 50\%$ displaying how far the MBH radiation reaches.

Readers should also note that the enclosed gas masses at the virial radius (80 kpc proper) are almost identical between Sim-SF and Sim-RMF, implying there has been *no massive gas expulsion driven by the MBH*. This is one of the key differences from previous numerical studies. Very strong gas expulsions were frequently observed in previous studies in which the MBH feedback energy is only thermally deposited to a few neighboring gas particles (e.g. Springel et al., 2005b). In contrast, most of the gas is still bound to our simulated galaxies because (1) the energy released from our slowly growing MBH is relatively small (a possible "radio-mode" analogue),[5] (2)

[5] This is valid only for the results presented herein in which the mass accretion onto the MBH is highly suppressed by self-regulation. It remains yet to be seen whether more massive MBHs or fast growing MBHs (for example, in merging galaxies) do or do not unbind the gas from the galactic gravitational potential. The so-called "quasar-mode" feedback will be the topic of a future paper (See §6.2).

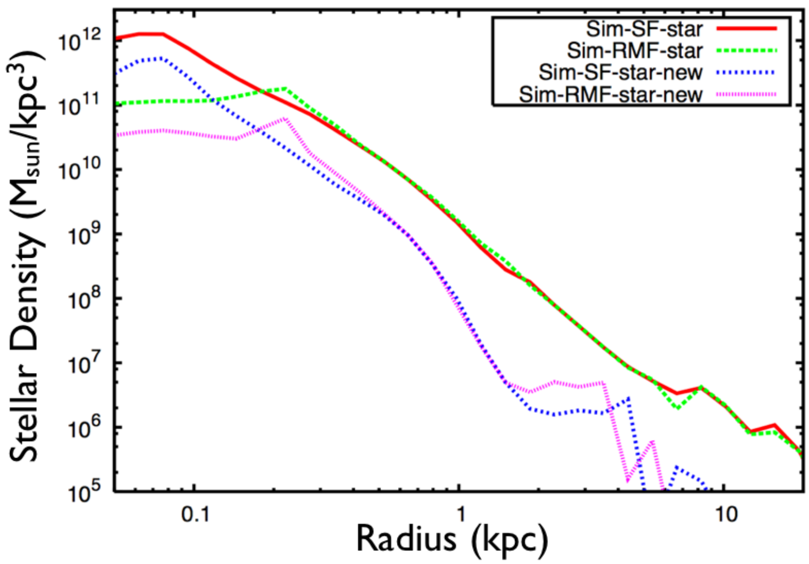

Fig. 3.9.— Stellar density profiles of total stars and young stars (molecular cloud particles of age < 100 Myr) in a 20 kpc sphere centered on the MBH at $z = 2.75$. The red solid line and the green dashed line represent Sim-SF and Sim-RMF, respectively. Locally suppressed star formation at the galactic center in Sim-RMF leads to a considerable reduction of stellar density in the region.

the gas mass to which the MBH energy is coupled is large in our radiative feedback formalism, and (3) the mass accretion rate onto our MBH is not high enough to repeatedly drive jets. Note again that the mechanical channel of MBH feedback is not a main driver of feedback in the presented calculation. The MBH has not doubled its mass at the end of our calculation (after 350 Myrs; see §3.2.4); and, with this highly suppressed mass accretion rate, jets have launched only a few tens of times in 350 Myr. We come back to the efficiency issue of mechanical feedback in §6.2.

To summarize, we have shown that MBH feedback, especially its radiation, alters the multiphase ISM of the surrounding gas and thus deprives the galactic inner core of cold, dense star-forming gas. Two consequences arise from the lack of star-forming gas at the galactic center: locally suppressed star formation, and the associated change in stellar distribution. We discuss these topics in the following sections.

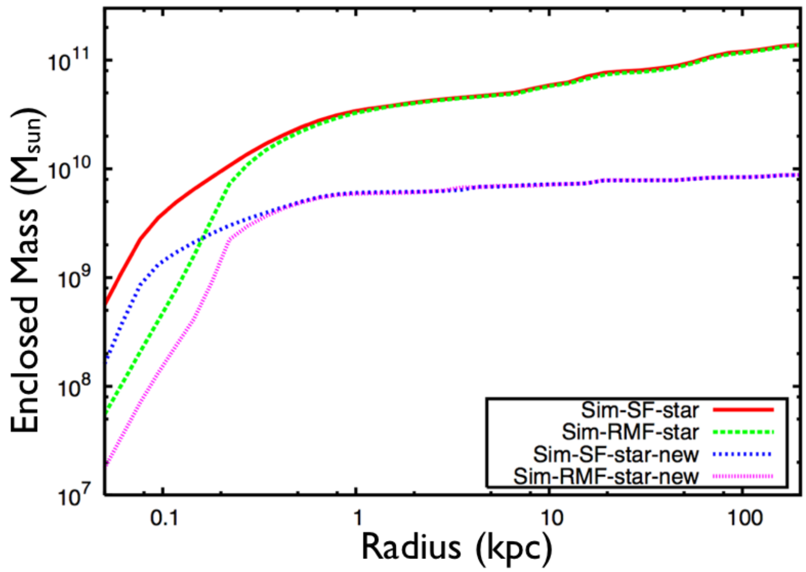

Fig. 3.10.— Enclosed mass profiles of total stars and young stars (molecular cloud particles of age < 100 Myr) centered on the MBH at $z = 2.75$. The red solid line and the green dashed line represent Sim-SF and Sim-RMF, respectively. The stellar mass enclosed in the 0.1 kpc sphere of Sim-RMF is about an order of magnitude smaller than that of Sim-SF.

3.2.3 Locally Suppressed Star Formation and the Change in Stellar Distribution

The inner core of the galaxy in Sim-RMF becomes a sterile environment for molecular cloud formation (star formation) because the gas is hot and turbulent, therefore Toomre stable. As a consequence, star formation is suppressed locally in the inner core, as shown in Figure 3.7. Figure 3.9 displays how the stellar mass density profile changes in the inner core region as a result of the locally suppressed star formation in Sim-RMF. Again we use the snapshot at $z = 2.75$, about 220 Myr after the MBH is placed at the center of the model galaxy. The stellar mass density at 0.1 kpc in Sim-RMF is only less than $\sim 20\%$ of that of Sim-SF. The mass density of young stars (age < 100 Myr) shows the similar drastic reduction.

The stellar masses enclosed within a radius r, $M_{\rm star}(<\rm r)$, are shown in Figure 3.10. The stellar mass enclosed within the 0.1 kpc sphere of Sim-RMF is almost

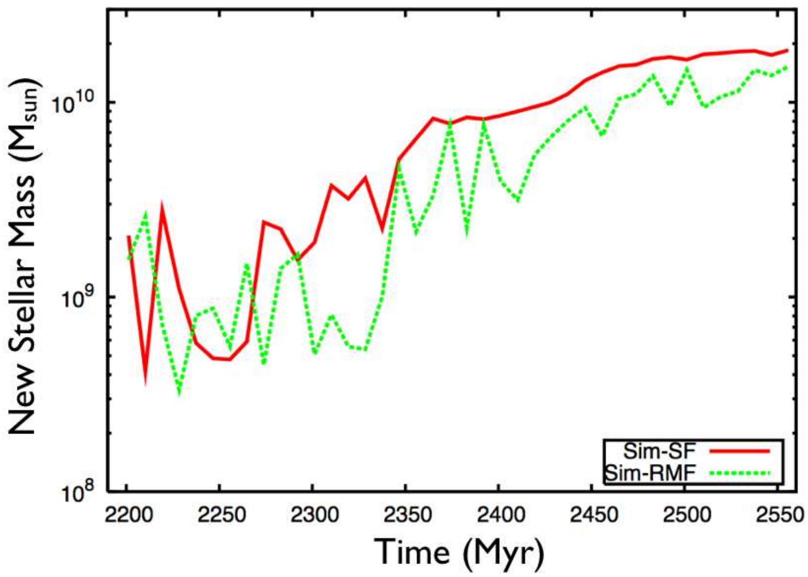

Fig. 3.11.— Star formation history in a 0.2 kpc sphere: the mass of new stars (molecular cloud particles born after the MBH is placed at 2190 Myr) inside a 0.2 kpc sphere centered on the MBH. The red solid line and the green dashed line represent Sim-SF and Sim-RMF, respectively. Since 2300 Myr the star formation activity of Sim-RMF in this region is suppressed.

an order of magnitude smaller than that of Sim-SF. The suppressed star formation replaces the steep inner cusp of stellar density profile with a flattened core ~ 0.3 kpc in radius; i.e. stars are less concentrated at the galactic center of Sim-RMF. Considering the relatively small amount of energy released from the slowly growing MBH, the difference between these two lines is quite remarkable. Together with Figure 3.8, one expects that the stellar to gas mass ratio inside the 0.2 kpc sphere of Sim-RMF will be much smaller than that of Sim-SF. Note also that the total stellar mass enclosed at the virial radius (80 kpc) is almost indistinguishable between Sim-SF and Sim-RMF. In other words, star formation in Sim-RMF is not globally suppressed, but only locally suppressed at the center. This is because our MBH feedback is not strong enough to unbind a large amount of gas (See §3.2.2), or to globally abolish cold, star-forming clumps in the entire ISM.

Figure 3.11 exhibits the evolution of the new stellar mass (molecular cloud particles born after the MBH is placed at 2190 Myr, or at $z = 3$) inside a 0.2 kpc sphere centered on the MBH. The plot demonstrates that since 2300 Myr the star formation activity in the inner core of Sim-RMF is suppressed. Naturally, alteration in the stellar distribution ensues at the center of the galaxy with an active MBH. Figure 3.12 strikingly contrasts the distribution of newly-formed stars (molecular cloud particles of age < 10 Myr).

- In the top row, a three dimensional rendering of newly-formed particles is constructed at a $\sim 45°$ angle from the disk plane. Here the light intensities of newly-formed particles are integrated along the lines of sight. At the center of the stellar distribution, i.e. the densest peak, lies the MBH particle.

- In the bottom row, newly-formed stellar masses are projected along the z-axis of the simulation box which makes a $\sim 47.2°$ angle with the angular momentum vector of the gas within a 5 kpc sphere centered on the MBH. The morphological difference at the inner core of the galaxy is particularly evident. Stars in Sim-SF are highly concentrated at the center, while stars in Sim-RMF are less concentrated but form spiral-like structures at ~ 0.2 kpc radius from the MBH.

In summary, it is shown that MBH feedback suppresses star formation locally at the galactic inner core, thus significantly changing the stellar distribution there. This new channel of feedback is particularly interesting because it is dominant only in the local surroundings of the MBH. Unlike stellar feedback, which operates globally, this new suppression mechanism does not require additional star formation and/or extensive mass expulsion out of the galactic potential.

3.2.4 Regulated Black Hole Growth

Heating by MBH feedback, which locally suppresses star formation, also makes the MBH to self-regulate its own growth. Figure 3.13 shows the MBH accretion history versus time for Sim-SF and Sim-RMF.

- The MBH in Sim-SF has grown exponentially to $3 \times 10^6 M_\odot$ in 350 Myr, already about >30 times more massive than its initial mass of $10^5 M_\odot$. The MBH

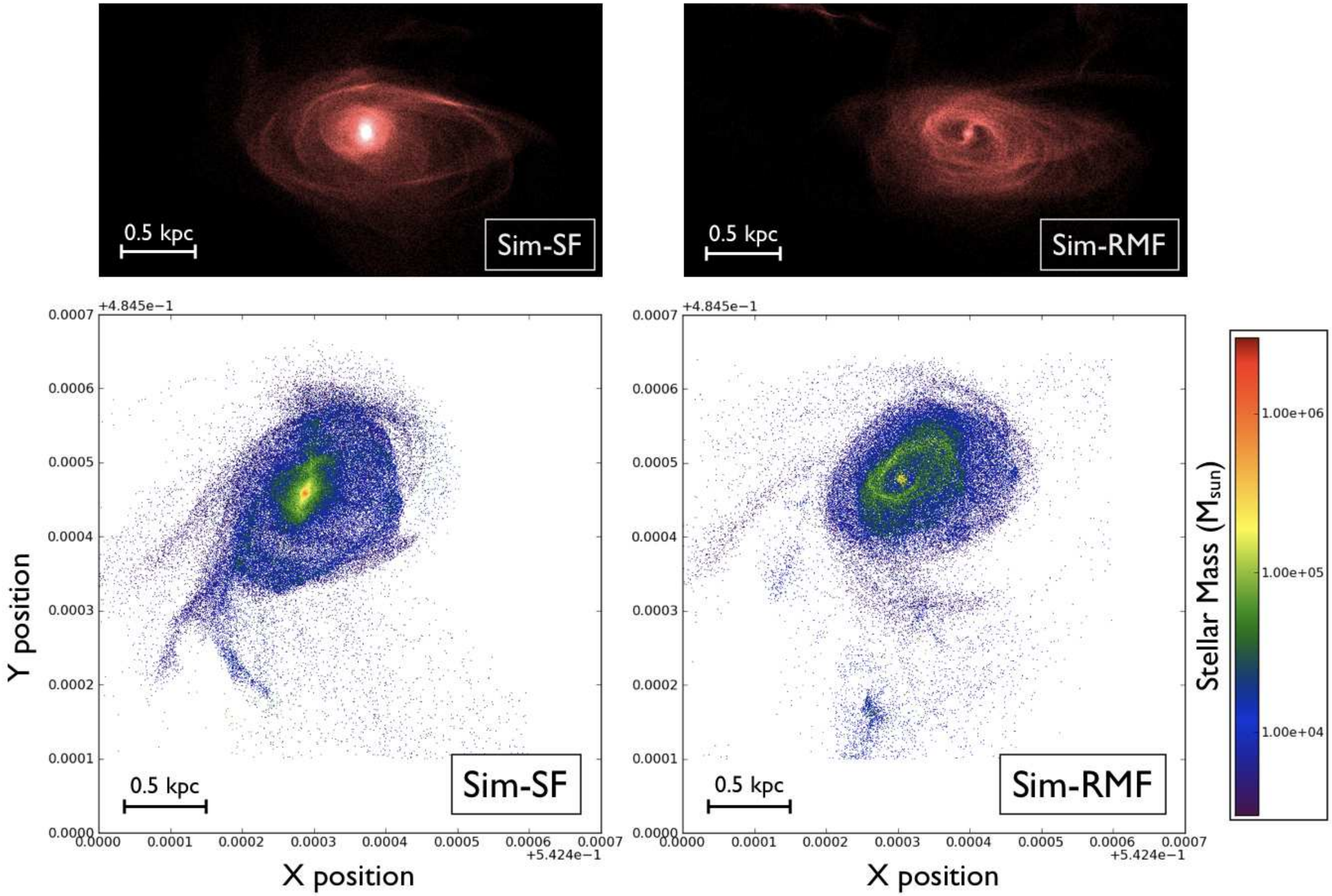

Fig. 3.12.— The distribution of newly-formed stars (molecular cloud particles of age < 10 Myr) at $z = 2.75$. Sim-SF on the left, and Sim-RMF on the right. Top: images of newly-formed stars constructed at a $\sim 45°$ angle from the disk plane. Visualization courtesy of Ralf Kaehler. Bottom: newly-formed stellar mass projected along the z-axis of the simulation box which makes a $\sim 47.2°$ angle with the gas angular momentum vector. Each frame is 3.0 kpc wide. The difference in stellar distribution is dramatic, especially in the < 0.5 kpc core.

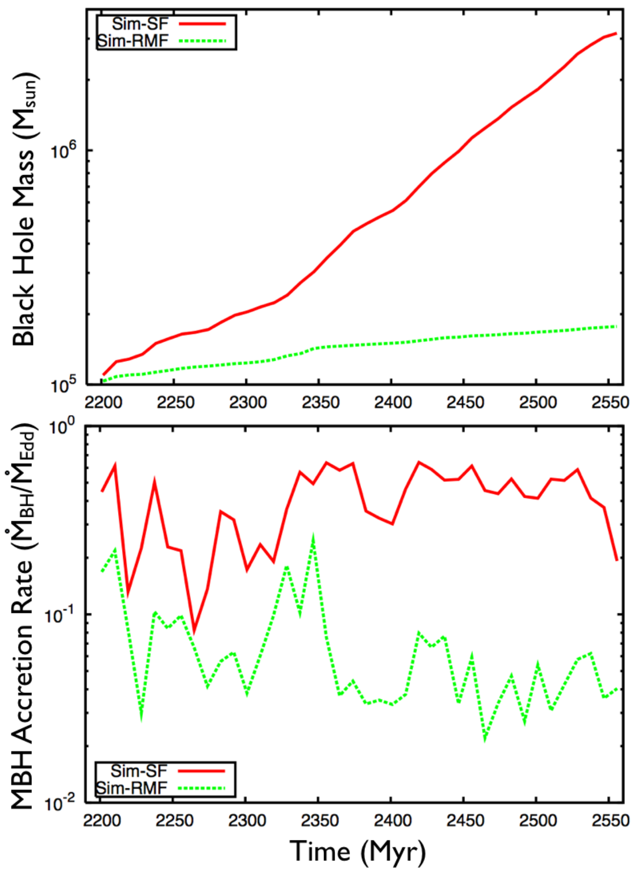

Fig. 3.13.— Top: black hole mass accretion history. Note that the mass of the MBH of Sim-RMF has not doubled during this period, while the MBH of Sim-SF has grown exponentially. Bottom: mass accretion rate onto the MBH in the unit of Eddington rate. In each panel, the red solid line and the green dashed line represent Sim-SF and Sim-RMF, respectively.

maintained the accretion rate of 0.2 - 0.6 $\dot{M}_{\rm Edd}$ during this time period, corresponding to the unhindered growth of the MBH when there is no mechanism to self-regulate itself other than stellar feedback.

- Over the course of the same period the MBH in Sim-RMF has grown by only $\sim 70\%$ to $1.7 \times 10^5 M_\odot$. The heated and diffused ISM in the vicinity of the MBH considerably suppresses the Bondi-Hoyle accretion estimate to as low as $\sim 0.02\ \dot{M}_{\rm Edd}$ in this period. This indicates that the MBH feedback described in previous sections is a possible "radio-mode" analogue where the accretion rate is $\sim 0.05\,\dot{M}_{\rm Edd}$ (Croton et al., 2006). It also presents a potential route to the relatively low mass MBH at the center of the Milky Way ($3 \times 10^6 M_\odot$).[6]

Therefore, the feedback from a MBH is confirmed as an effective mechanism for slowing down the accretion of gas onto itself. Without having to suddenly unbind all the surrounding gas, the MBH self-regulates its growth by heating up the neighborhood and keeping it hot for an extended period of time. This finding is consistent with the work by DeBuhr et al. (2010), who claimed that the growth of a MBH could be "self-regulated", rather than "supply-limited" (as in Springel et al., 2005b; Teyssier et al., 2010b) where quasar-like MBH feedback drive energetic large-scale outflows to unbind a significant amount of gas.

3.3 Summary

A state-of-the-art numerical framework which fully incorporates gas, stars, and a central massive black hole is developed. Our simulation, for the first time, followed the comprehensive evolution of a massive star-forming galaxy with self-consistently modeled stars and a MBH. Our novel framework renders a completely different, yet physically more accurate picture of how a galaxy and its embedded MBH evolve under each other's influence, providing a powerful means in understanding the coevolution of galaxies and MBHs. Our main results and new advancements are as follows.

1. *Molecular Cloud Formation and Feedback:* We have included a new model of molecular cloud formation and stellar feedback in our code (§2.2.4 to 2.2.5). Unlike previous star formation recipes based on the Schmidt relation, a particle spawns when a gas cell of a typical molecular cloud size, 15.2 pc, actually becomes Jeans unstable. Then the molecular cloud particle gradually produces stellar mass while returning a large fraction of mass back to the gas with thermal

[6] Authors again caution that the initial MBH mass ($10^5 M_\odot$) and final masses in both Sim-SF and Sim-RMF lie below the Magorrian et al. (1998) relationship, when 10% of the stellar mass is assumed to be in the bulge. The choice of a relatively small initial MBH mass may have caused a "radio-mode"-like MBH feedback, and a slower mass growth of the black hole.

feedback energy, modeling the observed slow star formation in molecular clouds. Thermal stellar feedback is shown to self-regulates star formation (§3.2.1).

2. *Massive Black Hole Accretion and Feedback:* We have successfully developed a self-consistent model of accretion of gas onto a MBH and its radiative and mechanical feedback effects (§2.2.6 to 2.2.8). Gas accretion onto the MBH is estimated with the Bondi-Hoyle formula, but without any boost factor, as we begin to resolve the Bondi radius. Monochromatic X-ray photons from the MBH are followed through three dimensional adaptive ray tracing, rendering the radiative feedback of a MBH; here, rays of photons ionize and heat the gas, and exert momentum onto the gas. Finally, the mechanical feedback of the MBH is represented by bipolar jets with velocities of $\sim 10^3$ km s^{-1} launched from the vicinity of the MBH accretion disk, well resolved in our high-resolution AMR simulations. Our approach is significantly different from the previous recipes for MBH feedback in galactic scale simulations to date (e.g. Springel et al., 2005b; Sijacki et al., 2007; Booth and Schaye, 2009; Teyssier et al., 2010b), yet more accurately presents the physics of MBHs when properly incorporated with a high dynamic range.

3. *Locally Suppressed Star Formation:* By investigating the coevolution of a $9.2 \times 10^{11} M_\odot$ galactic halo and its $10^5 M_\odot$ embedded MBH at $z \sim 3$, we show that MBH feedback, especially its radiation, heats the surrounding ISM up to 10^6 K through photoionization and Compton heating and thus locally suppresses star formation in the inner core of a galaxy (§3.2.2). The feedback also considerably changes the stellar distribution at the galactic center. This new channel of feedback from a slowly growing MBH is particularly interesting because it is only locally dominant, and does not require the heating of gas globally on the disk, or instigate a massive gas expulsion out of the galactic potential (§3.2.3).

4. *Self-regulated Black Hole Growth:* MBH feedback is also demonstrated to be an effective mechanism for slowing down the accretion of gas onto the MBH itself. Without necessarily unbinding all of its surrounding gas, the MBH self-regulates its growth by keeping the surrounding ISM hot for an extended period of time

(§3.2.4). Therefore, our results possibly are consistent with a "radio-mode" analogue of MBH feedback.

Our method limits the use of *ad hoc* formulation and instead more accurately models the physics of galaxy formation. As a result, four key components of galactic scale physics, (a) molecular cloud formation, (b) stellar feedback, (c) MBH accretion, and (d) MBH feedback, work self-consistently in one comprehensive framework. As an example, the radiation and jets from the MBH heat up the surrounding gas and create hot regions, but the thermal couplings of the radiative and mechanical energy are all carried out by the shock-capturing radiation hydrodynamics AMR scheme itself, not by any presupposed thermal deposition model. In our framework, one should also be able to couple small-scale physics (such as molecular cloud formation and feedback) with large-scale physics (such as quasar-driven galactic outflows) without any sub-resolution model. These first results undoubtedly demonstrate that we can now develop an unabridged, self-consistent numerical framework for both galaxies and MBHs.

Chapter 4

Merging of Galaxies on Adaptive Mesh Refinement

"The important thing in science is not so much to obtain new facts as to discover new ways of thinking about them."
— William Bragg (1890-1971)

In hierarchical structure formation, merging of galaxies is frequent and known to dramatically affect their properties. To comprehend these interactions high-resolution simulations are indispensable because of the nonlinear coupling between pc and Mpc scales. To this end, we present the first adaptive mesh refinement (AMR) simulation of two merging, low mass, initially gas-rich galaxies ($1.8 \times 10^{10} M_{\odot}$ each), including star formation and feedback. With galaxies resolved by $\sim 2 \times 10^7$ total computational elements, we achieve unprecedented resolution of the multiphase interstellar medium, finding a widespread starburst in the merging galaxies via shock-induced star formation. The high dynamic range of AMR also allows us to follow the interplay between the galaxies and their embedding medium depicting how galactic outflows and a hot metal-rich halo form. These results demonstrate that AMR provides a powerful tool in understanding interacting galaxies.

The results are published in *The Astrophysical Journal Letters*, 2009, Volume 694, L123, and in First Stars III Conference AIP Conference Proceedings, Volume 990, pp. 429-431 (2008). These articles are coauthored by John Wise and Tom Abel.

4.1 Introduction

Decades of work have been devoted to the study of interacting and merging galaxies, as they play essential roles not only in shaping present-day galaxies (Toomre, 1977, "merger hypothesis"), but also in constructing large scale structures from the bottom up (White and Rees, 1978, "hierarchical structure formation"). Because of the nonlinear coupling between pc (star forming regions) and Mpc scales (the distance at which tidal interactions occur) accurate numerical studies are imperative to comprehend the evolution of interacting galaxies. Although the morphology of merger remnants has been well reproduced by N-body simulations since the pioneering work by Toomre and Toomre (1972), and various physical characteristics and merger-driven starbursts have been successfully analyzed with smoothed particle hydrodynamics (SPH) simulations (Barnes and Hernquist, 1996; Mihos and Hernquist, 1996; Springel et al., 2005a,b; Di Matteo et al., 2005; Cox et al., 2006a,b; Mayer et al., 2007; Li et al., 2007a; Saitoh et al., 2008), a complete, self-consistent simulation of galaxy mergers has not yet been perfected.

First, SPH simulations tend to have coarse resolution in an interstellar medium (ISM), leading to the over-mixture of different gas phases (Agertz et al., 2007; Tasker et al., 2008). Therefore, straightforward SPH simulations might have complications in realizing a multiphase medium, in capturing shock-induced star formation, in converting thermal feedback to a kinetic motion, and thus in showing how feedback makes a difference in galactic evolution self-consistently, though different formulations and sub-resolution models alleviated the problems (Marri and White, 2003; Springel and Hernquist, 2003a; Barnes, 2004; Scannapieco et al., 2006).

Second, since gaseous halos and an intergalactic medium (IGM) have not been sufficiently resolved in SPH simulations, it is not easy to investigate the interplay between a galactic disk and a diffuse embedding medium. For instance, Cox et al. (2006a) emphasized that a galactic halo should be included to accurately study the galactic wind and the enrichment process powered by feedback and mergers. Yet because of their Lagrangian nature and smoothing scheme, SPH simulations might not have sufficient resolution to follow the evolution of the diffuse medium and the

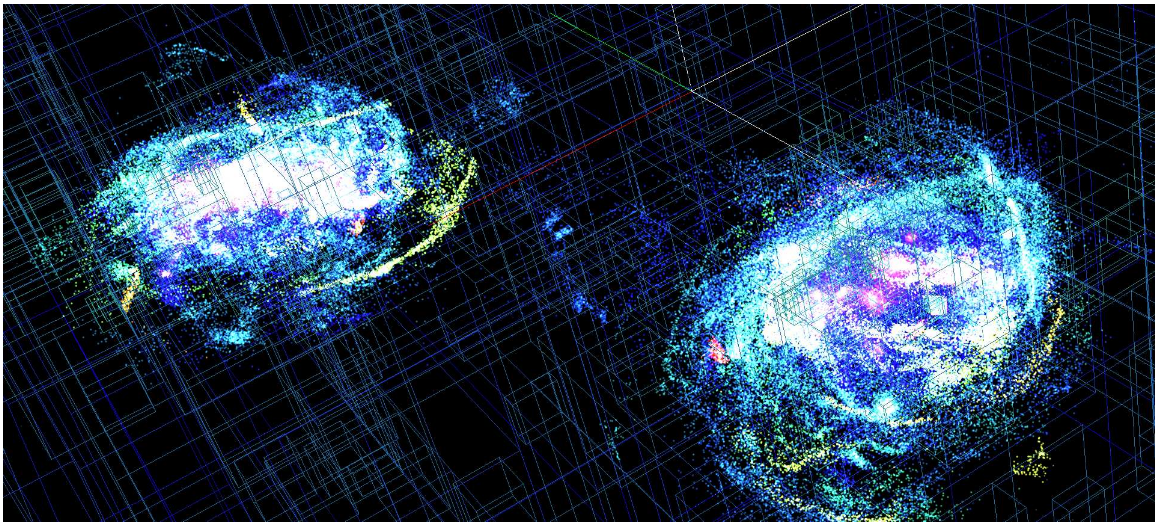

Fig. 4.1.— The snapshot of merging galaxies on adaptive mesh refinement. Visualization by Ji-hoon Kim and Tom Abel with *PartiView*, an interactive data visualization tool developed by National Center for Supercomputing Applications (NCSA), publicly available at http://www.haydenplanetarium.org/universe/partiview. Particles represent the clusters of stars colored by their ages. The boxes show adaptive meshes used in the calculation.

galactic outflow.

In light of these needs, an adaptive mesh refinement (AMR) technique potentially provides a uniquely useful tool to address these issues, allowing us to realize a self-consistent, high-resolution galaxy merger simulation. As proven by an increasing number of groups (Tassis et al., 2003, 2008; Kravtsov and Gnedin, 2005; Ceverino and Klypin, 2009; Dubois and Teyssier, 2008) AMR simulations have been highly successful in resolving the detailed structure of galactic evolution. In order to make use of the advantages of AMR such as the high dynamic range and reliable shock resolution, we utilize the AMR code *Enzo* (Bryan et al., 2001; O'Shea et al., 2004). In this *Letter*, we focus on the the first of its kind AMR simulation of two merging, low mass, initially gas-rich galaxies, including star formation and feedback, with special emphases on shock-induced star formation and the hot gas outflows.

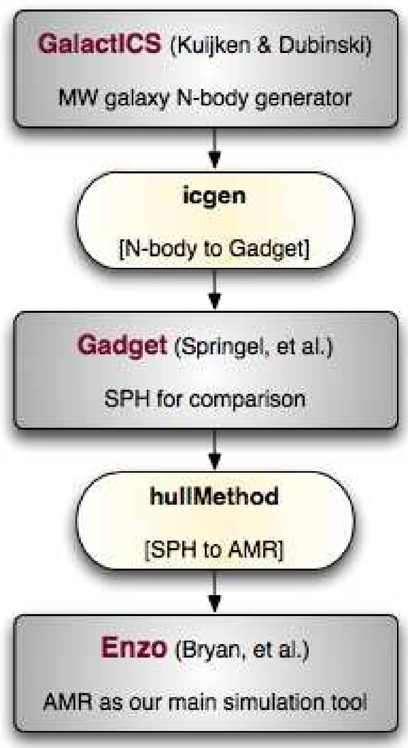

Fig. 4.2.— Dataset conversion pipeline from *GalactICS* (Kuijken and Dubinski, 1995) to *Gadget* (Springel et al., 2001), and then to *Enzo*

4.2 The Simulations

We first present a method to interpolate particle data onto an Eulerian adaptive mesh. This allows us to study galaxy mergers and evolution using the cosmological adaptive mesh refinement (AMR) code *Enzo* (Bryan and Norman, 1997; O'Shea et al., 2004). This pipeline also makes it straightforward to compare smooth particle hydrodynamics (SPH) simulations with AMR simulations of the same physical system. We also present the evolution of a stable disk galaxy and test whether the same system moving at 220 km/s across the grid show the same physical evolution.

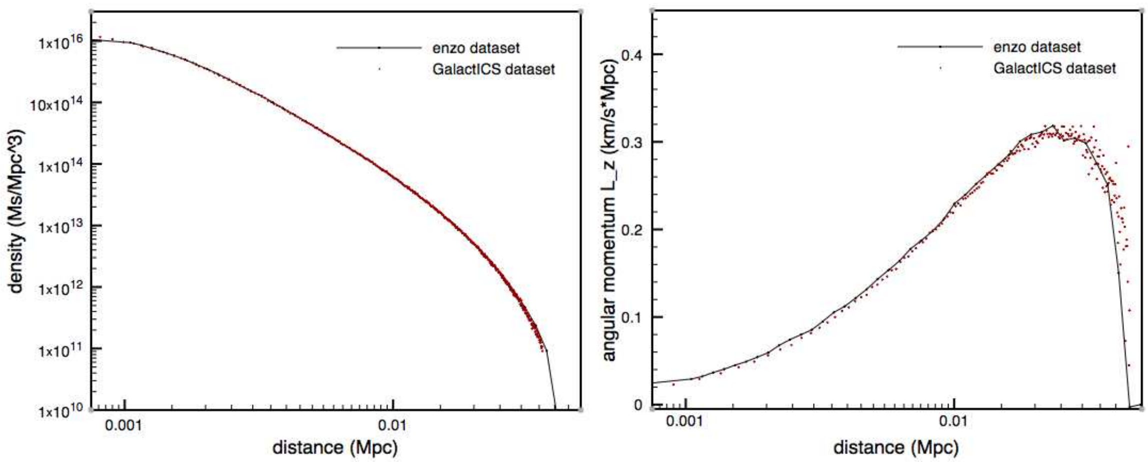

Fig. 4.3.— Comparison of radial profiles before and after the data conversion pipeline: gas radial density (left) and mass weighted gas angular momentum L_z (right) calculated in GalactICS/icgen (dots) and in *Enzo* (solid line)

4.2.1 Data Conversion Pipeline

We developed a data conversion method which converts a galactic N-body dataset of *GalactICS* (Kuijken and Dubinski, 1995) to an SPH dataset for *Gadget* (Springel et al., 2001), and then to an adaptive mesh for *Enzo* employing Delaunay tessellation onto an oct-tree structure. This pipeline, illustrated in Figure 4.2, inherently facilitates a comparison test between SPH and AMR simulations of the same physical system.

GalactICS to Gadget converter *icgen* can generate gas particles in disk and halo by splitting collisionless particles of N-body data. Because the fraction of dark matter particles in N-body data are transformed to halo SPH particles with the same velocity dispersion, they will virialize to the desired virial temperature automatically.

Gadget to *Enzo* converter *hullMethod* employs IDL function `qhull` (Delaunay triangulation) and `qgrid3` (linear interpolation) to reconstruct the density map using particle dataset. It uses an oct-tree structure to grid particle data onto an adaptively refined mesh. This conversion routine is similar to Delaunay tessellation field estimator (DTFE) method (Pelupessy et al., 2003) except the fact that we use the density value at each particles' position precalculated by Gadget's density estimator.

Using the particle data of a galactic sized halo with both the dark matter and the gas Kim et al. (2008) demonstrated the compatibility of the initial N-body dataset and the adaptive mesh produced through the pipeline. For example, Figure 4.3 shows radial profiles calculated at two different places of the conversion process: at the start (*GalactICS*) and at the end (*Enzo*). We can observe clear agreement between the two datasets confirming sufficient validity and functionality of our pipeline. A suite of functionality checks finds very satisfactory results enabling us to study galaxy evolution with AMR.

4.2.2 Simulation Code

Included Physics

The high-resolution Eulerian AMR code *Enzo* captures the gravitational collapse of turbulent fragmentation with very high spatial resolution (e.g. Wise et al., 2008) and attains multiphase gas dynamics in the ISM as it sharply resolves shocks and phase boundaries (Tassis et al., 2003; Slyz et al., 2005; Agertz et al., 2007; Tasker et al., 2008). *Enzo* also contains all relevant physics previously discussed in simulating galaxy evolution processes (Tasker and Bryan, 2006, 2008).

We employ the ZEUS hydrodynamics module included in *Enzo* to evolve the gas. Radiative cooling is used by adopting Sarazin and White (1987) to follow the equilibrium cooling function down to 10^4 K, and Rosen and Bregman (1995) further down to 300 K. This treatment will ensure a thin galactic disk forms by being cooled below 10^4 K, the approximate T_{vir} of the ISM in a galactic disk. The cutoff at 300 K roughly models the temperature floor provided by nonthermal pressure such as cosmic rays and magnetic fields (Rosen and Bregman, 1995).

Galaxies are placed in a box of 4 Mpc on a side to ensure enough space for galactic tidal interactions and to reduce any boundary effect. The top grid of 128^3 cells is allowed to recursively refine up to 13 levels based on the baryonic mass and the dark matter mass in each cell, achieving 3.8 pc resolution in the ISM. This value is in accord with the Jeans length for a dense gas clump of $n = 10^3$ cm^{-3}, at which a corresponding Jeans mass of $2 \times 10^3 M_\odot$ collapses to form a star particle. In this way, merging galaxies are resolved with $\sim 2 \times 10^7$ total computational elements, surpassing any numerical studies conducted thus far on galaxy mergers including gas.

Our star formation criteria are based on Cen and Ostriker (1992) with several important modifications. A cell of size Δx produces a star particle of $m_* = \epsilon \rho_{\rm gas} \Delta x^3$ (ϵ=0.5, a star formation efficiency) when *(i)* the gas density exceeds $n_{\rm thres} = 10^3$ cm^{-3}, *(ii)* the flow is converging, *(iii)* the cooling time is shorter than the dynamical time, and *(iv)* the particle produced has at least $10^3 M_\odot$. We do not impose any stochastic star formation unlike Tasker and Bryan (2006) or Stinson et al. (2006). With these revisions, our criteria guarantee that a star particle forms before an unphysically large mass begins to accrete onto any unresolved dense gas clump.

The energy loss by radiative cooling can be replenished by thermal stellar feedback. For each star particle, 5×10^{-6} of its rest mass energy and 25% of its mass are returned to the gas over the dynamical time of the particle. This corresponds to 10^{51} ergs per every $110 M_\odot$ deposited as stellar mass and represents various types of feedback such as protostellar outflows (Li and Nakamura, 2006), photoionization (McKee, 1989), stellar winds, and Type II supernovae explosions (Tasker and Bryan, 2006). This thermal feedback heats $\sim 10^3 M_\odot$ in a $<$10 pc cell up to $\sim 10^7$ K, but a multiphase medium is naturally established because the cooling time of these hot cells is always much longer than the sound crossing time.

Advection Test

Lastly, we put *Enzo* to the test for translational invariance. Many research topics, such as high-resolution galaxy mergers with diffuse gas halos, would benefit from an AMR approach to galaxy simulations. Therefore validating an acceptable level of translational invariance of the AMR code (i.e. how *practical* it is in the context of problem in which the code is utilized?) is very important (Tasker et al., 2008).

To check the translational invariance of the simulation code, we performed a simulation that compares two isolated galaxies: one is fixed in space and the other is moving at 220 km/s across the grid. Each has total mass of $3.16 \times 10^{11} M_\odot$ with 1.5% gas in disk and halo. It has 10^5 dark matter particles and 2.2×10^5 star particles, all of which are set up through the pipeline previously described. To draw a proper comparison, the background intergalactic medium of the moving galaxy also

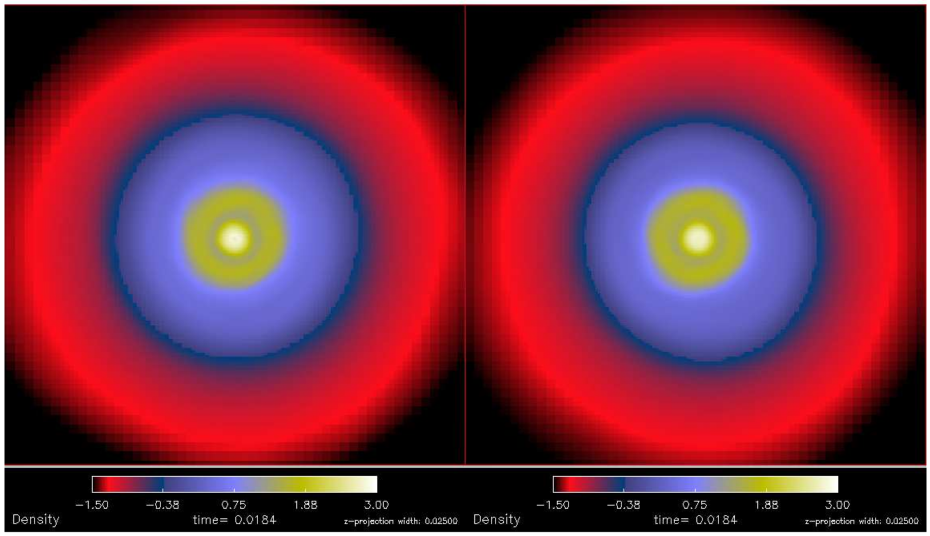

Fig. 4.4.— Face-on gas surface density of the stationary galaxy (left) and the moving galaxy (right) after 1.36 Gyrs. The right one has moved by 0.31 Mpc. The width shown is 0.1 Mpc.

moves at 220 km/s. We use 3-dimensional ZEUS hydrodynamics algorithm in *Enzo* while we assume adiabatic cooling and no star formation or feedback. The maximum resolution in this calculation is 120 pc.

Figures 4.4 and 4.5 depict gas surface density and gas circular velocity. These two galaxies show the same physical evolution and a very close resemblance of profiles. The moving galaxy simulation takes about 50% more calculation time than that of the stationary galaxy. Even though these model galaxies don't seem to be stable enough to maintain their initial profiles, this results from unrealistic physical conditions, such as adiabatic cooling, and should not affect our conclusion.

These early tests described above are encouraging and demonstrate that *Enzo* is well suited for studying galaxy evolution as has been shown previously by Tasker and Bryan (2006).

4.2.3 Initial Conditions

The individual galaxy progenitor we modeled has a total mass of $1.8 \times 10^{10} M_\odot$ with 10% in gas (R_{vir} = 65 kpc at z=0). Because we generate gas grids by splitting

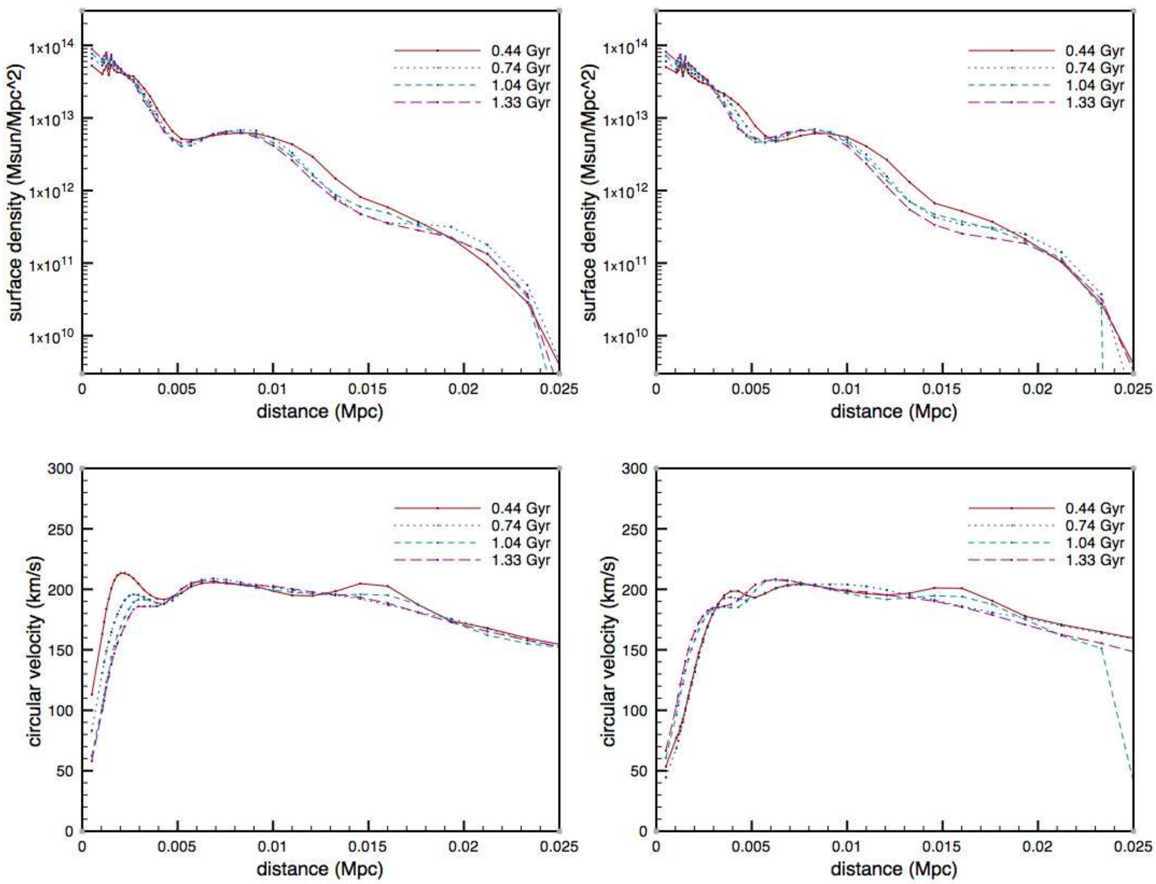

Fig. 4.5.— Comparison of galaxy profiles for the first 1.36 Gyrs: gas surface density (top) and gas circular velocity (bottom) for the stationary galaxy (left column) and the moving galaxy (right column).

10^5 collisionless particles in N-body data with the same density profile and velocity dispersion, the gas will virialize to the desired T_{vir} of the galactic halo automatically. A spin parameter λ=0.055 is given to cause the progenitor to form a disk galaxy with a gaseous halo within a few hundred Myrs. In addition, this galaxy progenitor is bathed in a warm (10^5 K) diffuse background IGM; an initial metallicity of $10^{-4}Z_{\odot}$ is also set up everywhere to follow the metallicity evolution. For a merger simulation, two identical galaxy progenitors are separated by 100 kpc and set on a prograde hyperbolic (e=1.1) coplanar collision course with a pericentric distance of 4 kpc. The initial separation is large enough to form individual galaxies before the first passage,

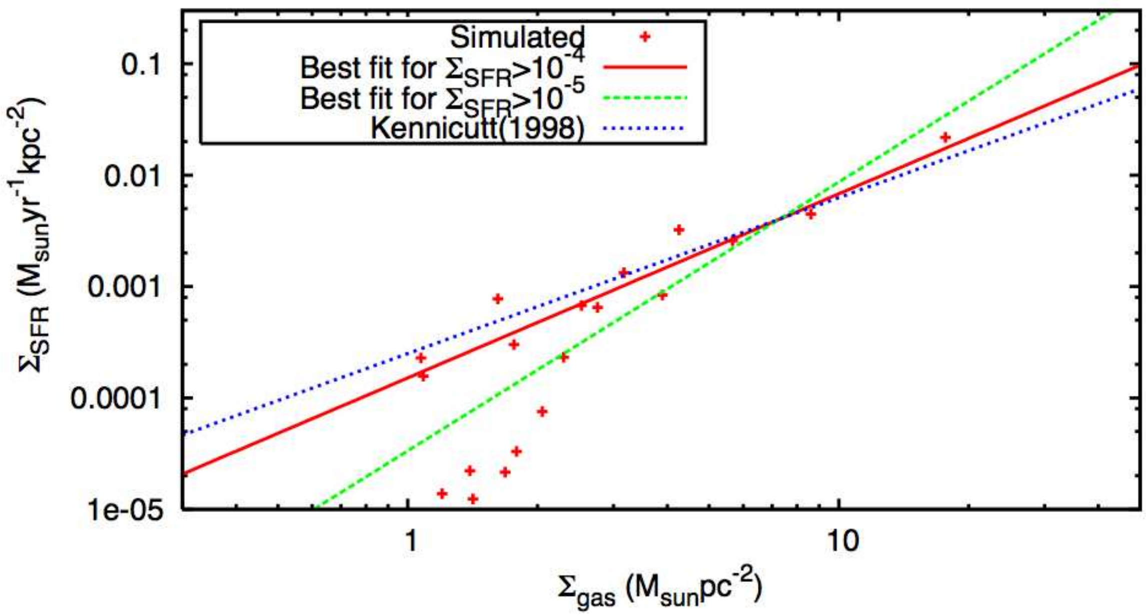

Fig. 4.6.— The global K-S relation for an isolated galaxy: time variation of the relationship between global SFR and gas surface density. Each data point represents a different epoch, equally spaced in 5 Gyr. The solid line is the best fit for simulated data of $\Sigma_{\rm SFR} > 10^{-4} M_{\odot}{\rm yr}^{-1}{\rm kpc}^{-2}$, and the dashed line for $\Sigma_{\rm SFR} > 10^{-5} M_{\odot}{\rm yr}^{-1}{\rm kpc}^{-2}$. The dotted line is from Kennicutt (1998).

and to observe the collision interface between the two gaseous halos.

4.3 Results

4.3.1 Properties of An Isolated Galaxy Model

We first examine how well our isolated galaxy formation simulation fits the global Kennicutt-Schmidt (K-S) relation between global star formation rate (SFR) and gas surface density, namely $\Sigma_{\rm SFR} \propto {\Sigma_{\rm gas}}^{1.4}$ (Kennicutt, 1998). To calculate both densities, we select a disk of radius 2.8 kpc so that 95% of created stars is contained in it after 5 Gyr; the gas surface density is averaged over the cells where the gas density exceeds $n = 4.0 \times 10^{-3}\,{\rm cm}^{-3}$. Figure 4.6 shows our star formation criteria and feedback correctly match the observed K-S relation, as other simulation works did (e.g.

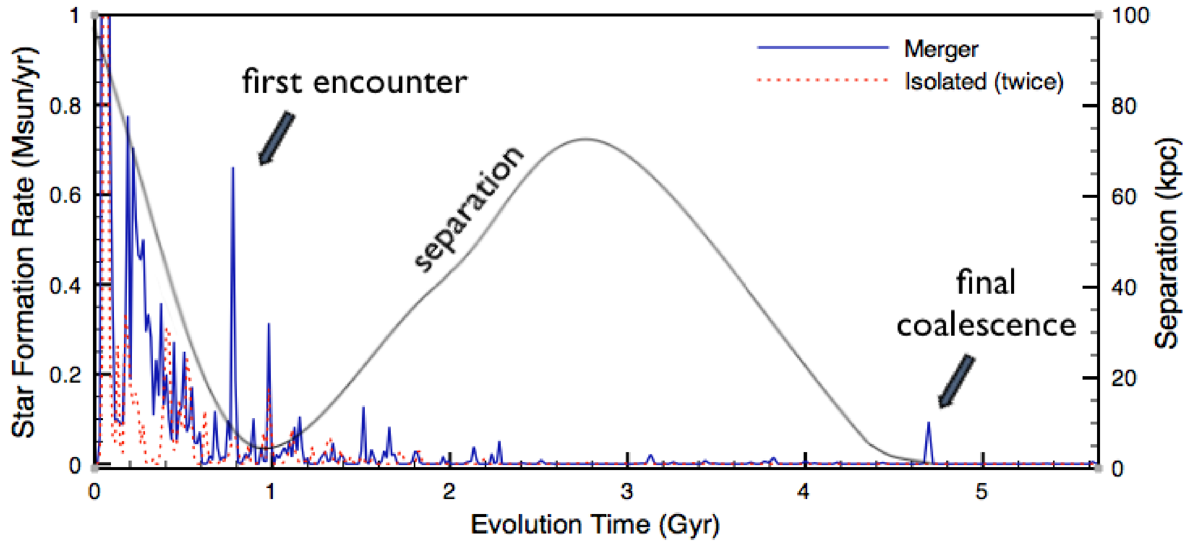

Fig. 4.7.— The global SFR as a function of time during the galaxy merger run and the isolated galaxy formation run (twice the value). The separation between the centers of two galaxies is also displayed.

Robertson and Kravtsov, 2008). The closest match to the K-S relation occurs when we restrict the fit to $\Sigma_{\rm SFR} > 10^{-4} M_{\odot}{\rm yr}^{-1}{\rm kpc}^{-2}$, which happens mostly in the first 2 Gyr, following an observational cutoff as in Kennicutt (1998).

4.3.2 Star Formation History in A Galaxy Merger

The global SFR of the merger simulation is displayed in Figure 4.7. It presents the initial stellar disk formation for each galaxy in the first ~0.6 Gyr, and several merger-driven starbursts afterwards, notably when two galaxies first encounter (~0.8 Gyr) and when they finally coalesce to form one galaxy (~4.7 Gyr). A low SFR between these two bursts confirms the regulated star formation by stellar feedback.

Snapshots of the merger sequence at four different epochs are compiled in Figure 4.8. The top row shows the density-weighted projection of density, in which irregular gas filaments, bridges and rings are formed by the compression of gas and turbulence. The middle row depicts the temperature sliced at the collisional plane, where cold gas

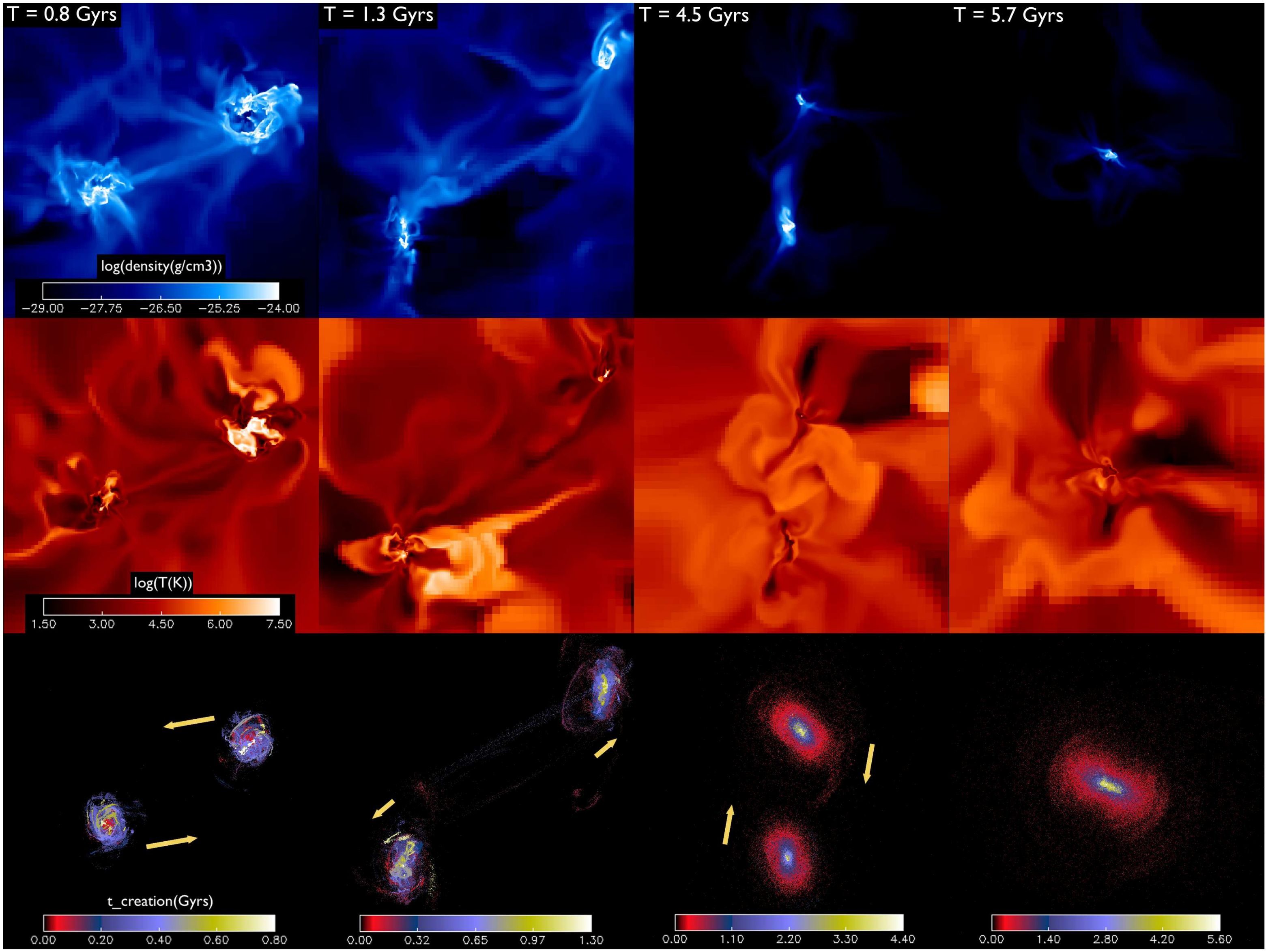

Fig. 4.8.— Density-weighted projection of density (top), temperature sliced at the orbital plane (middle), and stellar distributions colored by creation time (bottom) in the central 40 kpc, after 0.8, 1.3, 4.5, and 5.7 Gyr. High-resolution images and movies are available at http://www.slac.stanford.edu/∼mornkr/.

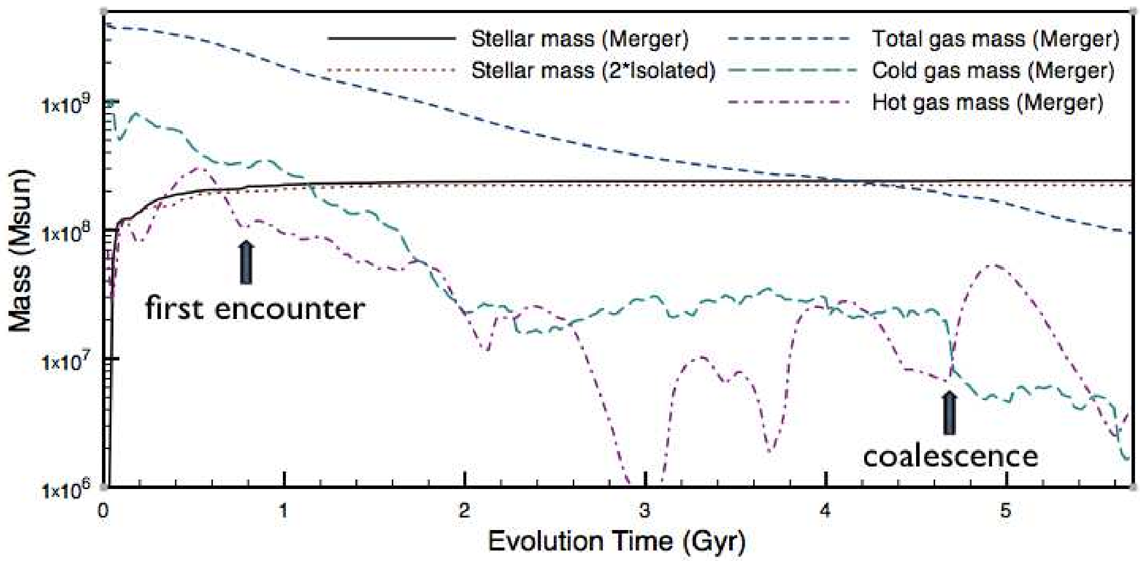

Fig. 4.9.— The evolution of the stellar mass (solid line for the merger run and dotted line for twice the value of the isolated galaxy) and the gas mass remaining in the central 200 kpc cube (short dashed line). Cold (T $< 10^3$ K) and hot (T $> 10^5$ K) gas masses are also shown (long dashed line and dot-dash line, respectively).

clumps and hot supernovae bubbles coexist side by side forming a complex, yet well-resolved multiphase medium. It also reveals how hot supernovae bubbles propagate through the diffuse embedding medium of the halo and the IGM. In the bottom row of stellar distributions colored by creation time, both merger-induced nuclear starbursts *and* shock-induced widespread starbursts are noticeable. Because of the finer resolution in the ISM, it is easier to resolve local dense clumps driven by shocks and the ensuing star formation. In contrast, SPH simulations often report predominantly nuclear starbursts (Barnes, 2004).

4.3.3 Gas Outflows and Formation of A Hot Gaseous Halo

The evolution of the stellar and gas mass in the central 200 kpc box is plotted in Figure 4.9. The gas expulsion via stellar feedback and galactic interaction is pronounced as more than 90% of the gas has been expelled in the first 4 Gyr. This gas eventually escapes the gravitational potential of the system or has not had enough time to fall back onto the galaxies. This massive gas depletion is prominent especially in low mass mergers because of the shallow gravitational well. As for the merger remnant at 5.7 Gyr, the remaining gas mass is $\sim$35% of the stellar mass and still decreasing rapidly. The amount of cold gas (T $<10^3$ K) available for future star formation is only $<$1% of the stellar mass, depicting how star formation is quenched by feedback heating and gas expulsion.

The gas disrupted by galactic interaction and heated by feedback creates a galactic wind of $>$200 km/s reaching as far as 1 Mpc from the simulated merging galaxies. This hot metal-loaded outflow is responsible for building the gaseous halo around galaxies as well as enriching some regions of the IGM up to a supersolar metallicity. As a result, a hot metal-rich halo is generated ($\rho \sim 10^{-29}$gcm^{-3}, T $\sim 10^{6-7}$ K) and sustained by continuous stellar feedback, as suggested by analytic models (e.g. Tang et al., 2008). Although the galactic outflows and the halo are very diffuse, their evolution is easily followed in AMR, as can be clearly seen in Figure 4.10 of the joint probability distribution functions (PDFs) on density-temperature planes. It also illustrates the wide range of densities and temperatures that are followed here.

4.4 Summary

Our simulation, for the first time, followed the self-consistent evolution of low mass merging galaxies with AMR at unprecedented resolution. Our findings are as follows.

First, as AMR naturally establishes a multiphase medium without any sub-resolution model, we have captured shock-induced star formation that occurs when merging galaxies compress the intervening gas (Barnes, 2004; Saitoh et al., 2008). The well-resolved shocks trigger a widespread starburst, in accord with observations (e.g. Schweizer, 2006). Further, the overcooling problem is absent as in Ceverino and Klypin (2009) because the multiphase medium is resolved by $<$10 pc cells, and the thermal feedback is sufficient to heat such small cells up to $\sim 10^7$ K.

Second, utilizing the high dynamic range and the Eulerian nature of AMR, we have followed the evolution of the hot diffuse medium of gaseous halos and the IGM as far as 1 Mpc away from the galaxies. This allows us to explore the interplay

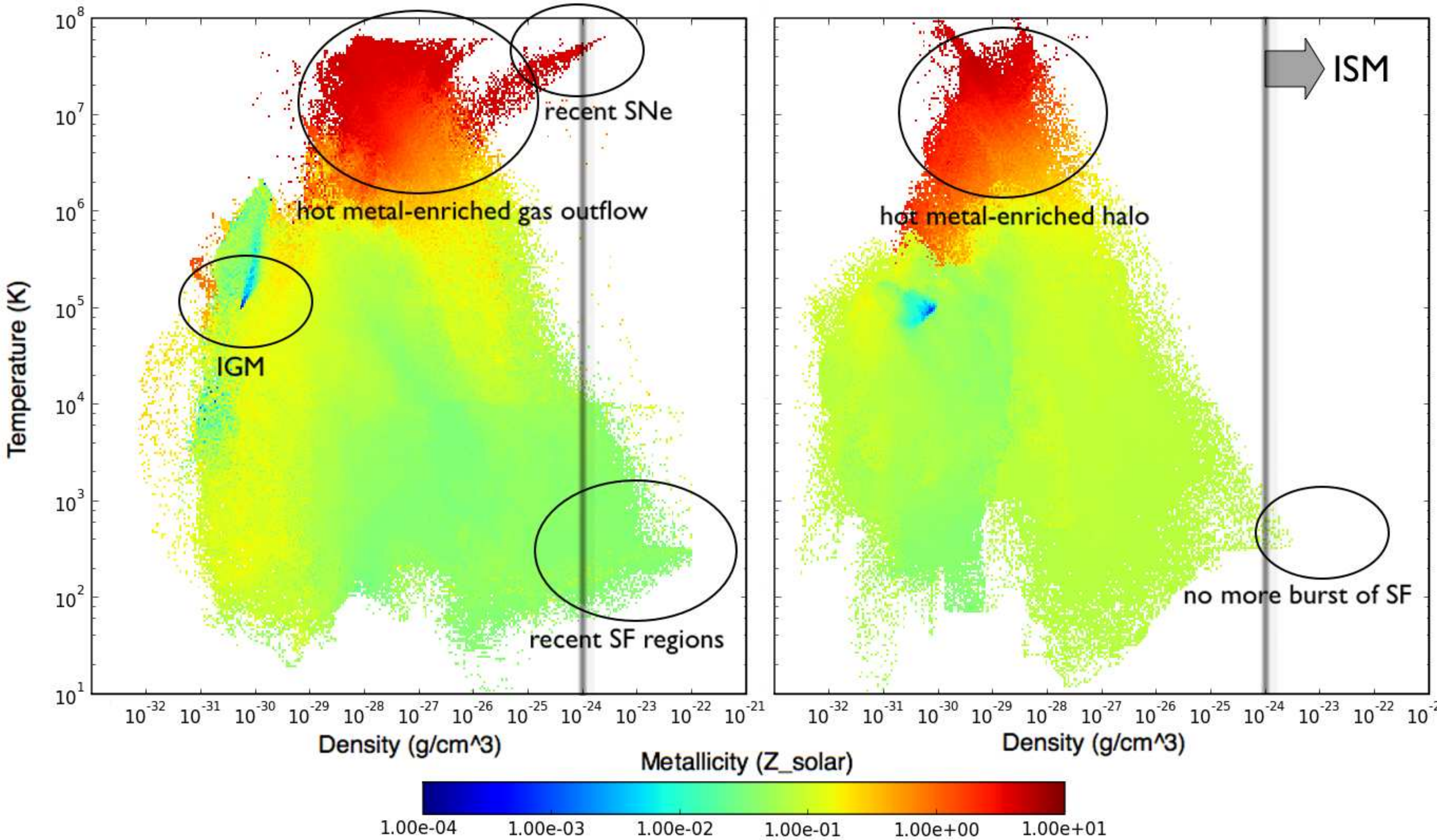

Fig. 4.10.— Joint density-temperature PDFs, colored by metallicity, for a 400 kpc sphere centered on the galaxy, after 0.8 Gyr (left) and 5.7 Gyr (right). Star forming regions, supernovae bubbles, gas outflows, and the halo are pointed out, proving the wide range of densities and temperatures followed here.

between the galactic outflows and the embedding medium and to demonstrate that a hot metal-rich halo forms around the galaxies from stellar feedback (Cox et al., 2006a). The massive gas expulsion in low mass merging galaxies leads to a high mass-to-light ratio, as it creates a merger remnant without much cold gas left for later star formation.

Although it should be considered provisional, our result brings compelling evidence that AMR delivers a uniquely powerful tool in understanding merging galaxies, while it addresses several issues SPH has suffered from. Comprehensive parameter studies should follow, especially in the efficiency of stellar feedback and the metal yields of stars; the results should be compared and calibrated with observations such as the mass-metallicity relation (Tremonti et al., 2004), galactic outflows (Martin, 2006), galactic morphology (Park and Choi, 2008), and gas to stellar mass ratio (Gavazzi et al., 2008). Physics such as UV photoelectric heating, cosmic rays, and magnetic fields are missing in this work, but will need to be considered in the future.

Chapter 5

Galaxy Mergers with Stars and Massive Black Holes

"The most exciting phrase to hear in science, the one that heralds new discoveries, is not 'Eureka!' but 'That's funny.' "
— Issac Asimov (1920-1992)

Merging of galaxies is important not just because it is the way to form larger systems in the bottom-up hierarchical structure formation, but because it is known to trigger massive star formation and active galactic nuclei (AGN). In order to comprehend this process, we carry out a simulation of two merging galaxies, $2.1 \times 10^{11} M_\odot$ each, with their $10^5 M_\odot$ embedded massive black holes (MBHs), portraying an analogue of merger-induced quasar-mode feedback by fast growing MBHs for which the accretion rates are $> 5\%$ of the Eddington limit. We find that the feedback from the fast growing MBHs helps to reduce the global star formation on the disk. When compared with the feedback by a slowly growing MBH, these MBHs drive more frequent jets creating sizable bubbles at the galactic centers.

This chapter is included in the publication which will be submitted to *The Astrophysical Journal*. This paper is coauthored by John Wise, Marcelo Alvarez, and Tom Abel.

5.1 Introduction

In the hierarchical structure formation paradigm of ΛCDM cosmology, merging of galaxies is a major piece of the puzzle in understanding the evolution of galaxies. A direct collision between the galactic gas content in galaxy mergers instigates massive starbursts, and triggers quasar activities (Hopkins et al., 2008). The morphology and properties of the galaxies are also drastically altered by the direct mechanical agitation, violent relaxation, and induced star formation. Especially when two comparable mass galaxies merge, the remnant could often be devoid of the star-forming gas; this is because the fuel for star formation has been violently consumed in the merger-driven starburst, and also because the triggered quasar occasionally prompts massive gas expulsion. Hence, such major mergers are thought to be responsible for creating giant red ellipticals.

In the final phase of the galaxy merger, the massive black holes (MBHs) at the centers of the galaxies merge, too. Merging of black holes is believed to cause a rapid growth of a supermassive black hole (SMBH) which would not have been feasible had it accumulated its mass only by gas accretion (Haiman and Loeb, 2001). In fact, successive merging of galaxies is considered to be one of many viable scenarios to build SMBHs at high redshift (Fan et al., 2006; Shemmer et al., 2006) from stellar mass black holes of Pop III star remnants. Another evidence which suggests the interwoven evolution of galaxies and MBHs is the observation of tight correlations between the black hole masses and bulge masses (Magorrian et al., 1998; Häring and Rix, 2004), between the black hole masses and bulge velocity dispersions (Ferrarese and Merritt, 2000; Gebhardt et al., 2000; Gültekin et al., 2009), and even between the black hole masses and the numbers of galactic globular clusters (Burkert and Tremaine, 2010). These observations have led to a scientific consensus that the host galaxies and their embedded MBHs have grown together under each other's influence (Silk and Rees, 1998; Kauffmann and Haehnelt, 2000; Wyithe and Loeb, 2003).

Studying the merging of galaxies and MBHs, and the triggered feedback during the process is therefore critical to build a realistic theory of galaxy formation. Due to the nonlinear coupling between the widely different scales and physical processes involved, numerical simulations are naturally required to investigate this phenomenon. Indeed, high-resolution numerical simulations of galaxy mergers such as Springel et al. (2005b) and Di Matteo et al. (2005) (see also Johansson et al., 2009; Booth and Schaye, 2009) have provided remarkable insights to the problem. These studies have successfully reproduced the change of galactic morphology at various stages of mergers, the merger-induced starbursts at close encounters, and the sudden gas inflow towards the galactic center triggering the growth and feedback of MBHs.

Nevertheless, it worth noting that many previous simulations of merging galaxies with MBHs lack either (1) the sufficient numerical resolution or (2) the accurate descriptions of baryonic physics and MBH physics. As an example, Kim et al. (2009) demonstrated that having a $\sim$ 3.8 pc resolution in the interstellar medium is essential to properly capture the clumpy star formation on the disks and spirals (see also Teyssier et al., 2010a). The high dynamic range of adaptively refined mesh was instrumental also in keeping track of the interplay between galactic disks and the embedding halos. Yet such high resolution has been only occasionally attained by previous studies of merging galaxies. Furthermore, complications still remain in describing galactic baryonic physics in simulations. For example, the key challenge in quasar formation studies is to describe how the MBH acquires its mass, and how it affects its host galaxy through feedback. However, previous studies have had to empirically boost the Bondi accretion estimate by 10 - 300 to compensate for coarse resolution (see the discussions by Booth and Schaye (2009) and Kim et al. (2010)). Poor resolution has also forced simulators to skip the detailed thermalization process below the resolution limit, and to simply thermally deposit a fixed fraction of the MBH feedback energy in the vicinity of the MBH (e.g. Springel et al., 2005b; Li et al., 2007b; Sijacki et al., 2009). These sub-resolution approaches often add too many tunable parameters to an already complicated problem, thus making it hard to explore the problem with least number of prior assumptions.

However, thanks to the expeditious developments of both numerical techniques and computer hardwares, more accurate simulations are now feasible at cheaper costs with better numerical resolution. And new ways to overcome the limitations of previous galaxy merger simulations with MBHs are begining to emerge. Taking the full advantage of the numerical techniques available, in the earlier paper in this series (Kim et al., 2010), a self-consistent numerical framework for galactic scale simulations is developed which is ideal to track how galaxies and MBHs evolve under each other's influence. The high-resolution adaptive mesh refinement (AMR) code *Enzo* was modified to model the formation and feedback of molecular clouds at their characteristic scale of 15.2 pc and the accretion of gas onto a MBH. Rather than using the thermal feedback prescription, they employed two channels of MBH feedback: radiative feedback (X-ray photons followed through full 3D adaptive ray tracing) and mechanical feedback (bipolar jets resolved in high-resolution AMR). Utilizing this framework, they investigated the coevolution of a massive star-forming galaxy and its embedded MBH at $z \sim 3$ in a cosmological ΛCDM simulation. They found that the MBH feedback locally suppresses star formation in the galactic inner core, and self-regulates its own growth by keeping the surrounding interstellar medium hot for an extended period of time.

In this second paper of the series, we extend the use of the same numerical framework of Kim et al. (2010) with slight modifications to carry out a simulation of two merging galaxies, $2.1 \times 10^{11} M_\odot$ each, with $10^5 M_\odot$ embedded MBHs. We avoid the use of an *ad hoc* prescription of MBH feedback, and focus on how the interstellar medium (ISM) and star formation on the disks are affected by triggered MBH feedback in mergers. While Kim et al. (2010) explored the quiescent form of feedback by a slowly growing MBH (a "radio-mode" analogue), merging of galaxies in this work would cause the gas funnel into galactic centers triggering a more violent form of feedback (possibly a "quasar-mode" mode analogue; Hopkins et al., 2008).

This article is organized as follows. The brief explanation on the simulation code is given in §5.2, and the initial condition of our experiments is described in §5.3. §5.4 is devoted to the results of our experiments, with an emphasis on the feedback-regulated star formation. We also discuss the possible future directions of this project. Assembled in §5.5 are the summary and conclusions.

5.2 Simulation Code

Our enhanced version of *Enzo-2.0*[1] (Bryan and Norman, 1997; Norman and Bryan, 1999; Norman et al., 2007) contains all relevant physics previously discussed in galactic simulations as well as several new physics discussed in detail in Kim et al. (2009) and Kim et al. (2010). The comprehensive framework developed by Kim et al. (2010) is designed to circumvent the limitations of previous studies and follow the actual physical processes between gas, stars, and MBHs. This allows us to perform a fully self-consistent galactic simulation integrating all galactic components simultaneously. While the detailed descriptions are given in Kim et al. (2010) we briefly summarize the key features, focusing on a few modifications when compared with Kim et al. (2010).

5.2.1 Hydrodynamics, Refinement, and Chemistry

We use the ZEUS hydrodynamics module included in *Enzo* to solve the Euler equations for the collisional fluid (Stone and Norman, 1992a,b; Anninos and Norman, 1994). Dark matter, stars, and MBHs are treated as collisionless particles. The grids are adaptively refined by factors of 2 in each axis on gas and particle overdensities. The mass thresholds, $M_{\rm ref}$, above which a cell refines are functions of a refinement level l as

$$M^l_{\rm ref,gas} = 2^{-0.817l} M^0_{\rm ref,gas} \quad \text{and} \quad M^l_{\rm ref,part} = 2^{-0.419l} M^0_{\rm ref,part} \tag{5.1}$$

with $M^0_{\rm ref,gas} = M^0_{\rm ref,part} = 1.2 \times 10^7 M_\odot$. This makes the simulation super-Lagrangian, refining the grids more on small scales. At $l = 11$ it gives 15.2 pc resolution. This value is in accord with the Jeans length for a dense gas clump of $n = 125$ cm^{-3} at $\sim$200 K, at which point a corresponding Jeans mass of 16000 $M_\odot$ collapses to spawn a molecular cloud particle. We choose the Courant-Friedrichs-Lewy safety number of 0.3 so the marching timestep is less than the time for the advecting wave to reach the adjacent cell. Non-equilibrium chemistry model is employed to track H, H$^+$,

[1] http://enzo.googlecode.com/

He, He^+, He^{++}, and e^- by following six collisional processes among them. At the same time, *Enzo*'s cooling module computes the radiative loss of internal gas energy (Anninos et al., 1997). The metallicity-dependent metal cooling rates are added to these primordial cooling rates: Sutherland and Dopita (1993) above 10^4 K; Glover and Jappsen (2007) below 10^4 K. Photoionization heating by the metagalactic UV background of quasars and galaxies is also considered (Haardt and Madau, 1996, 2001) with an approximate self-shielding (Cen et al., 2005).

5.2.2 Molecular Cloud Formation and Stellar Feedback

Our molecular cloud particle formation is based on Cen and Ostriker (1992) with important modifications. With the efficiency of $\epsilon_* = 0.5$, the finest cell of size $\Delta x =$ 15.2 pc and gas density $\rho_{\rm gas}$ produces a molecular cloud particle of mass

$$M_{\rm MC} = \epsilon_* \rho_{\rm gas} \Delta x^3 \tag{5.2}$$

when (a) the proton number density exceeds the threshold $n_{\rm thres} = 125\ {\rm cm}^{-3}$, (b) the velocity flow is converging, (c) the cooling time $t_{\rm cool}$ is shorter than the dynamical time $t_{\rm dyn}$ of the cell, and (d) the particle produced has at least $M_{\rm thres} = 8000\ M_\odot$. As a consequence, the gas in the finest cell is instantly converted into a particle as soon as the cell has accumulated more than $M_{\rm thres}/\epsilon_* = 16000\ M_\odot$, the Jeans mass at $n = 125$ ${\rm cm}^{-3}$ at ~ 200 K. It guarantees that a particle forms before an unphysically large mass begins to accrete onto any unresolved dense clump. Unlike previous star formation recipes based on the simple scaling of $\rho_{\rm SFR} \sim \rho_{\rm gas}^{1.5}$ (Schmidt, 1959), we deposit a particle when a gas cell of a typical molecular cloud size actually becomes Jeans unstable. For this reason, the particle formed in this way represents a *star-forming molecular cloud* that is self-gravitating, and thus decoupled from the gas on the grid. Each molecular cloud particle gradually turns 20% of the molecular cloud particle mass, $M_{\rm MC}$, into an actual stellar mass, $M_{\rm star}(t)$, over 12 $t_{\rm dyn}$. This models the slow star formation observed in molecular clouds (Krumholz and Tan, 2007). During that time, 7.5×10^{-7} of the rest mass energy of $M_{\rm star}$ and the rest of the molecular cloud mass, $0.8\,M_{\rm MC}$, are gradually returned into the cell in which the particle resides.[2] Meanwhile, 2% of the ejected mass is counted as metals, contributing to the metal enrichment of the interstellar medium.

5.2.3 Massive Black Hole Accretion in A Turbulent Medium

A seed black hole of $10^5 M_\odot$ is placed at the center of each merging galaxy. We estimate the rate of gas accretion by employing the modified Bondi-Hoyle formula in a turbulent vorticity-dominated medium, restricted by the Eddington limit (Bondi, 1952; Krumholz et al., 2006).[3]

$$\begin{aligned}\dot{M}_{\rm BH} &= \texttt{min}\,(\dot{M}_{\rm Edd}\,,\,\dot{M}_{\rm turb}) && (5.3)\\ &= \texttt{min}\left(\dot{M}_{\rm Edd}\,,\,\sqrt{\dot{M}_{\rm B}^2+\dot{M}_\omega^2}\right) && (5.4)\\ &= \texttt{min}\left(\frac{4\pi G M_{\rm BH} m_{\rm p}}{\epsilon_{\rm r}\sigma_{\rm T} c}\,,\,\frac{4\pi G^2 M_{\rm BH}^2 \rho_{\rm B}}{c_{\rm s}^3}\left[1+(0.34 f(\omega_*))^{-2}\right]^{-1/2}\right), && (5.5)\end{aligned}$$

Here $M_{\rm BH}$ is the mass of a MBH, $c_{\rm s}$ is the sound speed of the gas at the cell the MBH resides in, $m_{\rm p}$ is the mass of a proton, and $\sigma_{\rm T}$ is the Thomson scattering cross-section. The density $\rho_{\rm B}$ at the Bondi radius, $R_{\rm B} = 2GM_{\rm BH}/c_{\rm s}^2$, is extrapolated from the density $\rho_{\rm gas}$ of the cell where the MBH resides, as

$$\rho_{\rm B} = \rho_{\rm gas}\cdot\texttt{min}((\Delta x/R_{\rm B})^{1.5}, 1.0). \tag{5.6}$$

Here an $r^{-3/2}$ density profile is assumed inside the sphere of $R_{\rm B}$ (Wang et al., 2010). $f(\omega_*) = (1+\omega_*^{0.9})^{-1}$ is the function of dimensionless vorticity ω_*.

$$\omega_* = \frac{\omega R_{\rm B}}{c_{\rm s}} = |\nabla\times\mathbf{v}|\cdot\frac{2GM_{\rm BH}}{c_{\rm s}^2}\cdot\frac{1}{c_{\rm s}} \tag{5.7}$$

Note that $\dot{M}_{\rm turb}$ contains the suppression factor $[1+(0.34f(\omega_*))^{-2}]^{-1/2}$ to the Bondi-Hoyle rate due to the turbulence around the MBH. Also, the empirical boost factor

[2] 10^{51} ergs per every 750 $M_\odot$ of actual stellar mass formed

[3] Note the difference from §2.6 of Kim et al. (2010).

α of Springel et al. (2005b) is unnecessary in our formula because the high densities around the MBH is resolved with high-resolution AMR.[4] To minimize numerical artifacts, the gas mass accreting onto the MBH is subtracted uniformly from the cells within a Bondi radius.

5.2.4 Merging of Massive Black Holes

Merging of black holes is another way for MBHs to rapidly gain their masses. Yet, modeling the merging of black holes in galactic scale simulations is equally difficult as describing the gas accretion onto the black holes. When two galaxies merge, the MBHs at the galactic centers also fall together via (1) the in-spiral, (2) the ring-down, and then (3) the final coalescence. However, our numerical resolution is far from entering the regime of the general relativity and the gravitational wave generation which are needed to describe such processes (Centrella et al., 2010). Therefore we simply merge the two black holes when (a) they are separated by less than 50 pc, and (b) they are gravitationally bound (i.e. the relative velocity is smaller than the velocity of a circular orbit). This simple treatment is straightforward and popular in galactic or large scale simulations (e.g. Li et al., 2007b; Sijacki et al., 2009).

5.2.5 Massive Black Hole Feedback: Radiative and Mechanical

Enzo's radiative transfer module integrates the adaptive ray tracing technique with the hydrodynamics, energy, and chemistry solvers, and has been used in a variety of applications (Abel et al., 2007; Wise and Abel, 2010). Utilizing the similar machinery, first the luminosity of the MBH, $L_{\rm BH} = \epsilon_{\rm r} \dot{M}_{\rm BH} c^2$, is assigned to the radiation source. Then 768 ($= 12 \times 4^3$; *Healpix* level 3) rays are isotropically cast with a monochromatic energy of $E_{\rm ph} = 2$ keV, a characteristic temperature of an averaged quasar spectral energy distribution (SED; Sazonov et al., 2004, 2005; Ciotti and Ostriker, 2007). Each

[4] In order to resolve the gas around the MBH with the best resolution available, eight nearby cells close to the MBH are required to successively refine down to 15.2 pc at all times. See also the footnote 9 of Kim et al. (2010).

Table 5.1 Simulation Suite Description

Physics[a]		GM-SF	GM-RMF
Molecular cloud formation	(See §5.2.2)	○	○
Stellar feedback	(See §5.2.2)	○	○
MBH vorticity-dominated accretion	(See §5.2.3)	○	○
MBH mergers	(See §5.2.4)	○	○
MBH radiative feedback	(See §5.2.5)	×	○
MBH mechanical feedback	(See §5.2.5)	×	○

[a] For detailed explanation, see the referenced section. ○ = included, × = not included.

ray is traced until the ray reaches the edge of the computational domain or most of its photons are absorbed. It is adaptively split into four child rays whenever the area associated with a ray becomes larger than $0.2\,(\Delta x)^2$ of a local cell (Abel and Wandelt, 2002). Photons in the emitted ray interact with the surrounding gas in four ways: they (1) *photoionize* H, He, and He^+, (2) *photoheat* the gas with the excess energy above the ionization thresholds, (3) *Compton heat* the gas when they scatter off electrons (Ciotti and Ostriker, 2001), and (4) exert outward momentum to the gas when they are taken out from the ray either by photoionization or by Compton scattering. We consider the secondary ionization to estimate the photoionization and photoheating rates (Shull and van Steenberg, 1985). The radiation pressure on dust grains is ignored.

MBHs also inject the mass and momentum to describe the bipolar jets launched from the vicinity of the MBH. The kinetic power of the jets, as we introduce at $R_{\rm jet} = 30.4$ pc, is written as

$$P_{\rm kin} = \epsilon_{\rm kin} L_{\rm BH} = \epsilon_{\rm kin}\epsilon_{\rm r}\dot{M}_{\rm BH}c^2 = \frac{1}{2}\dot{M}_{\rm jet}v_{\rm jet}^2, \tag{5.8}$$

where $\dot{M}_{\rm jet}$ is the mass ejection rate of the jets, and $v_{\rm jet}$ is the jets velocity when introduced in the simulation. Hence $\epsilon_{\rm kin}$ encapsulates not only the acceleration of the jets powered by the central engine, but also the gravitational “redshift” from the scale of an accretion disk to a resolved scale of jets in simulations. With $\epsilon_{\rm kin} = 10^{-4}$ and $\eta_{\rm jet} = \dot{M}_{\rm jet}/\dot{M}_{\rm BH} = 0.05$ fixed, the initial velocity of the jets is given by

$$v_{\rm jet} = c \left(\frac{2\epsilon_{\rm kin}\epsilon_{\rm r}}{\eta_{\rm jet}} \right)^{1/2} = 6000 \ {\rm km\,s^{-1}} \tag{5.9}$$

for $\epsilon_{\rm r} = 0.1$. The resulting launch speed of the surrounding cells is found by averaging the momentum of jets and the preexisting gas in those cells (Wang et al., 2010). Every time the accumulated jet mass, $\Sigma\, \dot{M}_{\rm jet} dt$, exceeds the threshold of 200 $M_\odot$ it is injected in collimated bipolar jets of a width of five finest cells. The direction of the jets is parallel and anti-parallel to the total angular momentum of the accreted gas up to that point, with an added random angle of less than 10°.[5] Lastly, since the mechanical or the radiative feedback alone may not describe the whole picture, we include hybrid models in which each of these two channels constitutes a half of the MBH bolometric luminosity (GM-RMF; see Table 5.1).

5.3 Initial Conditions

We apply the physics of galaxy formation in our code to the context of two merging galaxies, $2.1 \times 10^{11} M_\odot$ each, with gaseous and stellar disks and embedded MBHs. The initial conditions of our experiments are first described.

5.3.1 Data Conversion Pipeline

The *Gadget-2* (Springel, 2005) initial condition generator *StarScream*[6] is used to create an N-body dataset of an isolated galaxy, to which we add gas particles by splitting collisionless particles. Then, the *Gadget*-to-*Enzo* converter *hullMethod* employs IDL functions `qhull` (Delaunay tessellation) and `qgrid3` (linear interpolation) to reconstruct a density map for *Enzo* AMR. It utilizes an oct-tree structure to grid particle

[5]Note the difference from §2.8 of Kim et al. (2010). This leeway angle of $< 10°$ is introduced because five cells around the MBH is insufficient to adequately resolve the launching angle of jets.

[6]I am grateful to Jay Billings for making his code available for this study, and commenting on my suggestions for improvements. Available at http://www.jayjaybillings.org/starscream/.

data onto an adaptively refined mesh. For details of the data conversion pipeline we refer the readers to Kim et al. (2008) and Kim et al. (2009).

5.3.2 Galactic and Orbital Parameters

We construct each galactic progenitor with 10^6 dark matter particles following the Navarro-Frenk-White profile with a concentration parameter of $c = 10$ (Navarro et al., 1996, 1997). Then the gas grids are generated by splitting the particles with a baryonic mass fraction of 10%. Because we provide the dark matter and the gas with the same density profile and velocity dispersion, the progenitor automatically virializes to a desired virial temperature of the halo. In addition, a collective rotation of spin parameter $\lambda = 0.05$ is given to cause a disk to form embedded in a gaseous halo within a few hundred Myrs. Finally, two of these identical galactic progenitors are set on a prograde parabolic collision course (eccentricity $e = 1.0$; Khochfar and Burkert, 2006), initially separated by 150 kpc, with a pericentric distance of 4 kpc. Each progenitor is tilted by 30° with respect to the orbital plane. The initial relative velocity is 165 $\mathrm{km\,s^{-1}}$. The progenitors are bathed in a diffuse background intergalactic medium of $5.0 \times 10^{-31}\mathrm{g\,cm^{-3}}$ at 10^5 K. An initial metallicity of $Z = 0.003\,Z_\odot$ is also set up everywhere to track the metallicity evolution.

At the start, this initial condition is evolved for 0.44 Gyrs with the coarse-resolution (121.6 pc) refinement strategy and star formation recipe, but without MBH accretion or feedback. This relaxation process is instrumental in creating natural *model galaxies*, each of which consists of a gaseous disk, a stellar disk, a gaseous halos and a dark matter halo. An added benefit is that the computational resources are not exhausted on resolving the artificial starburst at the start of the simulation, triggered simply because the gaseous halo of the NFW form is neither realistic nor stable. At the end of the relaxation, we split each collisionless particle – stars and dark matter – into 13 child particles (Kitsionas and Whitworth, 2002; Kim et al., 2010). Consequently, this procedure produces our initial condition where two model galaxies are beginning to collide into each other. A suite of high-resolution (15.2 pc) simulations are performed on this initial condition with optional advanced physics (Table 5.1).

Each model galaxy has a mass of $M_{\rm vir} = 2.1 \times 10^{11} M_\odot$ and correspondingly, a virial velocity of $v_{\rm vir} = 86$ km s^{-1} and a virial radius of

$$R_{\rm vir} = M_{\rm vir}^{1/3} \left[\frac{H_0^2 h^2 \Omega_{\rm m} \Delta_{\rm c}}{2G} \right]^{-1/3} = 188 \text{ kpc} \tag{5.10}$$

given $h = 0.71$, $\Omega_{\rm m} = 0.27$, and $\Delta_{\rm c} = 200$. The dark matter halo represented by 1.3×10^7 particles constitutes 90% of the total mass. The stellar disk of $\sim 1.6 \times 10^6$ particles contains $\sim 1.0 \times 10^{10} M_\odot$, whereas the rest, $\sim 9.9 \times 10^9 M_\odot$, is in gaseous form available for future star formation, either in the galactic ISM or in the embedding halo. Each molecular cloud particle represents 1600 to 8000 $M_\odot$ at this time, whereas each dark matter particle samples a collective mass of 14500 $M_\odot$. At the center of each model galaxy lies a $10^5 M_\odot$ MBH, a gravitational seed which we put at 0.44 Gyr and will accumulate the gas along the way. At this point, galaxies are ~ 75 kpc apart. This separation is large enough to allow merging galaxies to form a collisional interface between their gaseous halos. All in all, our setup mimics the period when relatively low mass galaxies merge in a fast assembly regime of structure formation.

5.4 Results

A suite of simulations with and without the MBH feedback is performed in order to investigate the evolution of merging galaxies with their embedded MBHs (GM-SF and GM-RMF; Table 5.1). Each of the calculations is performed on 16 processors of the Orange cluster[7] at Stanford University. Grids and particles altogether, each simulation is routinely resolved with $\sim 3.3 \times 10^7$ total computational elements ($\sim 3.0 \times 10^7$ particles and $\sim 150^3$ cells). To evolve the system for 1 Gyr (from 0.44 Gyr to 1.5 Gyr in simulation time), each of these runs typically takes ~ 25000 CPU hours.

[7]Infiniband-connected AMD, 8 cores per node, 4 GB memory per core

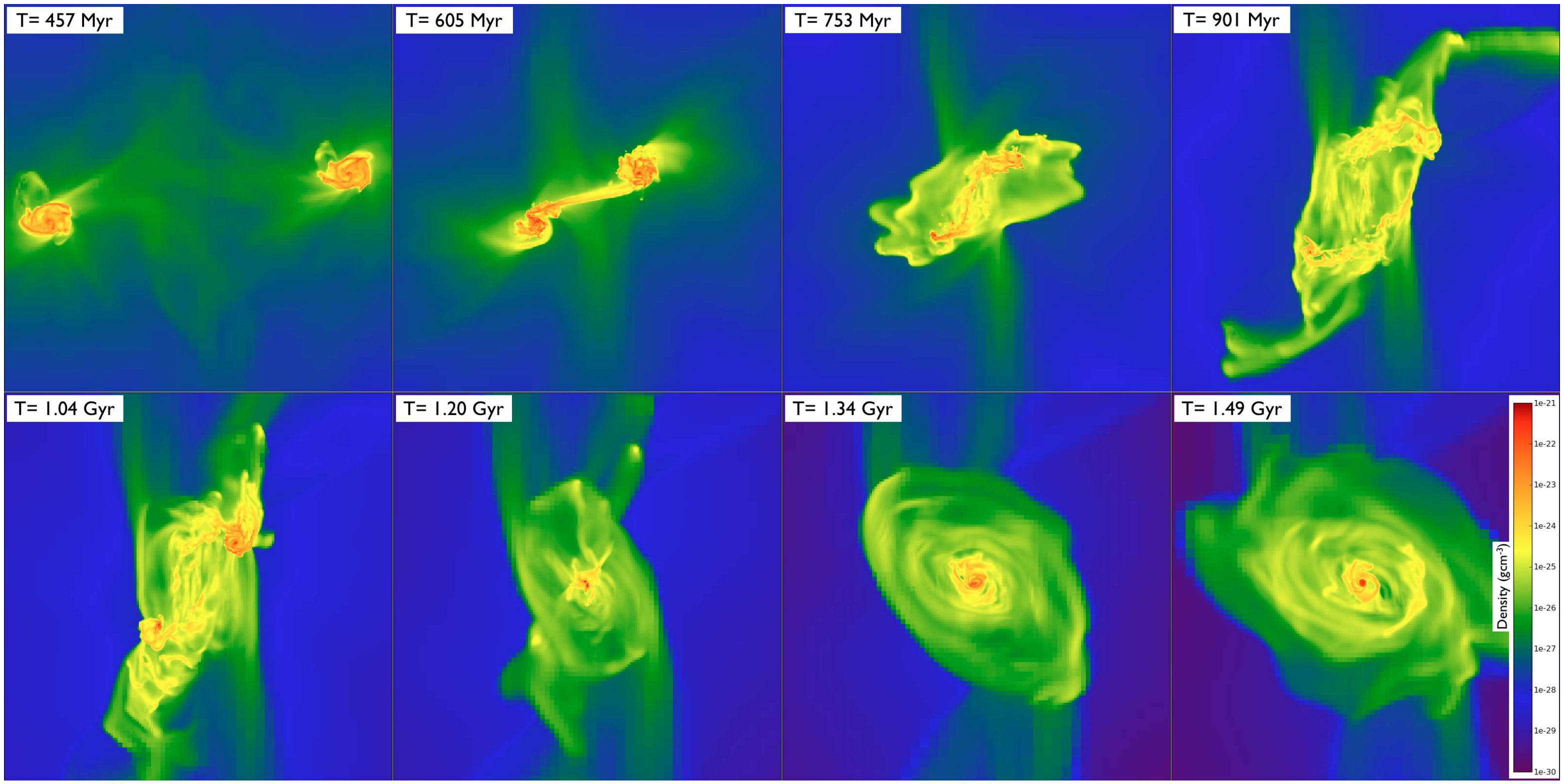

Fig. 5.1.— Density-weighted projection of density in the central 80 kpc, after 0.45, 0.61, 0.75, 0.90, 1.04, 1.20, 1.34, and 1.49 Gyr ($\sim$ 0.15 Gyrs between the frames). Note that both galaxies are 30° tilted with respect to the orbital plane. High-resolution images and movies are available at http://www.jihoonkim.org/.

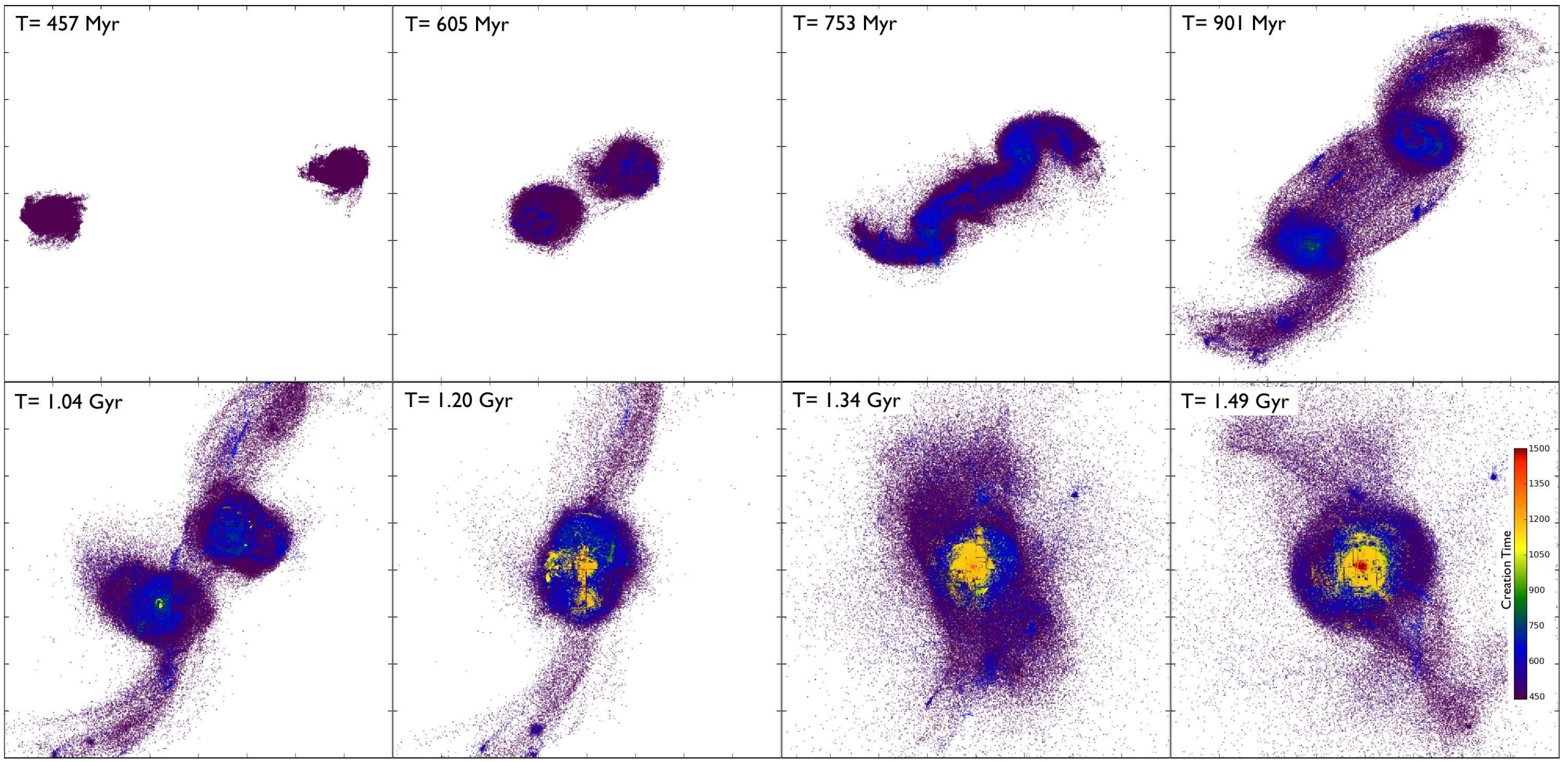

Fig. 5.2.— Stellar distributions colored by creation time in the central 80 kpc, after 0.45, 0.61, 0.75, 0.90, 1.04, 1.20, 1.34, and 1.49 Gyr ($\sim$ 0.15 Gyrs between the frames). Stars existed before 0.44 Gyr are colored purple.

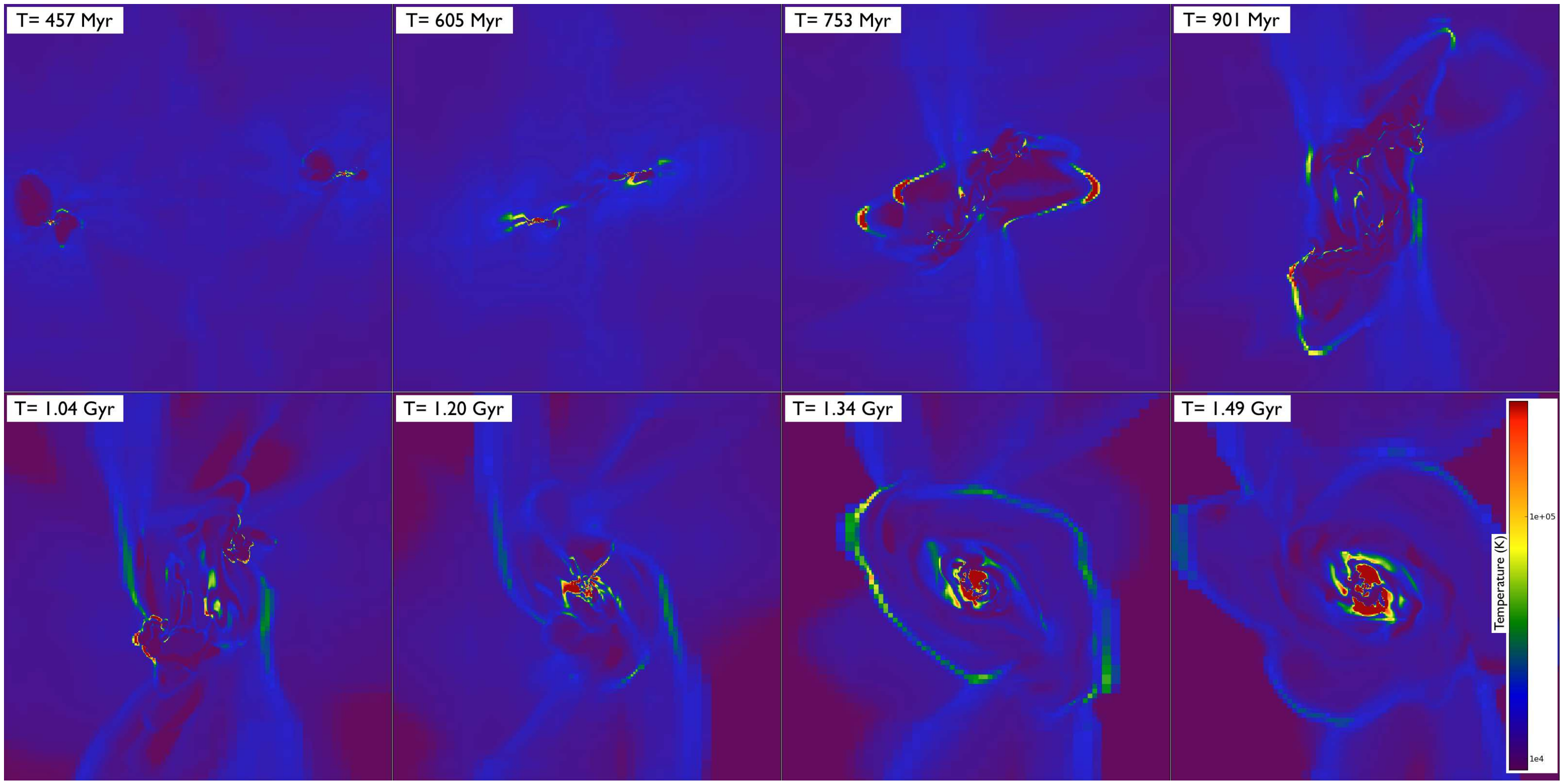

Fig. 5.3.— Temperature sliced through the orbital plane in the central 80 kpc, after 0.45, 0.61, 0.75, 0.90, 1.04, 1.20, 1.34, and 1.49 Gyr ($\sim$ 0.15 Gyrs between the frames). The temperature ranges from 9×10^3 K to 3×10^5 K.

5.4.1 Changes in Interstellar Medium and Star Formation

Merger Sequence Overview

The time sequence images of GM-RMF are compiled in Figures 5.1 to 5.3 for eight different epochs between 0.44 Gyr and 1.5 Gyr. Figure 5.1 depicts the density-weighted projection of density, in which clumps and filaments of gas are pronounced. When galaxies first pass by each other (at ~ 0.65 Gyr) and when finally coalesce (at ~ 1.2 Gyr),[8] the compression of the intervening gas triggers the formation of gas filaments and bridges, resulting in massive starbursts. The stars, i.e. molecular cloud particles, created during the mergers are displayed in Figure 5.2 colored by their creation time. Note that both galaxies are tilted by 30° with respect to the orbital plane (the plane on which the density is projected); thus, the apparent sizes of the galaxies are smaller than what they would appear at their respective face-on angles.

Figure 5.3 shows the temperature sliced at the plane of the collisional orbit, where hot bubbles driven by supernova explosions and the MBH feedback exist alongside the cold disks and filaments. With high-resolution AMR the multiphase medium is naturally achieved without any sub-resolution prescription (e.g. Springel and Hernquist, 2003a). A natural advantage of the AMR approach is that the interactions between different phases of gas – for example, between the expanding supernova bubbles and the diffuse galactic halos – is inherently included in this calculation.[9]

Global Impact of MBH Feedback

In the stellar mass evolution of Figure 5.4, two episodes of massive star formation are prominent: one during the first encounter (between 0.55 Gyr and 0.75 Gyr), and the other during the final coalescence phase (between 1.1 Gyr and 1.2 Gyr). This plot also well demonstrates the impact of the MBH feedback. To measure the importance of the MBH feedback in regulating global star formation, the overall increases in stellar masses are compared 1 Gyr after the MBHs are seeded and their feedback activated.

[8] The two MBHs merge at 1.38 Gyr in GM-SF, and at 1.31 Gyr in GM-RMF.

[9] Note again that the cold disks do not lie on the orbital plane, but intersect with it making 30° angle. This is why the full extent of the baryonic disks is not shown.

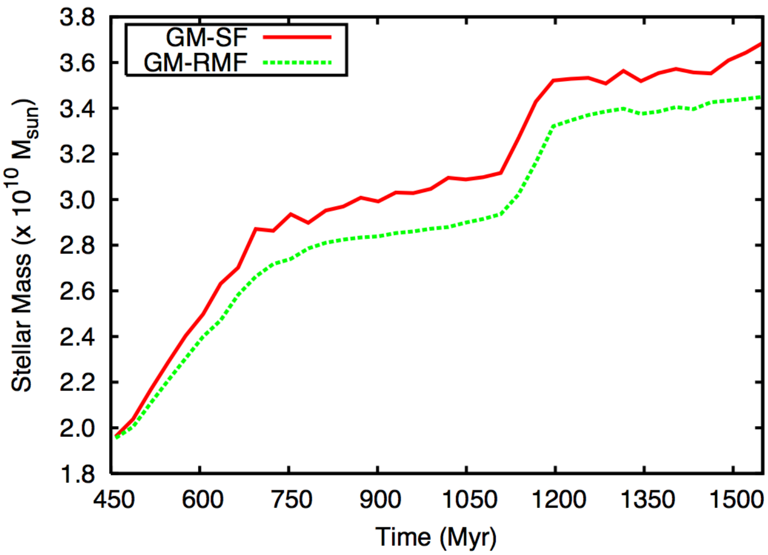

Fig. 5.4.— The evolution of stellar mass in the central 60 kpc sphere. The red solid line and the green dashed line represent GM-SF and GM-RMF, respectively. The increase in stellar mass of GM-RMF 1 Gyr after the MBH feedback is turned on is 15% smaller than that of GM-SF.

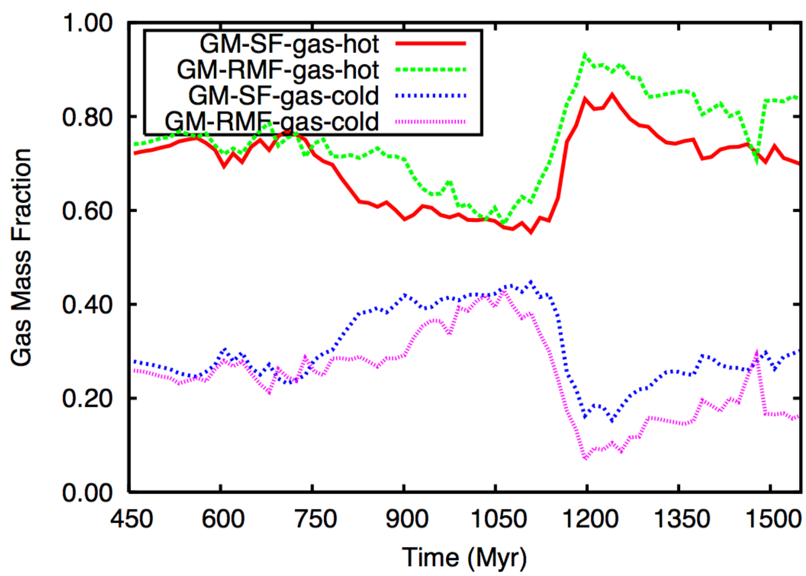

Fig. 5.5.— The evolution of gas mass fraction in the central 60 kpc sphere. The gas below 10^4 K is considered to be cold, above 10^4 K hot. The MBH feedback makes the interstellar medium hotter, sometimes reducing the cold gas fraction by more than 40%. The jumps in hot gas fraction coincides with the star formation peaks.

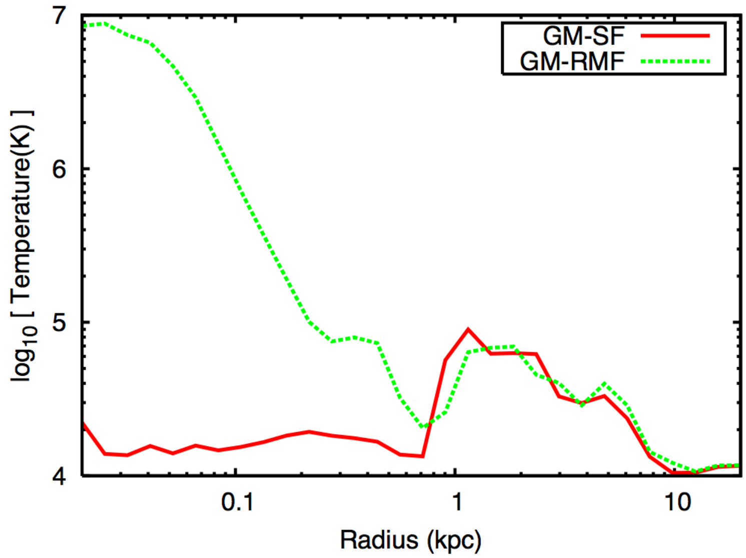

Fig. 5.6.— The mass-weighted radial profile of temperature in a 20 kpc sphere centered on the MBH at 1.49 Gyr. The red solid line and the green dashed line represent GM-SF and GM-RMF, respectively. The temperature within 1 kpc sphere is raised by the radiation and shocks by the MBH feedback.

The total stellar mass increase in GM-RMF at 1.5 Gyr is 15% smaller than that of GM-SF. In Figure 5.5, the fractional composition of interstellar gas by temperature explains how star formation is suppressed. First, note that the interstellar gas forms the multiphase medium and lively changes its composition. And in GM-RMF it is unmistakable that the two channels of MBH feedback, radiative and mechanical, make the interstellar medium hotter, increasing the hot gas mass fraction by up to 15% and reducing the cold gas fraction by up to 40% when compared with GM-SF. When the gas cells are heated through X-ray radiation or through shocks created by the MBH, they have harder time to turn into molecular cloud particles. It is because these cells are so hot that they seldom cool down to a typical molecular cloud temperature in a dynamical time (i.e. cooling time $t_{\rm cool} \gg$ dynamical time $t_{\rm dyn}$). Note also that the jump in hot gas mass fraction at 1.1 Gyr coincides with the star formation peak in Figure 5.4; the triggered star formation combined with the prompted MBH feedback heats up the interstellar gas.

To see the impact of MBH feedback more clearly, we analyze a snapshot of our

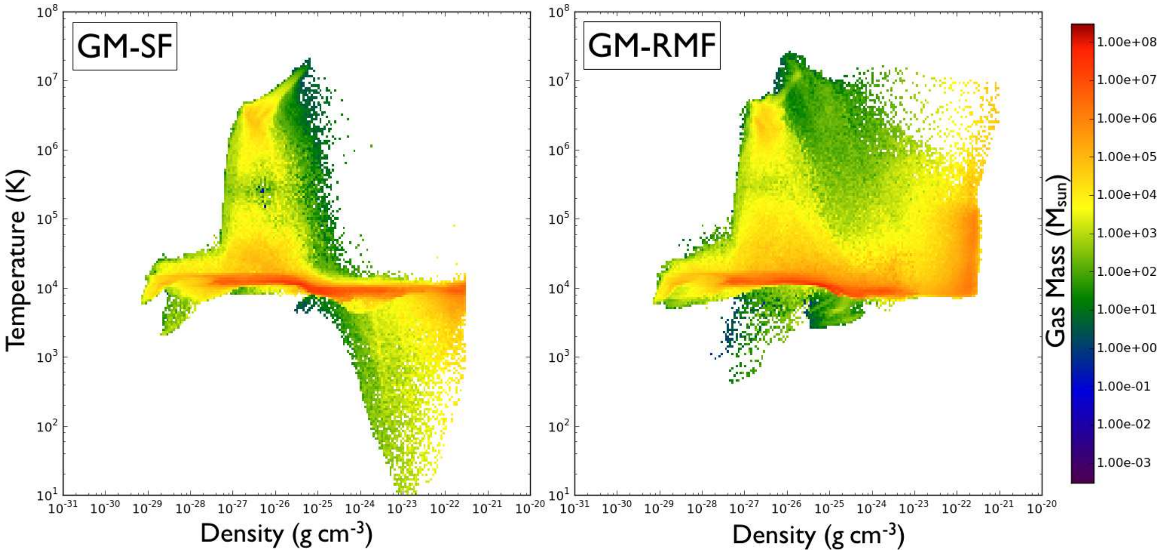

Fig. 5.7.— Joint probability distribution functions of gas density and temperature colored by the gas mass in each bin. The data is for a 20 kpc sphere centered on the MBH at 1.49 Gyr. GM-SF on the left, and GM-RMF on the right. Feedback from the MBH heats the gas up to 10^7 K prohibiting the gas from turning into stars.

simulation. Figures 5.6 to 5.8 are taken at 1.49 Gyr (corresponding to the last panel in Figures 5.1 to 5.3) when both the galaxies and their embedded black holes are merged, showing the state of the gas in the inner 20 kpc sphere centered on the MBH. First, the mass-weighted profile of temperature in the inner region is shown in Figure 5.6. While the temperature in GM-SF largely sits at 10^4 K, the temperature in GM-RMF within 1 kpc radius is raised up to 10^7 K. This temperature increase is even higher than what was found in Kim et al. (2010). The difference may portray the variation between the feedback by a slowly growing MBH in a massive isolated galaxy and the one by a fast growing MBH in a merger remnant. It is also worth to note that the 1 kpc distance out to which the gas is heated by MBH feedback is consistent with the findings in Sazonov et al. (2005) and Kim et al. (2010). The broad temperature peak between 1 to 10 kpc correlates with the hot bubbles inflated by supernova explosions above the galactic plane.

Likewise, Figure 5.7 illustrates how the cold dense gas is eliminated by the MBH feedback. The hot dense gas in GM-RMF (T $>$ 10^5 K, $\rho > 10^{-22}$ g cm^{-3}) shows a

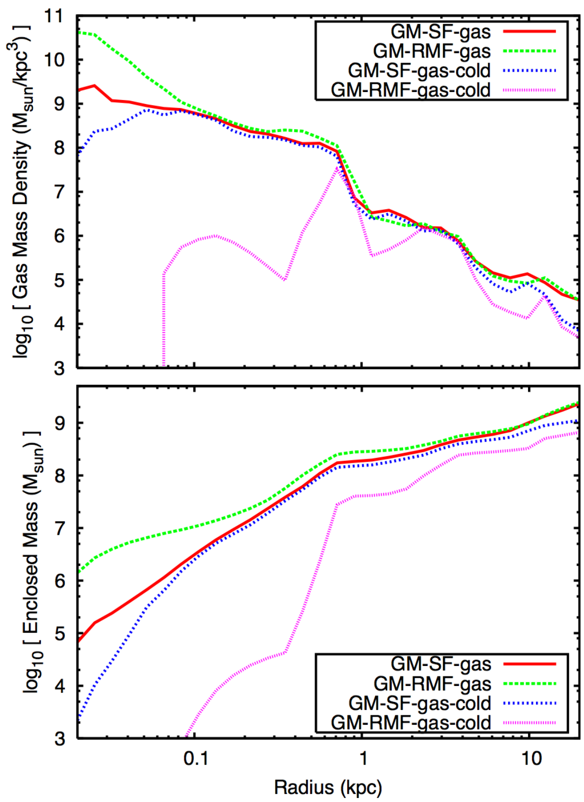

Fig. 5.8.— Radial gas density (top) and enclosed mass profiles (bottom) centered on the MBH at 1.49 Gyr. In GM-RMF the MBH feedback keeps larger amount of gas at the galactic center (green dashed line) compared to GM-SF (red solid line).

clear departure from GM-SF. The gas profiles from this snapshot are also displayed in Figure 5.8. In GM-RMF the MBH feedback keeps larger amount of gas within 1 kpc from the galactic center when compared with GM-SF. Only a small fraction of the gas in this region is below 10^4 K whereas in GM-SF most of the gas is cold. As noted, the heating of the interstellar gas is by the MBH through two channels: radiative and mechanical. We discuss both mechanisms in the following.

Heating by MBH Radiative Feedback

The radiation from the MBH is absorbed by the gas. Figure 5.9 reveals the total amount of radiation absorbed to heat up the gas inside the central 60 kpc sphere. The absorbed radiation energy for heating includes (1) the heating by the excess

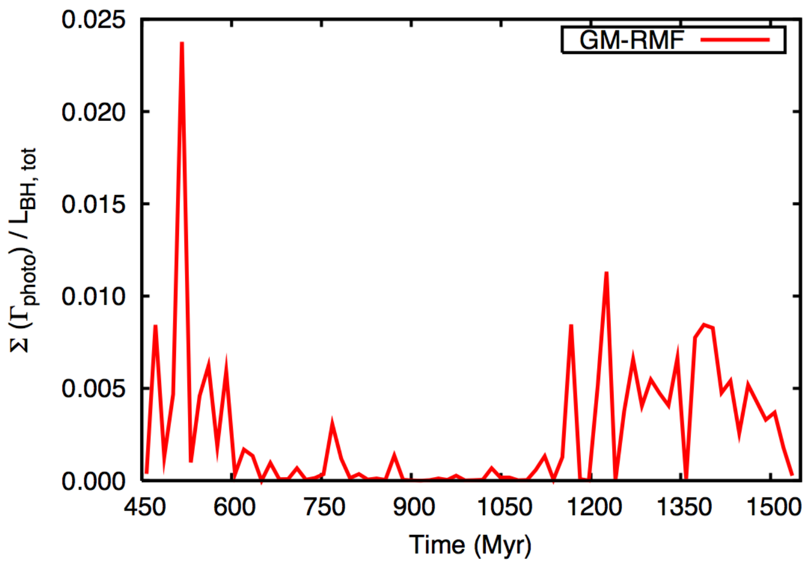

Fig. 5.9.— The fraction of MBH feedback energy used to heat up the gas in the central 60 kpc sphere. The radiation absorbed to heat up the gas reach up to 2.5% of the total bolometric luminosity of the MBH.

energy above the ionization thresholds of H, He, and He^+, and (2) the Compton heating when photon - electron scatterings occur. The total absorbed energy for heating is then divided by the total bolometric luminosity of the MBH, $L_{\rm BH}$, to get the fraction

$$f_{\rm rad,\,heat} = \frac{\int_V \Gamma_{\rm rad,\,heat} dV}{L_{\rm BH}} = \frac{\int_V \Gamma_{\rm rad,\,heat} dV}{\epsilon_{\rm r} M_{\rm BH} c^2}. \tag{5.11}$$

Figure 5.9 shows that $f_{\rm rad,\,heat}$ averages 0.3% and reaches up to 2.5%. In other words, about 0.3% of the total bolometric luminosity of the MBH on average is used to radiatively heat the surrounding gas. We remind the readers that in GM-RMF only a half of $L_{\rm BH}$ comes out as radiation, and the other half is used in the mechanical channel. Hence $f_{\rm rad,\,heat}$ does not include the energy which was injected into the interstellar medium as a mechanical energy. It does not include the energy used to ionize the species, either.[10]

[10] $f_{\rm rad,\,heat}$ is therefore not the same as the fraction of $L_{\rm BH}$ that is thermally coupled to surrounding gas, i.e. $\epsilon_{\rm f}$ in Springel et al. (2005b) or Booth and Schaye (2009).

The thermalization of the MBH radiation energy is a major factor in heating the gas around the MBH up to 10^7 K as shown in Figures 5.6 and 5.7. We caution the readers that the amount of radiation captured by the gas would depend on the density of the surrounding gas resolved, and therefore on the numerical resolution of the simulation. The value of $f_{\rm rad,\,heat}$ we find in Figure 5.9 would mean the lower bound of captured MBH radiation if the resolution was insufficient. See §5.4.2 for related discussions.

Propagation of Jets by MBH Mechanical Feedback

Recently it is postulated that the energy injection by strong bipolar winds at the center of a galaxy could inflate large bubbles expanding into the galactic halo. Most notably, the prominent gamma-ray bubbles identified by the *Fermi Gamma-ray Space Telescope* above and below the galactic center of the Milky Way galaxy are dubbed "Fermi bubbles" and garnering much attention. These bubbles are believed to be driven by the galactic winds of massive supernova explosions, or by strong active galactic nuclei (AGN) activities (e.g. Su et al., 2010; Guo and Mathews, 2011). As the feasibility of this scenario needs be tested via numerical experiments, it is well-timed to examine whether the mechanical channel of our MBH feedback is indeed capable of launching energetic jets and inflating observable size bubbles.

Figures 5.10 and 5.11 illustrate how the mechanical feedback of the MBH works in our simulation. The sequential images in each Figure present the temperature and density in the central 10 kpc sliced through the MBH at eight different epochs between 1.464 Gyr and 1.475 Gyr (after two black holes are merged). The large momentum of the bipolar jets from the MBH inflates low density, high temperature bubbles of 3 to 5 kpc in size. The bilobular bubbles are perpendicular to the dense disk shown as a cold dense filament from left to right. At 1.466 Gyr, a clear shock front reaching high temperature up to 10^7 K is noticeable. The initial expansion speed of the shocks is measured to reach 500 $\mathrm{km\,s^{-1}}$. Although it should be considered provisional, the bilobular morphology of the bubbles created this way seem to suggest that the Fermi bubbles could have been naturally inflated by the MBH mechanical feedback of duration < 10 Myrs. However, the expanding gas mostly falls back into

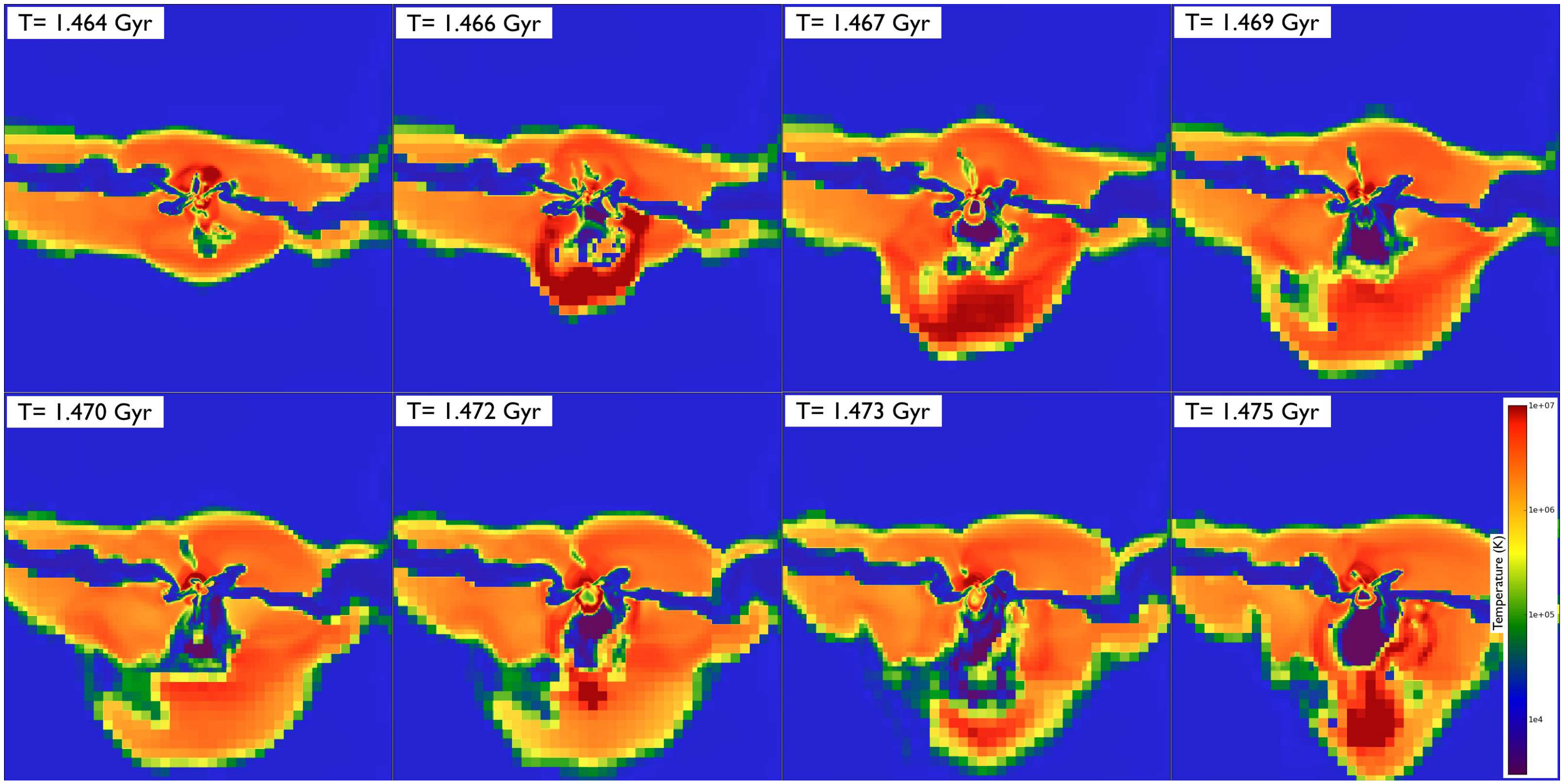

Fig. 5.10.— Sequence images of launching of the jets. Temperature in the central 10 kpc sliced through the MBH from 1.464 Gyr to 1.475 Gyr ($\sim$ 1.5 Myrs between the frames). The temperature ranges from 3×10^3 K to 10^7 K.

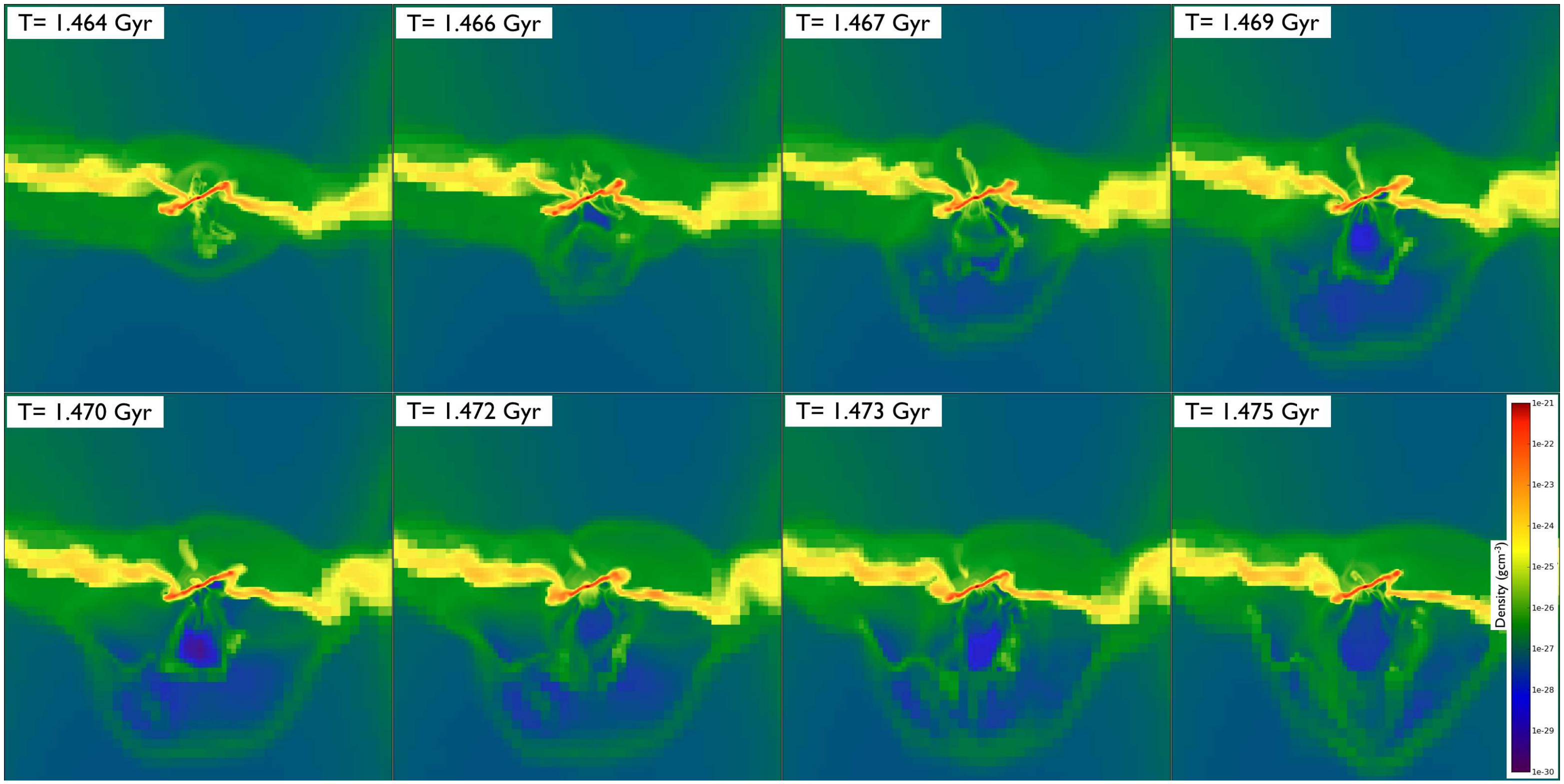

Fig. 5.11.— Sequence images of launching of the jets. Density in the central 10 kpc sliced through the MBH from 1.464 Gyr to 1.475 Gyr ($\sim$ 1.5 Myrs between the frames).

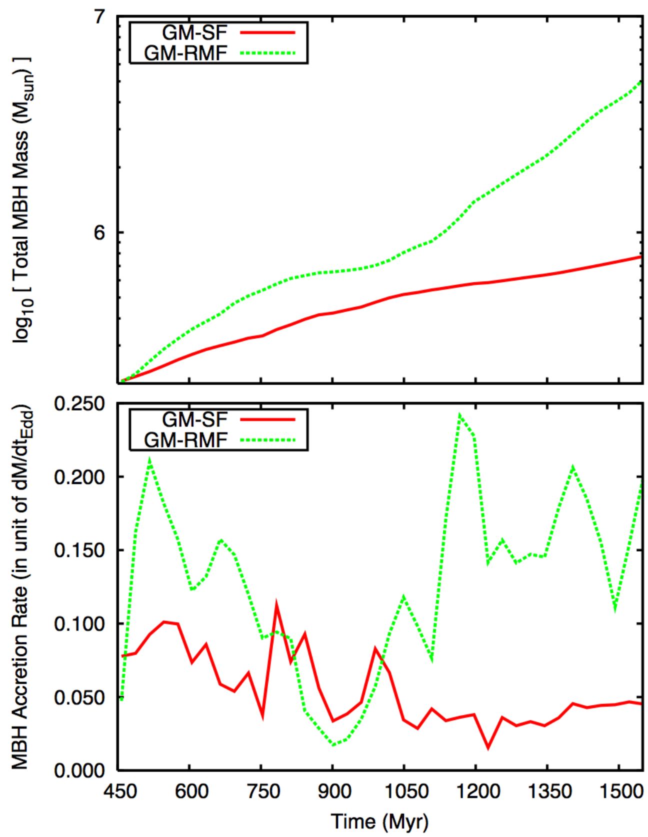

Fig. 5.12.— Top: the total black hole mass accretion history. Bottom: the mass accretion rates onto the MBHs in the unit of the Eddington rate. In each panel, the red solid line and the green dashed line represent GM-SF and GM-RMF, respectively.

the potential well, and rarely escapes the galactic halo. Overall, only a negligible amount of gas – if at all – is expelled out of the galactic potential by the MBH mechanical feedback (see Figure 5.8). This contrasts with the previous simulations of Springel et al. (2005b) and others in which a massive expulsion of gas by the AGN activity is frequently observed during major mergers of galaxies.

5.4.2 Black Hole Growth and Related Issues

Figure 5.12 displays the growth history of the combined mass of two MBHs in our simulations. As expected the accretion rates are $\geq 5\%$ of the Eddington limit during mergers, indicating that our simulation may portray an analogue of merger-induced quasar-mode feedback by fast growing MBHs (Croton et al., 2006). However, two problems immediately stand out. The most notable one is that the run with the MBH feedback (GM-RMF) exhibits faster growth of black hole masses than the run without the MBH feedback (GM-SF) does. Another problem is that the final coalescence of galaxies at 1.1 Gyr does not seem to cause an increase in the black hole accretion rate in GM-SF. (On the other hand, it does cause a rise in the accretion rate in GM-RMF.) This finding does not seem to agree well with the previous numerical experiments such as Springel et al. (2005b) and Di Matteo et al. (2005) in which black hole accretion rates and star formation rates coincide well.

These disagreements might be explained by the differences in numerical prescriptions to describe MBHs, between previous studies and ours. Before anything else, the ways in which the MBH energy is coupled to the gas differ from each other. In Springel et al. (2005b) and many studies that followed, a fixed fraction of the MBH energy is thermally and isotropically added to the gas in the smallest resolved volume in the vicinity of the MBH. This sub-resolution prescription skips the thermalization process below the resolution limit of 50 to 100 pc. It often creates strong shocks and easily expels a large amount of gas out of the galactic potential. In contrast, the radiative and mechanical feedback of MBHs in our work do not necessarily generate such powerful and isotropic shocks. Rather, our feedback channels also demonstrate strong directionality in two ways: (1) the radiation escapes preferentially towards the direction perpendicular to the dense galactic disk, and (2) the jets are directed along the total angular momentum of the accreted gas, which usually asymptotes to the overall galactic rotation axis (see Figure 5.11).[11]

We suggest that the physical processes we modeled in our work need to be re-examined to tackle these outstanding problems. First and foremost, our feedback machinery needs to be scrutinized to see how well it reflects the reality. In what follows, we describe possible improvements and future directions which are tested or considered.

[11] The directionality of the MBH feedback may in fact better reflect the nature. For example, recent studies have argued that the MBH feedback may preferentially remove the dilute hot gas, while not affecting the cold stream (van de Voort et al., 2011).

MBH Mechanical Feedback in Random Directions

To alleviate the strong directionality of MBH feedback in our machinery, we have tested simulations in which bipolar jets of the MBH mechanical feedback are launched in random directions. The observations of X-shaped radio galaxies (XRGs) where the radio jets rapidly changes their directions by large angles (Merritt and Ekers, 2002; Gopal-Krishna et al., 2003) motivate this consideration. However we do not observe any significant improvement from the earlier results.

MBH Radiative Feedback Captured with More Resolution

It is possible that the numerical resolution of our simulations is still not fine enough to fully capture the thermalization of MBH radiation. If the gas near the MBH is not properly resolved, the optical depth of the radiation could be small even at the smallest resolved distance (Omma et al., 2004). Because the amount of radiation captured by the gas cells depends on the density of the resolved gas, the captured MBH radiation in Figure 5.9 could likely mean the lower bound of the real value. For this reason we have performed a simulation of a $2.1 \times 10^{11} M_{\odot}$ isolated galaxy with $<$ pc resolution and found that $f_{\rm rad,\,heat}$ defined in §5.4.1 generally increases (up to $f_{\rm rad,\,heat} \sim 5\%$). Increased radiative heating might aid the MBH in self-regulating its own growth. More analysis on simulations of higher resolution need to be carried out.

Kinetic Stellar Feedback

Stellar feedback in galactic scale numerical simulations has been traditionally modeled with the thermal injection of energy. Lately, however, another approach using momentum kicks is being investigated in order to overcome the limitation of the thermal prescription (Hopkins et al., 2011).[12] Figure 5.13 illustrates the schematic views

[12] It is well-known that the thermal stellar feedback in SPH simulations is not effective in launching galactic winds. It is because the injected thermal energy quickly dissipates by numerical diffusion. This has led some simulators to adopt a phenomenological treatment in which gas particles are vertically launched manually, or the cooling of the internal energy is temporarily forbidden (e.g. Springel and Hernquist, 2003a). Now to overcome this limitation Hopkins et al. (2011) uses the fact that even if thermal energy numerically dissipates in SPH, momentum doesn't.

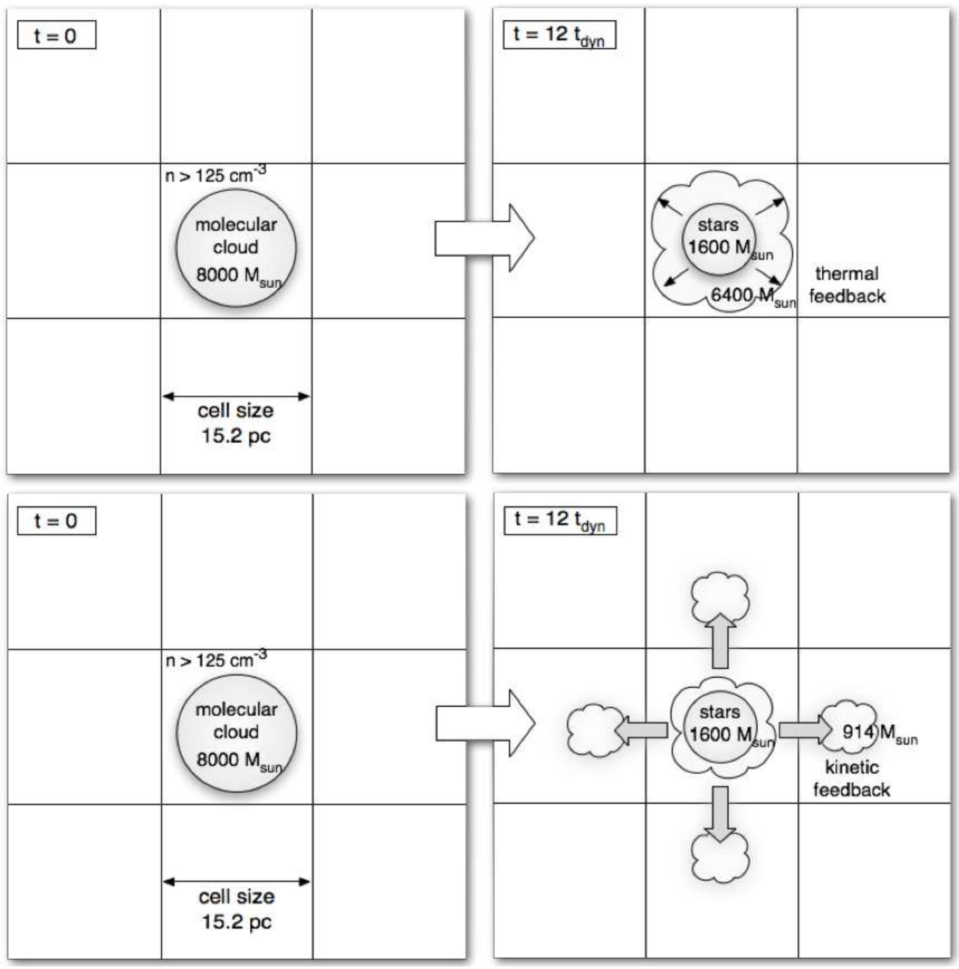

Fig. 5.13.— Schematic view of the thermal and kinetic stellar feedback.

of thermal and kinetic stellar feedback implemented in *Enzo*. The kinetic stellar feedback prescription injects mass and momentum to the six nearby cells. The initial velocity of the injected mass is calculated so that the total kinetic energy is equal to the thermal feedback energy adopted in Kim et al. (2010). This new mechanism renders old stars naturally sit in low dense regions, and may depict the realistic picture of how stellar feedback disturbs the galactic disk and the black hole accretion disk. Preliminary tests show that this new form of feedback is successful in effectively suppressing the global star formation. However we still observe that the MBH accretion is not self-regulated.

Magnetohydrodynamics

Lastly, we work on a simulation with magnetic fields, inspired by the studies of the jets in the presence of magnetic fields (e.g. Dubois et al., 2009; Wang et al., 2010). In full magnetohydrodynamics (MHD) calculations, magnetic fields are shown to aid the jets in depositing outflow momentum onto the infalling gas. In turn, jets can distort and carry the magnetic field, modifying its distribution.[13] The interaction between the jets and the magnetic fields might enhance the effectiveness of the MBH mechanical feedback and help the MBH regulate further gas accretion onto itself.

Enzo adopts the Dedner et al. (2002) formulation of MHD equations, in which the divergence-free condition of the magnetic field, $\nabla \cdot \mathbf{B} = 0$, is enforced by hyperbolic cleaning incorporated with the projection method (Toth, 2000). The piecewise linear method is used for spatial reconstruction (van Leer, 1979), while fluxes are computed with the local Lax-Friedrichs Riemann solver (Kurganov and Tadmor, 2000). The total variation diminishing second order Runge-Kutta method is used to perform time integration (Shu and Osher, 1988).[14] For initial conditions, we seed a uniform magnetic field of 0.1 nG initially directed along the galactic rotation axis. A set of simulations with and without the magnetic field is planned to explore whether the magnetic fields could help the jets drive massive gas expulsion, thereby quenching star formation and the growth of black holes.

5.5 Summary

For the first time, we carried out a comprehensive high-resolution simulation of two merging galaxies, $2.1 \times 10^{11} M_\odot$ each, with their $10^5 M_\odot$ embedded MBHs, portraying an analogue of merger-induced quasar-mode feedback by fast growing MBHs. Our main findings are as follows.

[13] In this type of simulations, the direction or the collimation of the jets is unaffected by the magnetic field. It is feasible, however, in MHD calculations of the relativistic plasma jets with sub-parsec resolution (e.g. McKinney and Blandford, 2009).

[14] These methods coupled with *Enzo* AMR are extensively tested in a variety of experiments such as relativistic jets (Wang et al., 2008), galaxy formation (Wang and Abel, 2009), and star cluster formation (Wang et al., 2010).

1. *Self-consistent Study of Merging Galaxies:* Our AMR framework comprehensively incorporates gas, stars, and central MBHs in one framework, and allows us to explore how galaxies and MBHs coevolve and influence each other during comparable mass mergers. It simultaneously resolves both the dense interstellar medium and the diffuse intergalactic medium, and easily couples small scale physics (e.g. star formation and feedback, MBH accretion and feedback) and large scale phenomena (e.g. galactic outflow, bilobular bubbles inflated by MBHs) without sub-resolution prescription.

2. *Suppressed Star Formation:* We show that MBH feedback can heat the interstellar medium up to 10^7 K through radiation and shocks. The MBH feedback reduces the global cold gas fraction by up to 40%, and suppresses the star formation by 15% after 1 Gyr. These MBHs also drive more frequent and powerful jets creating sizable bubbles at the galactic centers (§5.4.1).

3. *Black Hole Growth and Related Issues:* The accretion rates are $\geq 5\%$ of the Eddington limit during the merger, indicating that our simulation may portray an analogue of merger-induced "quasar-mode" feedback by fast growing MBHs. However, we find that the run with the MBH feedback exhibits faster growth of black hole masses than the run without the MBH feedback. We suggest that the physical processes we modeled in our work need to be reexamined to tackle these problems. For example, including magnetic fields may aid jets in depositing outflow momentum onto the infalling gas, thus help the MBH self-regulate its own growth (§5.4.2).

Chapter 6

Conclusions and Future Work

"The significant problems we face cannot be solved at the same level of thinking we were at when we created them."
— Albert Einstein (1879-1955)

Every astronomer must have at some point found himself spellbound and awed by the spectacular images of galaxies taken by the Hubble Space Telescope. Trillions of stars orbiting in giant spiral structures, well-defined dust lanes right across the stellar lights, the big moment in the violent fireworks of galaxy mergers. All of these leave us dumbfound for a while in search of the laws and truth behind the mesmerizing beauty. However, it is equally astonishing to learn that we do not yet have a well-established theory to explain how such galaxies have formed and evolved.

The Universe is built from the bottom up and as such, galaxies are the basic building block of the large scale structures. Therefore a reliable theory of galaxy formation is in great demand not only to explain the beautiful galactic images themselves, but also to offer a basis to elucidate the formation of the large scale structures. The purpose of this thesis has been to demonstrate that such theory can be perfected through refined numerical simulations. We have developed a state-of-the-art numerical framework which self-consistently models the interplay between galactic components: dark matter, gas, stars, and massive black holes. Utilizing this tool we have demonstrated that such interactions needs to be adequately considered and described in order to comprehend the star formation history, black hole accretion history, and cosmological evolution of galaxies.

In this chapter, we discuss the original conclusions and future applications of this thesis work. Listed in §6.1 are the main conclusions focusing on the impact of our new approach in understanding the evolution of galaxies. Ideas on how to improve our numerical approach are summarized in §6.2. Possible future work and projects, including the formation of high-redshift supermassive black holes, are also discussed in §6.3 and §6.4. A portion of this chapter is included in the publication submitted to *The Astrophysical Journal* which is coauthored by John Wise, Marcelo Alvarez, and Tom Abel.

6.1 Conclusions

6.1.1 Building A Self-consistent Numerical Framework for Galaxy Formation

We developed a fully self-consistent galaxy formation simulation integrating dark matter, gas, stars, and massive black holes (MBHs) in one comprehensive framework (Kim et al. (2010); Chapter 2). Our unique framework has the following novel features.

- *Molecular cloud formation*: *Enzo* is modified to model the formation of molecular clouds at its characteristic scale of 15.2 pc. We self-consistently deposit a particle when a gas cell of a molecular cloud size actually becomes Jeans unstable.

- *Stellar feedback*: The molecular cloud particle then gradually produces stellar mass while returning a large fraction of mass back to the gas with thermal feedback energy. It models the observed slow star formation in molecular clouds.

- *MBH accretion*: Gas accretion rate onto a MBH is estimated assuming a Bondi-Hoyle accretion but without any empirical boost factor (e.g. as in Springel et al., 2005b), since high-resolution AMR resolves the high densities near the MBH.

- *MBH radiative and mechanical feedback*: Monochromatic X-ray photons from the MBH is followed through full 3D adaptive ray tracing rendering the radiative feedback of the MBH. Here photons ionize and heat the gas, and exert momentum onto the gas. Bipolar jets with velocities of $\sim 10^3$ km s^{-1} are launched from the vicinity of the MBH, well resolved in high-resolution adaptive mesh. Our approach is significantly different from the previous recipes for MBH feedback in galactic scale simulations to date (e.g. Springel et al., 2005b; Sijacki et al., 2007; Booth and Schaye, 2009; Teyssier et al., 2010b), yet more accurately presents the physics of MBHs when properly incorporated with a high dynamic range.

6.1.2 Galaxy Formation with Stars and MBHs

With a much improved numerical tool in hand, we investigated the coevolution of a $9.2 \times 10^{11} M_\odot$ galaxy and its $10^5 M_\odot$ embedded MBH at redshift 3 in a ΛCDM simulation (Kim et al. (2010); Chapter 3). Our simulation, for the first time, followed the comprehensive evolution of a massive star-forming galaxy with self-consistently modeled stars and a MBH, evolving under each other's influence. Our method limits the use of *ad hoc* formulation and instead more accurately models the physics of galaxy formation. Therefore, one should also be able to couple small-scale physics (such as molecular cloud formation and feedback) with large-scale physics (such as quasar-driven galactic outflows) without any sub-resolution model. Our main results are as follows.

- *Molecular Cloud Formation and Feedback:* Unlike previous star formation recipes based on the Schmidt relation, a particle spawns when a gas cell of a typical molecular cloud size, 15.2 pc, actually becomes Jeans unstable. Then thermal stellar feedback is shown to self-regulates star formation.

- *Locally Suppressed Star Formation:* We show that MBH feedback, especially its radiation, heats the surrounding ISM up to 10^6 K through photoionization and Compton heating and thus locally suppresses star formation in the inner core of a galaxy. The feedback also considerably changes the stellar distribution at the galactic center. This new channel of feedback from a slowly growing MBH is particularly interesting because it is only locally dominant, and does not require the heating of gas globally on the disk, or instigate a massive gas expulsion out of the galactic potential.

- *Self-regulated Black Hole Growth:* MBH feedback is also demonstrated to be an effective mechanism for slowing down the accretion of gas onto the MBH itself. Without necessarily unbinding all of its surrounding gas, the MBH self-regulates its growth by keeping the surrounding ISM hot for an extended period of time. Therefore, our results possibly are consistent with a "radio-mode" analogue of MBH feedback.

6.1.3 Merging of Galaxies on Adaptive Mesh Refinement

We performed the very first adaptive mesh refinement (AMR) simulation of two merging galaxies, $1.8 \times 10^{10} M_{\odot}$ each, including star formation and feedback (Kim et al. (2009); Chapter 4). Our simulation, for the first time, followed the self-consistent evolution of low mass merging galaxies with AMR at unprecedented resolution. Although it should be considered provisional, our result brings compelling evidence that AMR delivers a uniquely powerful tool in understanding merging galaxies, while it addresses several issues SPH has suffered from.

- *Multiphase Medium and Shock-induced Star Formation:* First, as AMR naturally establishes a multiphase medium without any sub-resolution model, we have captured shock-induced star formation that occurs when merging galaxies compress the intervening gas. The well-resolved shocks trigger a widespread starburst, in accord with observations. Further, the overcooling problem is absent because the multiphase medium is resolved by $<$10 pc cells, and the thermal feedback is sufficient to heat such small cells up to $\sim$10^7 K.

- *Hot Gas Outflow:* Second, utilizing the high dynamic range and the Eulerian nature of AMR, we have followed the evolution of the hot diffuse medium of gaseous halos and the IGM as far as 1 Mpc away from the galaxies. This allows us to explore the interplay between the galactic outflows and the embedding medium and to demonstrate that a hot metal-rich halo forms around the galaxies from stellar feedback. The massive gas expulsion in low mass merging galaxies leads to a high mass-to-light ratio, as it creates a merger remnant without much cold gas left for later star formation.

6.1.4 Galaxy Mergers with Stars and MBHs

We also carried out a comprehensive high-resolution simulation of two merging galaxies, $2.1 \times 10^{11} M_\odot$ each, with their $10^5 M_\odot$ embedded MBHs, portraying an analogue of merger-induced quasar-mode feedback by fast growing MBHs (Kim et al. (2011); Chapter 5). Our main findings are as follows.

- *Suppressed Star Formation:* We show that MBH feedback can heat the interstellar medium up to 10^7 K through radiation and shocks. The MBH feedback reduces the global cold gas fraction by up to 40%, and suppresses the star formation by 15% after 1 Gyr. These MBHs also drive more frequent and powerful jets creating sizable bubbles at the galactic centers.

- *Black Hole Growth and Related Issues:* The accretion rates are $\geq 5\%$ of the Eddington limit during the merger, indicating that our simulation may portray an analogue of merger-induced "quasar-mode" feedback by fast growing MBHs. However, we find that the run with the MBH feedback exhibits faster growth of black hole masses than the run without the MBH feedback. We suggest that the physical processes we modeled in our work need to be reexamined to tackle these problems. For example, including magnetic fields may aid jets in depositing outflow momentum onto the infalling gas, thus help the MBH self-regulate its own growth.

6.2 Improvement on Physics

While proven to be fruitful already in producing robust results, our comprehensive galaxy formation framework is only the first step forward in the right direction. Imminent future projects and improvements are as follows.

6.2.1 Improving Mechanical Feedback

In the results presented herein, mechanical feedback is energetically secondary to radiative feedback because the mass accreted onto the MBH is not large enough to repeatedly drive jets. These infrequent jets easily penetrate the ISM without necessarily creating sizable shocks or entraining a large amount of gas. However, a few mechanisms will be considered in the future which could have enhanced the effectiveness of jets. Magnetic fields could aid the jets in efficiently depositing outflow momentum onto the infalling gas, as was shown by the studies on the evolution of jets in the presence of magnetic fields (Dubois et al., 2009; Wang et al., 2010). Cosmic rays accelerated by relativistic jets and shock fronts (Skillman et al., 2008) could boost the effectiveness of jets, too.

6.2.2 Improving Radiative Feedback

For now, monochromatic X-ray photons are utilized to carry the energy of MBH radiation (§2.2.7); however, a better model will be needed to describe the polychromatic energy distribution of MBH radiation. Ideally one wants to have a large number of spectral energy bins, each of which is separately followed through three-dimensional ray tracing. Given the computationally challenging nature of polychromatic radiative transfer, however, tabulated rates of photoionization and photoheating as functions of optical depth can be a good alternative. Moreover, to accurately quantify the radiative feedback on the gas in the vicinity of a MBH, the pressure force on dust grains needs to be computed. This could have increased the radiation pressure in the presented results, especially in the central $<$ kpc region. For this purpose, dust models in Rocha et al. (2008) will need to be considered.

6.2.3 Adding Supplementary Feedback Channels

A MBH particle in our work represents not just the black hole itself, but also includes accreting gas and stars deep within the galactic nucleus. Thus, there is a need for other feedback channels, such as stellar winds from a nuclear disk (Ciotti et al., 2009). The nuclear disk winds can be implemented as thermal deposition of energy, working in conjunction with the aforementioned radiative and mechanical feedback. Stellar UV radiation from the nuclear disk can also be incorporated into the radiative feedback of the MBH. Including this supplementary feedback will reveal the multi-faceted nature of the coupling of MBH energy with its surroundings.

6.2.4 Improving Accretion Estimate

The accretion estimate using the Bondi-Hoyle formula will need to be improved, especially when the gas disk around the MBH can be resolved down to the Bondi radius. Different estimates such as the ones considering gas angular momentum (Hopkins and Quataert, 2010; Levine et al., 2010) are attractive candidates that should be explored.

6.2.5 Nonthermal Pressure Sources

Nonthermal pressure sources such as magnetic fields (Wang and Abel, 2009), stellar UV radiation, and cosmic rays are missing in this work, but should be included in future simulations.

6.2.6 Parameter Studies

More comprehensive parameter studies should follow, especially in the parametrization of MBH feedback and the efficiency of stellar feedback. The results should be compared and calibrated with observations such as bulge to disk mass ratio and gas to stellar mass ratio (e.g. Gavazzi et al., 2008), or with analytical investigations (e.g. Sazonov et al., 2005). In particular, the disk-bulge decomposition of simulated galaxies will be the subject of subsequent analysis of our simulations.

6.2.7 Joining Forces with Other Astrophysics Codes

We also recognize that the results from our experiment can provide the community with better sub-resolution models for MBH physics. For example, the radial profile of heating rates by the MBH in our simulation can be tabulated; in a coarsely resolved particle-based simulation, one can deposit thermal energy according to this radial

Fig. 6.1.— A snapshot of a galaxy simulated in *Enzo* and visualized with *Sunrise* (Jonsson et al., 2010). Seen from a 60 angle (top) and an edge-on angle (bottom). The reddening by dust absorption and reemission is included; note the prominent dust lane across the edge-on image. Visualization courtesy of Patrik Jonsson and Matthew Turk.

dependence into a volume larger than a typical smoothing kernel. This can be a useful means for improving the particle-based simulations as well as for speeding up future large-scale AMR calculations, such as the formation of high-redshift quasars and the reionization of intergalactic helium.

Very detailed structures of the star forming galaxies are imprinted in our high-resolution galactic dataset at a wide range of scales. Therefore, using the tools for generating mock observations and spectra (e.g. Jonsson et al., 2010), our simulated galaxies on AMR can produce the most precise simulation counterpart against the observation of active star-forming galaxies. The influence of dust obscuration and galactic wind would be engraved in the synthesized galactic images and spectra (Figure 6.1).

6.3 Formation of High-redshift Quasars

For the first time, a numerical framework which self-consistently simulates galaxies and MBHs is ready (Kim et al., 2009, 2010, 2011). Expanding upon extensive experience in galactic simulations, we will apply this tool to one of the most challenging, yet highly rewarding tasks in contemporary astrophysics: building high-redshift quasars with unabridged descriptions of galaxy - MBH interactions. Details of the proposed projects are as follows.

6.3.1 Scientific Motivation

Computer simulations are astronomers laboratories. Theories of galaxy formation must be put to the test through computational experiments. However, the numerical frameworks to date hardly encompass all the important physics at galactic scale, such as star formation or MBH feedback. Therefore, our new framework which self-consistently models stars and MBHs with less tunable parameters brings a unique perspective to a wide range of galaxy formation studies in which simulations have had hard time in reproducing observations:

1. What makes giant elliptical galaxies red with little star formation activity?

2. Can MBH feedback suppress star formation without having to blow out all the gas out of the galactic potential as some simulated quasars do (e.g. Springel et al., 2005b))?

3. How do galaxies maintain high angular momentum disks and avoid making secular bulges that are too massive?, etc.

Among all these problems, the most troubling one is the existence of high-redshift quasars. The discovery of high-redshift quasars (Fan et al., 2006) poses a serious challenge to ΛCDM cosmology: How did the MBH acquire such a huge mass in such a short time < 1 Gyr? The commonly adopted scenario starts with a seed BH of $10^{2-3} M_\odot$ formed from a collapsing Population III star at $z \sim 20$ (Heger and Woosley, 2002). Then, a sequence of galaxy mergers and subsequently, merging of their embedded BHs builds a MBH of up to $10^9 M_\odot$ at $z \sim 6$ (Haiman and Loeb, 2001). Numerical evaluation of this scenario requires us to secure the two most important pillars of contemporary astrophysics:

1. Dark matter cosmology: How rare is the density peak which later evolves to a massive quasar hosting halo? How have dark matter (DM) halos merged to form this massive halo?

2. Baryonic physics: How does gas fall into the gravitational potential of a DM halo? How is the gas consumed by star formation and BH accretion? How do stellar and MBH feedback in turn change the interstellar medium and self-regulate their growths?

While DM cosmology is relatively well constrained through analytic studies, many complications still remain in describing galactic baryonic physics even in the most recent numerical attempts (Li et al., 2007b; Sijacki et al., 2009). For example, the key challenge in studies of quasar formation is to describe how a MBH acquires its mass, and how it affects its host galaxy through feedback. However, previous studies have empirically boosted the Bondi accretion estimate by 10 - 300 to compensate for coarse resolutions (Booth and Schaye, 2009). Poor resolution has also forced simulators to skip the thermalization process below the resolution limit, and to simply thermally deposit MBH feedback energy near the MBH (e.g. Springel et al., 2005b)). These sub-resolution approaches often add too many tunable parameters to an already complicated problem. Therefore, a self-consistent numerical framework we developed for galactic simulations will be ideal to track how galaxies and MBHs have evolved under each others influence to form high-redshift quasars.

6.3.2 Building High-redshift Quasars with Unabridged Physics

By simulating quasars in early universe in a self-consistent numerical framework, we can prove or falsify the validity of the pillars of contemporary astrophysics. While challenging, this calculation is well-timed as observations provide good constraints on galactic evolution, and numerical resolution reaches ever so close to resolve individual galaxies in a ($\sim$ Gpc)^3 volume. Combining thorough experience in carrying out galactic and cosmological simulations with MBHs (Kim et al., 2009, 2010, 2011) and *Enzo*'s intensive radiation calculation capability, we are well poised to perform a state-of-the-art calculation to assess the accretion history of MBHs in the early universe.

Required Physics and Enabling Techniques

1. *Multi-scale physics*: To simulate high-redshift quasars whose number density is < 10 Gpc^{-3} at $z \sim 6$, a simulation box of $(500\ h^{-1}\mathrm{Mpc})^3$ is necessary (Sijacki et al., 2009). Meanwhile, ~ 50 pc resolution is required to resolve the gas inflow around $\sim 10^5 M_\odot$ BHs as well as the characteristic scale of molecular clouds. This multi-scale simulation with a dynamic range of $\sim 10^7$ will be achieved by employing *Enzo* adaptive mesh refinement.

2. *Hydrodynamics*: The shock-capturing Riemann solver is ideal to depict the mechanical feedback of MBHs: bipolar jets of $\sim 10^3\ \mathrm{km\,s^{-1}}$ (Kim et al., 2010). The *Enzo* magnetohydrodyanmics (MHD; Wang and Abel, 2009) module has been tested in galactic simulations with MBHs, and will continue to be improved in order to measure how magnetic fields aid jets in efficiently depositing outflow momentum onto the infalling gas and boost galactic nonthermal pressure (Dubois et al., 2009; Wang et al., 2010).

3. *Radiation sources*: From $z \sim 15$ to $z \sim 6$ a sequence of ~ 10 mergers is expected to form a $> 10^{13} M_\odot$ halo hosting a quasar at $z \sim 6$. Therefore, at least ~ 10 MBHs in each merging halo need to be described as sources of radiation. We will use coupled radiative transfer module tested with > 30 radiation sources (Wise and Abel, 2010). In addition, an auxiliary radiative transfer machinery has been being built to heat and ionize the gas using pre-tabulated rates, to account for the polychromatic energy distribution of MBH radiation.

4. *Refined MBH physics*: A MBH particle resolved by ~ 50 pc resolution represents not just the BH itself, but also includes stars and accreting gas deep within the galactic nucleus. Therefore, one should improve the physics around MBH, such

as stellar winds from a nuclear disk (Ciotti et al., 2009). The nuclear disk wind has been implemented as the injection of thermal energy, tested to work in conjunction with the aforementioned MBH radiative and mechanical feedback.

5. *Other galactic scale physics*: We will maintain the basic formalism of the molecular cloud formation and stellar feedback, along with the 6-species chemistry ($\mathrm{H, H^+, He, He^+, He^{++}, e^-}$) and cooling below 10^4 K, as were previously detailed.

Proposed Simulation Strategy

1. *Low-resolution stage*: We first identify a massive DM halo of $\sim 10^{13} M_\odot$ at $z \sim 6$ by running a coarse adiabatic run in a $(500\,h^{-1}\mathrm{Mpc})^3$ box. Then we recenter the density field around this halo and set up a new initial condition that contains a small-scale power as well, with a 512^3 root grid and a series of three nested grids of twice finer resolution each. The grid at level 3 encloses the Lagrangian volume of the quasar-hosting halo and manifests the equivalent resolution of 4096^3 unigrid. This method saves a computational expense of performing a 4096^3 root grid calculation being refined everywhere, and is well demonstrated in Kim et al. (2010) (Chapter 3).

2. *High-resolution stage*: We then impose $\sim$ 50 pc resolution while introducing physics modules described in Kim et al. (2010) (Chapter 2). With a 512^3 root grid box of $(500\,h^{-1}\mathrm{Mpc})^3$ refined by factors of two along each axis, this resolution corresponds to a maximum refinement level of 12 at $z \sim 6$, very feasible on parallelized *Enzo*. Using the inline halo finder, a $10^{4-5} M_\odot$ seed BH is placed every time the host halo reaches a total mass of $10^{10} M_\odot$. With novel radiative transfer techniques such as truncating the ray tracing at the virial radius of a MBH hosting halo, or ray merging (Wise and Abel, 2010), the simulation performance is expected to scale up well with the number of processors.

3. *Analysis and mock observations*: We propose a suite of simulations with varying modes of MBH feedback to measure how the self-regulating MBH feedback

affects the build-up of high-redshift quasars. We will investigate how the BH accretion and star formation are influenced by halo merger events and the inclusion of different MBH feedback, magnetic fields, etc. Our high-resolution simulation will also provide exceptional datasets for synthesized galactic spectra and images which embody the galactic star formation history and dust distribution. These simulated observations (Figure 6.1) will be readily comparable with observations of early universe by HST, Spitzer, and JWST in the future (Gardner et al., 2006).

Extending The Scope

An immediate extension of the proposed project is to study the interwoven destiny of galaxies and MBHs, remarkably imprinted in the relation between the MBH masses and bulge stellar velocity distributions ($M_{\rm BH} - \sigma_{\rm bulge}$; e.g. Ferrarese and Merritt, 2000). It will be possible to carry out close inspection on each merging event and the rapid BH growth therein down to lower redshift, followed by a remnants analysis with disk-bulge decomposition (Di Matteo et al., 2008). The redshift evolution of the $M_{\rm BH} - \sigma_{\rm bulge}$ relation can be compared to the observed data (e.g. SDSS by Woo et al., 2008), with which we can calibrate our MBH models and put a powerful constraint on the coevolution of galaxies and MBHs.

Another extension is to explore the reionization history of the intergalactic helium by high-redshift quasars. Since it requires a larger number of radiation sources, subresolution models of MBH physics derived from the earlier work could be used to speed up the calculation. For example, the radial profile of heating rates by a MBH in small scale simulations (as in Kim et al., 2010) can first be tabulated. Then, in coarsely resolved large-scale simulations, one can inject thermal energy with this radial dependence. Moreover, by integrating the ionizing radiation escaping the high-redshift quasars, one can put a stronger constraint on the relative contributions of Population III stars and quasars for hydrogen reionization, whose signature will be better measured by JWST and ALMA (Gardner et al., 2006).

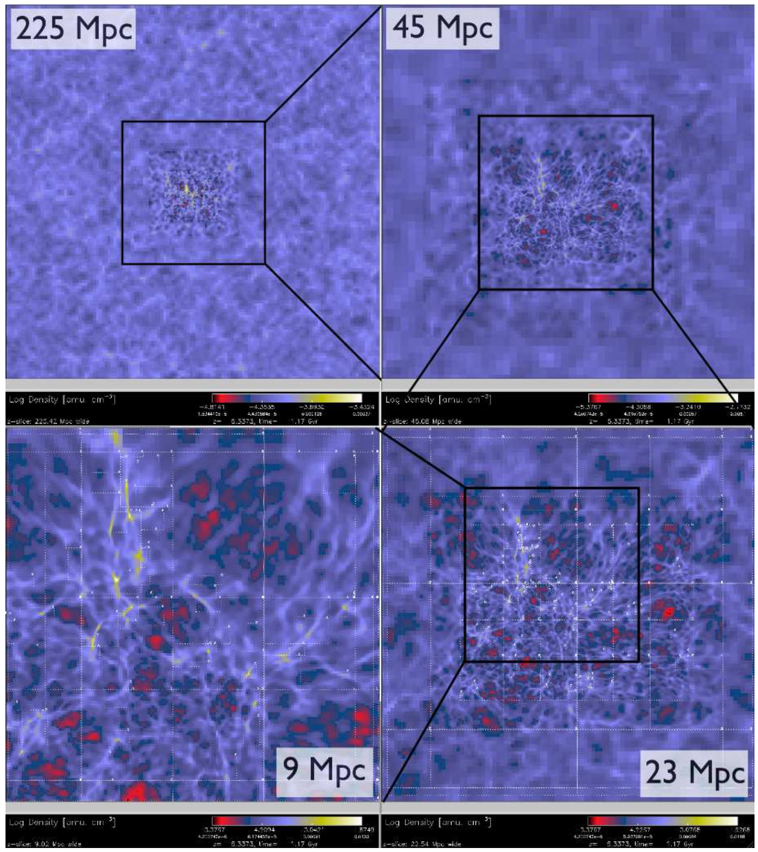

Fig. 6.2.— A snapshot of a galaxy cluster simulation with the initial condition of effective resolution of 4096^3. The initial condition is generated for $(1\,h^{-1}\mathrm{Gpc})^3$ at $z = 30$, and the snapshot is taken at $z = 5.3$.

6.4 Further Applications of the Numerical Framework

The publicly available astrophysical code *Enzo* and its implementation of stellar physics and MBH physics can be straightforwardly deployed in other settings. Among many, we report two of such possibilities which are also under active investigation.

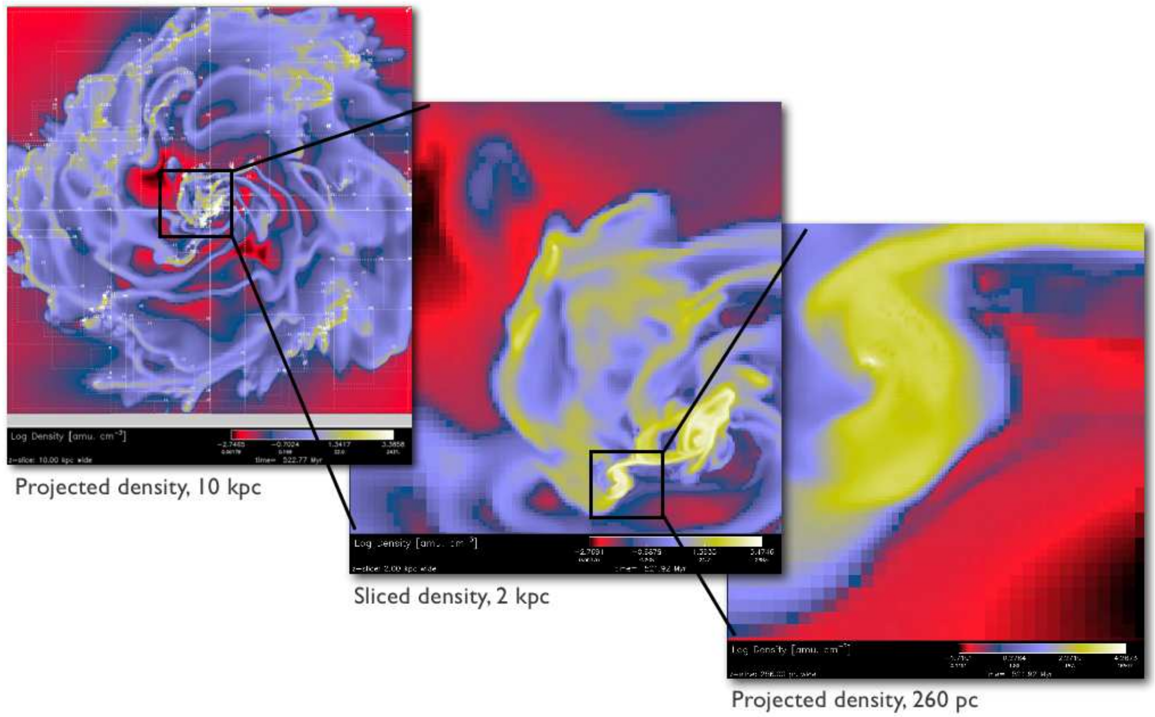

Fig. 6.3.— A snapshot of a star cluster simulation in a galactic context reaching the resolution of 0.47 pc for a $2 \times 10^{11} M_{\odot}$ galaxy.

6.4.1 Stopping of Cooling Catastrophe in Galaxy Clusters

The same numerical framework for galactic scale simulations can be employed for other applications such as simulations of galaxy clusters. Figure 6.2 shows a snapshot of such simulation with an initial condition of effective resolution of 4096^3 in $(1\,h^{-1}\text{Gpc})^3$, created with the MUlti-Scale Initial Condition generator (*MUSIC*) by Hahn and Abel (2011). The mechanical feedback of active galactic nuclei (AGN) at the centers of massive clusters can be turned on with constant energy input at around $z = 2 - 3$. The so-called *cooling catastrophe* in the cluster simulation may be stopped or regulated by the energetic AGN jets (Dubois et al., 2010).

6.4.2 Stellar Cluster Formation in Galactic Context

The high dynamic range of *Enzo* can be employed to observe the formation of individual star clusters in the context of evolving galaxies. Figure 6.3 demonstrates a snapshot of such attempt where more resolution (up to 0.47 pc) is imposed while particles are split via the technique described in §3.1.1. The cooling curve shown in Figure 1.1 needs to be used to include the effect of radiative cooling by molecular hydrogen in dense regions ($n_{\rm H} > 10^{7-8}\,{\rm cm}^{-3}$). This new approach will overcome the limitations of typical star cluster simulations where a single stars cluster forms in an idealized set up (e.g. Wang et al., 2010).

The theory of galaxy formation is still incomplete and stained with numerous unknowns. However, it also ironically signifies that now is the great time for astrophysicists to contribute to the perfection of the galaxy formation theory. As has been illustrated in the candidate's thesis, numerical studies of galaxy formation will help us overcome the problems and hurdles the contemporary researchers experience. What is even more encouraging is that the numerical investigation of galaxy formation has enormous room for improvements, and its potential is only starting to be discovered. Ever improving simulation data, joined with the wealth of observations, will gradually make us open our eyes to the truth and beauty of the Universe.

Bibliography

Aarseth, S. J., Turner, E. L., and Gott, III, J. R. (1979). N-body simulations of galaxy clustering. I - Initial conditions and galaxy collapse times. *ApJ*, 228:664–683.

Abadi, M. G., Navarro, J. F., Steinmetz, M., and Eke, V. R. (2003). Simulations of Galaxy Formation in a Λ Cold Dark Matter Universe. II. The Fine Structure of Simulated Galactic Disks. *ApJ*, 597:21–34.

Abel, T. (2011). rpSPH: a novel smoothed particle hydrodynamics algorithm. *MNRAS*, pages 196–+.

Abel, T., Anninos, P., Zhang, Y., and Norman, M. L. (1997). Modeling primordial gas in numerical cosmology. *New Astronomy*, 2:181–207.

Abel, T. and Wandelt, B. D. (2002). Adaptive ray tracing for radiative transfer around point sources. *MNRAS*, 330:L53–L56.

Abel, T., Wise, J. H., and Bryan, G. L. (2007). The H II Region of a Primordial Star. *ApJ*, 659:L87–L90.

Agertz, O., Moore, B., Stadel, J., Potter, D., Miniati, F., Read, J., Mayer, L., Gawryszczak, A., Kravtsov, A., Nordlund, Å., Pearce, F., Quilis, V., Rudd, D., Springel, V., Stone, J., Tasker, E., Teyssier, R., Wadsley, J., and Walder, R. (2007). Fundamental differences between SPH and grid methods. *MNRAS*, 380:963–978.

Agertz, O., Teyssier, R., and Moore, B. (2011). The formation of disc galaxies in a ΛCDM universe. *MNRAS*, 410:1391–1408.

Alladin, S. M. (1965). The Dynamics of Colliding Galaxies. *ApJ*, 141:768–+.

Allen, S. W., Dunn, R. J. H., Fabian, A. C., Taylor, G. B., and Reynolds, C. S. (2006). The relation between accretion rate and jet power in X-ray luminous elliptical galaxies. *MNRAS*, 372:21–30.

Alvarez, M. A., Wise, J. H., and Abel, T. (2009). Accretion onto the First Stellar-Mass Black Holes. *ApJ*, 701:L133–L137.

Anninos, P., Zhang, Y., Abel, T., and Norman, M. L. (1997). Cosmological hydrodynamics with multi-species chemistry and nonequilibrium ionization and cooling. *New Astronomy*, 2:209–224.

Anninos, W. Y. and Norman, M. J. (1994). Nonlinear hydrodynamics of cosmological sheets. 1: Numerical techniques and tests. *ApJ*, 429:434–464.

Antonucci, R. (1993). Unified models for active galactic nuclei and quasars. *ARA&A*, 31:473–521.

Antonuccio-Delogu, V. and Silk, J. (2008). Active galactic nuclei jet-induced feedback in galaxies - I. Suppression of star formation. *MNRAS*, 389:1750–1762.

Arp, H. (1966). *Atlas of peculiar galaxies.* Pasadena: California Inst. Technology, 1966.

Bailin, J., Kawata, D., Gibson, B. K., Steinmetz, M., Navarro, J. F., Brook, C. B., Gill, S. P. D., Ibata, R. A., Knebe, A., Lewis, G. F., and Okamoto, T. (2005). Internal Alignment of the Halos of Disk Galaxies in Cosmological Hydrodynamic Simulations. *ApJ*, 627:L17–L20.

Bakes, E. L. O. and Tielens, A. G. G. M. (1994). The photoelectric heating mechanism for very small graphitic grains and polycyclic aromatic hydrocarbons. *ApJ*, 427:822–838.

Balogh, M. L., Pearce, F. R., Bower, R. G., and Kay, S. T. (2001). Revisiting the cosmic cooling crisis. *MNRAS*, 326:1228–1234.

Barnes, J. and Efstathiou, G. (1987). Angular momentum from tidal torques. *ApJ*, 319:575–600.

Barnes, J. and Hut, P. (1986). A hierarchical O(N log N) force-calculation algorithm. *Nature*, 324:446–449.

Barnes, J. E. (1988). Encounters of disk/halo galaxies. *ApJ*, 331:699–717.

Barnes, J. E. (2004). Shock-induced star formation in a model of the Mice. *MNRAS*, 350:798–808.

Barnes, J. E. and Hernquist, L. (1992a). Dynamics of interacting galaxies. *ARA&A*, 30:705–742.

Barnes, J. E. and Hernquist, L. (1992b). Formation of dwarf galaxies in tidal tails. *Nature*, 360:715–717.

Barnes, J. E. and Hernquist, L. (1996). Transformations of Galaxies. II. Gasdynamics in Merging Disk Galaxies. *ApJ*, 471:115–+.

Barnes, J. E. and Hernquist, L. E. (1991). Fueling starburst galaxies with gas-rich mergers. *ApJ*, 370:L65–L68.

Baugh, C. M. (2006). A primer on hierarchical galaxy formation: the semi-analytical approach. *Reports on Progress in Physics*, 69:3101–3156.

Benson, A. J. (2010). Galaxy formation theory. *Phys. Rep.*, 495:33–86.

Berger, M. J. and Colella, P. (1989). Local adaptive mesh refinement for shock hydrodynamics. *Journal of Computational Physics*, 82:64–84.

Berger, M. J. and Oliger, J. (1984). Adaptive Mesh Refinement for Hyperbolic Partial Differential Equations. *Journal of Computational Physics*, 53:484–+.

Bertschinger, E. (1995). COSMICS: Cosmological Initial Conditions and Microwave Anisotropy Codes. *ArXiv Astrophysics e-prints*.

Bertschinger, E. (1998). Simulations of Structure Formation in the Universe. *ARA&A*, 36:599–654.

Bertschinger, E. (2001). Multiscale Gaussian Random Fields and Their Application to Cosmological Simulations. *ApJS*, 137:1–20.

Biretta, J. A. and Junor, W. (1995). The Parsec-Scale Jet in M87. *Proceedings of the National Academy of Science*, 92:11364–11367.

Biretta, J. A., Sparks, W. B., and Macchetto, F. (1999). Hubble Space Telescope Observations of Superluminal Motion in the M87 Jet. *ApJ*, 520:621–626.

Birnboim, Y. and Dekel, A. (2003). Virial shocks in galactic haloes? *MNRAS*, 345:349–364.

Blandford, R. D. and Payne, D. G. (1982). Hydromagnetic flows from accretion discs and the production of radio jets. *MNRAS*, 199:883–903.

Blandford, R. D. and Znajek, R. L. (1977). Electromagnetic extraction of energy from Kerr black holes. *MNRAS*, 179:433–456.

Bode, P., Ostriker, J. P., and Xu, G. (2000). The Tree Particle-Mesh N-Body Gravity Solver. *ApJS*, 128:561–569.

Bondi, H. (1952). On spherically symmetrical accretion. *MNRAS*, 112:195–+.

Bondi, H. and Hoyle, F. (1944). On the mechanism of accretion by stars. *MNRAS*, 104:273–+.

Booth, C. M. and Schaye, J. (2009). Cosmological simulations of the growth of supermassive black holes and feedback from active galactic nuclei: method and tests. *MNRAS*, 398:53–74.

Borgani, S., Murante, G., Springel, V., Diaferio, A., Dolag, K., Moscardini, L., Tormen, G., Tornatore, L., and Tozzi, P. (2004). X-ray properties of galaxy clusters and groups from a cosmological hydrodynamical simulation. *MNRAS*, 348:1078–1096.

Bournaud, F., Chapon, D., Teyssier, R., Powell, L. C., Elmegreen, B. G., Elmegreen, D. M., Duc, P., Contini, T., Epinat, B., and Shapiro, K. L. (2011). Hydrodynamics of High-redshift Galaxy Collisions: From Gas-rich Disks to Dispersion-dominated Mergers and Compact Spheroids. *ApJ*, 730:4–+.

Bridle, A. H. and Perley, R. A. (1984). Extragalactic Radio Jets. *ARA&A*, 22:319–358.

Bromm, V. and Loeb, A. (2003). Formation of the First Supermassive Black Holes. *ApJ*, 596:34–46.

Brook, C. B., Kawata, D., Martel, H., Gibson, B. K., and Bailin, J. (2006). Disk Evolution since z˜1 in a CDM Universe. *ApJ*, 639:126–135.

Bryan, G. L., Abel, T., and Norman, M. L. (2001). Achieving Extreme Resolution in Numerical Cosmology Using Adaptive Mesh Refinement: Resolving Primordial Star Formation. *ArXiv e-prints*, 112:arXiv:0112089.

Bryan, G. L. and Norman, M. L. (1997). Simulating X-Ray Clusters with Adaptive Mesh Refinement. In Clarke, D. A. and West, M. J., editors, *Computational Astrophysics; 12th Kingston Meeting on Theoretical Astrophysics*, volume 123 of *Astronomical Society of the Pacific Conference Series*, pages 363–368.

Bullock, J. S., Dekel, A., Kolatt, T. S., Kravtsov, A. V., Klypin, A. A., Porciani, C., and Primack, J. R. (2001). A Universal Angular Momentum Profile for Galactic Halos. *ApJ*, 555:240–257.

Burkert, A. and Tremaine, S. (2010). A Correlation Between Central Supermassive Black Holes and the Globular Cluster Systems of Early-type Galaxies. *ApJ*, 720:516–521.

Bush, S. J., Cox, T. J., Hernquist, L., Thilker, D., and Younger, J. D. (2008). Simulations of XUV Disks with a Star Formation Density Threshold. *ApJ*, 683:L13–L16.

Callegari, S., Kazantzidis, S., Mayer, L., Colpi, M., Bellovary, J. M., Quinn, T., and Wadsley, J. (2010). Growing Massive Black Hole Pairs in Minor Mergers of Disk Galaxies. *ArXiv e-prints*, 1002:arXiv:1002.1712.

Cattaneo, A., Faber, S. M., Binney, J., Dekel, A., Kormendy, J., Mushotzky, R., Babul, A., Best, P. N., Brüggen, M., Fabian, A. C., Frenk, C. S., Khalatyan, A., Netzer, H., Mahdavi, A., Silk, J., Steinmetz, M., and Wisotzki, L. (2009). The role of black holes in galaxy formation and evolution. *Nature*, 460:213–219.

Cattaneo, A. and Teyssier, R. (2007). AGN self-regulation in cooling flow clusters. *MNRAS*, 376:1547–1556.

Cen, R., Nagamine, K., and Ostriker, J. P. (2005). Quantitative Signatures of Galactic Superwinds on Lyα Clouds and Metal-Line Systems. *ApJ*, 635:86–99.

Cen, R. and Ostriker, J. P. (1992). Galaxy formation and physical bias. *ApJ*, 399:L113–L116.

Centrella, J., Baker, J. G., Kelly, B. J., and van Meter, J. R. (2010). The Final Merger of Black-Hole Binaries. *Annual Review of Nuclear and Particle Science*, 60:75–100.

Ceverino, D., Dekel, A., and Bournaud, F. (2010). High-redshift clumpy discs and bulges in cosmological simulations. *MNRAS*, 404:2151–2169.

Ceverino, D. and Klypin, A. (2009). The Role of Stellar Feedback in the Formation of Galaxies. *ApJ*, 695:292–309.

Chandrasekhar, S. (1943). Dynamical Friction. I. General Considerations: the Coefficient of Dynamical Friction. *ApJ*, 97:255–+.

Christensen, C. R., Quinn, T., Stinson, G., Bellovary, J., and Wadsley, J. (2010). Star Formation and Feedback in Smoothed Particle Hydrodynamic Simulations. II. Resolution Effects. *ApJ*, 717:121–132.

Ciotti, L. and Ostriker, J. P. (2001). Cooling Flows and Quasars. II. Detailed Models of Feedback-modulated Accretion Flows. *ApJ*, 551:131–152.

Ciotti, L. and Ostriker, J. P. (2007). Radiative Feedback from Massive Black Holes in Elliptical Galaxies: AGN Flaring and Central Starburst Fueled by Recycled Gas. *ApJ*, 665:1038–1056.

Ciotti, L., Ostriker, J. P., and Proga, D. (2009). Feedback from Central Black Holes in Elliptical Galaxies. I. Models with Either Radiative or Mechanical Feedback but not Both. *ApJ*, 699:89–104.

Ciotti, L., Ostriker, J. P., and Proga, D. (2010). Feedback from Central Black Holes in Elliptical Galaxies. III. Models with Both Radiative and Mechanical Feedback. *ApJ*, 717:708–723.

Colberg, J. M. and Di Matteo, T. (2008). Supermassive black holes and their environments. *MNRAS*, 387:1163–1178.

Cole, S., Lacey, C. G., Baugh, C. M., and Frenk, C. S. (2000). Hierarchical galaxy formation. *MNRAS*, 319:168–204.

Cole, S., Norberg, P., Baugh, C. M., Frenk, C. S., Bland-Hawthorn, J., Bridges, T., Cannon, R., Colless, M., Collins, C., Couch, W., Cross, N., Dalton, G., De Propris, R., Driver, S. P., Efstathiou, G., Ellis, R. S., Glazebrook, K., Jackson, C., Lahav, O., Lewis, I., Lumsden, S., Maddox, S., Madgwick, D., Peacock, J. A., Peterson, B. A., Sutherland, W., and Taylor, K. (2001). The 2dF galaxy redshift survey: near-infrared galaxy luminosity functions. *MNRAS*, 326:255–273.

Colella, P. and Woodward, P. R. (1984). The Piecewise Parabolic Method (PPM) for Gas-Dynamical Simulations. *Journal of Computational Physics*, 54:174–201.

Couchman, H. M. P. (1991). Mesh-refined P3M - A fast adaptive N-body algorithm. *ApJ*, 368:L23–L26.

Couchman, H. M. P., Thomas, P. A., and Pearce, F. R. (1995). Hydra: an Adaptive-Mesh Implementation of P 3M-SPH. *ApJ*, 452:797–+.

Cox, T. J., Di Matteo, T., Hernquist, L., Hopkins, P. F., Robertson, B., and Springel, V. (2006a). X-Ray Emission from Hot Gas in Galaxy Mergers. *ApJ*, 643:692–706.

Cox, T. J., Jonsson, P., Primack, J. R., and Somerville, R. S. (2006b). Feedback in simulations of disc-galaxy major mergers. *MNRAS*, 373:1013–1038.

Croton, D. J., Springel, V., White, S. D. M., De Lucia, G., Frenk, C. S., Gao, L., Jenkins, A., Kauffmann, G., Navarro, J. F., and Yoshida, N. (2006). The many lives of active galactic nuclei: cooling flows, black holes and the luminosities and colours of galaxies. *MNRAS*, 365:11–28.

Dalla Vecchia, C. and Schaye, J. (2008). Simulating galactic outflows with kinetic supernova feedback. *MNRAS*, 387:1431–1444.

de Avillez, M. A. (1999). Three-Dimensional Evolution of the Galactic Fountain. In Gibson, B. K. and Putman, M. E., editors, *Stromlo Workshop on High-Velocity Clouds*, volume 166 of *Astronomical Society of the Pacific Conference Series*, pages 103–+.

De Lucia, G. and Helmi, A. (2008). The Galaxy and its stellar halo - insights from a hybrid cosmological approach. *ArXiv e-prints*, 807:arXiv:0807.1109.

DeBuhr, J., Quataert, E., and Ma, C. (2010). The Growth of Massive Black Holes in Galaxy Merger Simulations with Feedback by Radiation Pressure. *ArXiv e-prints*, 1006:arXiv:1006.3312.

Dedner, A., Kemm, F., Kröner, D., Munz, C.-D., Schnitzer, T., and Wesenberg, M. (2002). Hyperbolic divergence cleaning for the mhd equations. *J. Comput. Phys.*, 175(2):645–673.

Dekel, A. and Birnboim, Y. (2006). Galaxy bimodality due to cold flows and shock heating. *MNRAS*, 368:2–20.

Dekel, A., Birnboim, Y., Engel, G., Freundlich, J., Goerdt, T., Mumcuoglu, M., Neistein, E., Pichon, C., Teyssier, R., and Zinger, E. (2009). Cold streams in early massive hot haloes as the main mode of galaxy formation. *Nature*, 457:451–454.

Di Matteo, T., Colberg, J., Springel, V., Hernquist, L., and Sijacki, D. (2008). Direct Cosmological Simulations of the Growth of Black Holes and Galaxies. *ApJ*, 676:33–53.

Di Matteo, T., Springel, V., and Hernquist, L. (2005). Energy input from quasars regulates the growth and activity of black holes and their host galaxies. *Nature*, 433:604–607.

Diemand, J., Kuhlen, M., and Madau, P. (2007). Dark Matter Substructure and Gamma-Ray Annihilation in the Milky Way Halo. *ApJ*, 657:262–270.

Diemand, J., Kuhlen, M., Madau, P., Zemp, M., Moore, B., Potter, D., and Stadel, J. (2008). Clumps and streams in the local dark matter distribution. *Nature*, 454:735–738.

Dubois, Y., Devriendt, J., Slyz, A., and Silk, J. (2009). Influence of AGN jets on the magnetized ICM. *MNRAS*, 399:L49–L53.

Dubois, Y., Devriendt, J., Slyz, A., and Teyssier, R. (2010). Jet-regulated cooling catastrophe. *ArXiv e-prints*, 1004:arXiv:1004.1851.

Dubois, Y. and Teyssier, R. (2008). On the onset of galactic winds in quiescent star forming galaxies. *A&A*, 477:79–94.

Dubois, Y. and Teyssier, R. (2010). Magnetised winds in dwarf galaxies. *A&A*, 523:A72+.

Efstathiou, G., Davis, M., White, S. D. M., and Frenk, C. S. (1985). Numerical techniques for large cosmological N-body simulations. *ApJS*, 57:241–260.

Efstathiou, G. and Eastwood, J. W. (1981). On the clustering of particles in an expanding universe. *MNRAS*, 194:503–525.

Eggen, O. J., Lynden-Bell, D., and Sandage, A. R. (1962). Evidence from the motions of old stars that the Galaxy collapsed. *ApJ*, 136:748–+.

Eisenstein, D. J. and Hu, W. (1999). Power Spectra for Cold Dark Matter and Its Variants. *ApJ*, 511:5–15.

Eke, V. R., Cole, S., and Frenk, C. S. (1996). Cluster evolution as a diagnostic for Omega. *MNRAS*, 282:263–280.

Enßlin, T. A., Pfrommer, C., Springel, V., and Jubelgas, M. (2007). Cosmic ray physics in calculations of cosmological structure formation. *A&A*, 473:41–57.

Fabian, A. C., Arnaud, K. A., Bautz, M. W., and Tawara, Y. (1994). ASCA observations of cooling flows in clusters of galaxies. *ApJ*, 436:L63–L66.

Fabian, A. C., Celotti, A., Blundell, K. M., Kassim, N. E., and Perley, R. A. (2002). The properties of the X-ray holes in the intracluster medium of the Perseus cluster. *MNRAS*, 331:369–375.

Fall, S. M. and Efstathiou, G. (1980). Formation and rotation of disc galaxies with haloes. *MNRAS*, 193:189–206.

Fan, X., Strauss, M. A., Becker, R. H., White, R. L., Gunn, J. E., Knapp, G. R., Richards, G. T., Schneider, D. P., Brinkmann, J., and Fukugita, M. (2006). Constraining the Evolution of the Ionizing Background and the Epoch of Reionization with z˜6 Quasars. II. A Sample of 19 Quasars. *AJ*, 132:117–136.

Fermi, E. (1954). Galactic Magnetic Fields and the Origin of Cosmic Radiation. *ApJ*, 119:1–+.

Ferrarese, L. and Ford, H. (2005). Supermassive Black Holes in Galactic Nuclei: Past, Present and Future Research. *Space Sci. Rev.*, 116:523–624.

Ferrarese, L. and Merritt, D. (2000). A Fundamental Relation between Supermassive Black Holes and Their Host Galaxies. *ApJ*, 539:L9–L12.

Font, A. S., Bower, R. G., McCarthy, I. G., Benson, A. J., Frenk, C. S., Helly, J. C., Lacey, C. G., Baugh, C. M., and Cole, S. (2008). The colours of satellite galaxies in groups and clusters. *MNRAS*, 389:1619–1629.

Foyle, K., Courteau, S., and Thacker, R. J. (2008). An N-body/SPH study of isolated galaxy mass density profiles. *MNRAS*, 386:1821–1844.

Fryxell, B., Olson, K., Ricker, P., Timmes, F. X., Zingale, M., Lamb, D. Q., MacNeice, P., Rosner, R., Truran, J. W., and Tufo, H. (2000). FLASH: An Adaptive Mesh Hydrodynamics Code for Modeling Astrophysical Thermonuclear Flashes. *ApJS*, 131:273–334.

Gardner, J. P., Mather, J. C., Clampin, M., Doyon, R., Greenhouse, M. A., Hammel, H. B., Hutchings, J. B., Jakobsen, P., Lilly, S. J., Long, K. S., Lunine, J. I., McCaughrean, M. J., Mountain, M., Nella, J., Rieke, G. H., Rieke, M. J., Rix, H., Smith, E. P., Sonneborn, G., Stiavelli, M., Stockman, H. S., Windhorst, R. A., and Wright, G. S. (2006). The James Webb Space Telescope. *Space Sci. Rev.*, 123:485–606.

Gavazzi, G., Giovanelli, R., Haynes, M. P., Fabello, S., Fumagalli, M., Kent, B. R., Koopmann, R. A., Brosch, N., Hoffman, G. L., Salzer, J. J., and Boselli, A. (2008). HI content and other structural properties of galaxies in the Virgo cluster from the Arecibo Legacy Fast ALFA Survey. *A&A*, 482:43–52.

Gebhardt, K., Bender, R., Bower, G., Dressler, A., Faber, S. M., Filippenko, A. V., Green, R., Grillmair, C., Ho, L. C., Kormendy, J., Lauer, T. R., Magorrian, J., Pinkney, J., Richstone, D., and Tremaine, S. (2000). A Relationship between Nuclear Black Hole Mass and Galaxy Velocity Dispersion. *ApJ*, 539:L13–L16.

Gibson, B. K., Courty, S., Sanchez-Blazquez, P., Teyssier, R., House, E. L., Brook, C. B., and Kawata, D. (2008). Hydrodynamical Adaptive Mesh Refinement Simulations of Disk Galaxies. *ArXiv e-prints*, 808:arXiv:0808.0576.

Gingold, R. A. and Monaghan, J. J. (1977). Smoothed particle hydrodynamics - Theory and application to non-spherical stars. *MNRAS*, 181:375–389.

Glover, S. C. O. and Jappsen, A. (2007). Star Formation at Very Low Metallicity. I. Chemistry and Cooling at Low Densities. *ApJ*, 666:1–19.

Gopal-Krishna, Biermann, P. L., and Wiita, P. J. (2003). The Origin of X-shaped Radio Galaxies: Clues from the Z-symmetric Secondary Lobes. *ApJ*, 594:L103–L106.

Governato, F., Brook, C. B., Brooks, A. M., Mayer, L., Willman, B., Jonsson, P., Stilp, A. M., Pope, L., Christensen, C., Wadsley, J., and Quinn, T. (2009). Forming a large disc galaxy from a z $\sim$ 1 major merger. *MNRAS*, 398:312–320.

Governato, F., Willman, B., Mayer, L., Brooks, A., Stinson, G., Valenzuela, O., Wadsley, J., and Quinn, T. (2007). Forming disc galaxies in ΛCDM simulations. *MNRAS*, 374:1479–1494.

Gültekin, K., Richstone, D. O., Gebhardt, K., Lauer, T. R., Tremaine, S., Aller, M. C., Bender, R., Dressler, A., Faber, S. M., Filippenko, A. V., Green, R., Ho, L. C., Kormendy, J., Magorrian, J., Pinkney, J., and Siopis, C. (2009). The M-σ and M-L Relations in Galactic Bulges, and Determinations of Their Intrinsic Scatter. *ApJ*, 698:198–221.

Gunn, J. E. and Gott, III, J. R. (1972). On the Infall of Matter Into Clusters of Galaxies and Some Effects on Their Evolution. *ApJ*, 176:1–+.

Guo, F. and Mathews, W. G. (2011). Fermi Bubbles: Evidence for a Possible Recent AGN Jet Activity in the Galaxy. *ArXiv e-prints*.

Guo, Q., White, S., Li, C., and Boylan-Kolchin, M. (2010). How do galaxies populate dark matter haloes? *MNRAS*, 404:1111–1120.

Haardt, F. and Madau, P. (1996). Radiative Transfer in a Clumpy Universe. II. The Ultraviolet Extragalactic Background. *ApJ*, 461:20–+.

Haardt, F. and Madau, P. (2001). Modelling the UV/X-ray cosmic background with CUBA. In D. M. Neumann & J. T. V. Tran, editor, *Clusters of Galaxies and the High Redshift Universe Observed in X-rays*.

Haehnelt, M. G. (1995). Momentum transfer by an internal source of ionizing radiation: an important feedback process during galaxy formation? *MNRAS*, 273:249–256.

Hahn, O. and Abel, T. (2011). Multi-scale initial conditions for cosmological simulations. *ArXiv e-prints*.

Haiman, Z. and Loeb, A. (2001). What Is the Highest Plausible Redshift of Luminous Quasars? *ApJ*, 552:459–463.

Häring, N. and Rix, H. (2004). On the Black Hole Mass-Bulge Mass Relation. *ApJ*, 604:L89–L92.

Heger, A. and Woosley, S. E. (2002). The Nucleosynthetic Signature of Population III. *ApJ*, 567:532–543.

Hernquist, L. (1987). Performance characteristics of tree codes. *ApJS*, 64:715–734.

Hernquist, L. (1993). N-body realizations of compound galaxies. *ApJS*, 86:389–400.

Hockney, R. W. and Eastwood, J. W. (1981). *Computer Simulation Using Particles*.

Hockney, R. W. and Eastwood, J. W. (1988). *Computer simulation using particles*.

Holmberg, E. (1941). On the Clustering Tendencies among the Nebulae. II. a Study of Encounters Between Laboratory Models of Stellar Systems by a New Integration Procedure. *ApJ*, 94:385–+.

Homan, D. C., Kadler, M., Kellermann, K. I., Kovalev, Y. Y., Lister, M. L., Ros, E., Savolainen, T., and Zensus, J. A. (2009). MOJAVE: Monitoring of Jets in Active Galactic Nuclei with VLBA Experiments. VII. Blazar Jet Acceleration. *ApJ*, 706:1253–1268.

Hopkins, P. F., Hernquist, L., Cox, T. J., and Kereš, D. (2008). A Cosmological Framework for the Co-Evolution of Quasars, Supermassive Black Holes, and Elliptical Galaxies. I. Galaxy Mergers and Quasar Activity. *ApJS*, 175:356–389.

Hopkins, P. F. and Quataert, E. (2010). How do massive black holes get their gas? *MNRAS*, pages 1085–+.

Hopkins, P. F., Quataert, E., and Murray, N. (2011). Self-Regulated Star Formation in Galaxies via Momentum Input from Massive Stars. *ArXiv e-prints*.

Jeans, J. H. (1902). The Stability of a Spherical Nebula. *Royal Society of London Philosophical Transactions Series A*, 199:1–53.

Johansson, P. H., Naab, T., and Burkert, A. (2009). Equal- and Unequal-Mass Mergers of Disk and Elliptical Galaxies with Black Holes. *ApJ*, 690:802–821.

Jonsson, P., Groves, B. A., and Cox, T. J. (2010). High-resolution panchromatic spectral models of galaxies including photoionization and dust. *MNRAS*, 403:17–44.

Joung, M. K. R. and Mac Low, M. (2006). Turbulent Structure of a Stratified Supernova-driven Interstellar Medium. *ApJ*, 653:1266–1279.

Junor, W., Biretta, J. A., and Livio, M. (1999). Formation of the radio jet in M87 at 100 Schwarzschild radii from the central black hole. *Nature*, 401:891–892.

Karl, S. J., Naab, T., Johansson, P. H., Kotarba, H., Boily, C. M., Renaud, F., and Theis, C. (2010). One Moment in Time - Modeling Star Formation in the Antennae. *ApJ*, 715:L88–L93.

Katz, N. (1992). Dissipational galaxy formation. II - Effects of star formation. *ApJ*, 391:502–517.

Kauffmann, G. and Haehnelt, M. (2000). A unified model for the evolution of galaxies and quasars. *MNRAS*, 311:576–588.

Kaufmann, T., Mayer, L., Wadsley, J., Stadel, J., and Moore, B. (2007a). Angular momentum transport and disc morphology in smoothed particle hydrodynamics simulations of galaxy formation. *MNRAS*, 375:53–67.

Kaufmann, T., Wheeler, C., and Bullock, J. S. (2007b). On the morphologies, gas fractions, and star formation rates of small galaxies. *MNRAS*, 382:1187–1195.

Kennicutt, Jr., R. C. (1989). The star formation law in galactic disks. *ApJ*, 344:685–703.

Kennicutt, Jr., R. C. (1998). The Global Schmidt Law in Star-forming Galaxies. *ApJ*, 498:541–+.

Kennicutt, Jr., R. C., Calzetti, D., Walter, F., Helou, G., Hollenbach, D. J., Armus, L., Bendo, G., Dale, D. A., Draine, B. T., Engelbracht, C. W., Gordon, K. D., Prescott, M. K. M., Regan, M. W., Thornley, M. D., Bot, C., Brinks, E., de Blok, E., de Mello, D., Meyer, M., Moustakas, J., Murphy, E. J., Sheth, K., and Smith, J. D. T. (2007). Star Formation in NGC 5194 (M51a). II. The Spatially Resolved Star Formation Law. *ApJ*, 671:333–348.

Kereš, D. and Hernquist, L. (2009). Seeding the Formation of Cold Gaseous Clouds in Milky Way-Size Halos. *ApJ*, 700:L1–L5.

Khochfar, S. and Burkert, A. (2006). Orbital parameters of merging dark matter halos. *A&A*, 445:403–412.

Kim, J.-H., Wise, J. H., and Abel, T. (2008). Galaxy Evolution with Adaptive Mesh Refinement. In *First Stars III*, volume 990 of *American Institute of Physics Conference Series*, pages 429–431.

Kim, J.-H., Wise, J. H., and Abel, T. (2009). Galaxy Mergers with Adaptive Mesh Refinement: Star Formation and Hot Gas Outflow. *ApJ*, 694:L123–L127.

Kim, J.-H., Wise, J. H., Alvarez, M. A., and Abel, T. (2010). Galaxy Formation with Self-consistently Modeled Stars and Massive Black Holes I: Feedback-regulated Star Formation and Black Hole Growth. *ApJ*, submitted.

Kim, J.-H., Wise, J. H., Alvarez, M. A., and Abel, T. (2011). Galaxy Formation with Self-consistently Modeled Stars and Massive Black Holes II: Mergers and Triggered Star Formation. *ApJ*, in preparation.

King, A. R. (2009). Black hole outflows. *MNRAS*, pages 1914–+.

King, I. (1962). The structure of star clusters. I. an empirical density law. *AJ*, 67:471–+.

Kitsionas, S. and Whitworth, A. P. (2002). Smoothed Particle Hydrodynamics with particle splitting, applied to self-gravitating collapse. *MNRAS*, 330:129–136.

Kitsionas, S. and Whitworth, A. P. (2007). High-resolution simulations of clump-clump collisions using SPH with particle splitting. *MNRAS*, 378:507–524.

Klypin, A., Trujillo-Gomez, S., and Primack, J. (2010). Halos and galaxies in the standard cosmological model: results from the Bolshoi simulation. *ArXiv e-prints*.

Klypin, A. A. and Shandarin, S. F. (1983). Three-dimensional numerical model of the formation of large-scale structure in the Universe. *MNRAS*, 204:891–907.

Komatsu, E., Smith, K. M., Dunkley, J., Bennett, C. L., Gold, B., Hinshaw, G., Jarosik, N., Larson, D., Nolta, M. R., Page, L., Spergel, D. N., Halpern, M., Hill, R. S., Kogut, A., Limon, M., Meyer, S. S., Odegard, N., Tucker, G. S., Weiland, J. L., Wollack, E., and Wright, E. L. (2011). Seven-year Wilkinson Microwave Anisotropy Probe (WMAP) Observations: Cosmological Interpretation. *ApJS*, 192:18–+.

Kormendy, J. and Richstone, D. (1995). Inward Bound—The Search For Supermassive Black Holes In Galactic Nuclei. *ARA&A*, 33:581–+.

Kotarba, H., Karl, S. J., Naab, T., Johansson, P. H., Dolag, K., Lesch, H., and Stasyszyn, F. A. (2010). Simulating Magnetic Fields in the Antennae Galaxies. *ApJ*, 716:1438–1452.

Kovalev, Y. Y., Lister, M. L., Homan, D. C., and Kellermann, K. I. (2007). The Inner Jet of the Radio Galaxy M87. *ApJ*, 668:L27–L30.

Kowalski, M., Rubin, D., Aldering, G., Agostinho, R. J., Amadon, A., Amanullah, R., Balland, C., Barbary, K., Blanc, G., Challis, P. J., Conley, A., Connolly, N. V., Covarrubias, R., Dawson, K. S., Deustua, S. E., Ellis, R., Fabbro, S., Fadeyev, V., Fan, X., Farris, B., Folatelli, G., Frye, B. L., Garavini, G., Gates, E. L., Germany, L., Goldhaber, G., Goldman, B., Goobar, A., Groom, D. E., Haissinski, J., Hardin, D., Hook, I., Kent, S., Kim, A. G., Knop, R. A., Lidman, C., Linder, E. V., Mendez, J., Meyers, J., Miller, G. J., Moniez, M., Mourão, A. M., Newberg, H., Nobili, S., Nugent, P. E., Pain, R., Perdereau, O., Perlmutter, S., Phillips, M. M., Prasad, V., Quimby, R., Regnault, N., Rich, J., Rubenstein, E. P., Ruiz-Lapuente, P., Santos, F. D., Schaefer, B. E., Schommer, R. A., Smith, R. C., Soderberg, A. M., Spadafora, A. L., Strolger, L., Strovink, M., Suntzeff, N. B., Suzuki, N., Thomas, R. C., Walton, N. A., Wang, L., Wood-Vasey, W. M., and Yun, J. L. (2008). Improved Cosmological Constraints from New, Old, and Combined Supernova Data Sets. *ApJ*, 686:749–778.

Koyama, H. and Inutsuka, S. (2002). An Origin of Supersonic Motions in Interstellar Clouds. *ApJ*, 564:L97–L100.

Kravtsov, A. V. and Gnedin, O. Y. (2005). Formation of Globular Clusters in Hierarchical Cosmology. *ApJ*, 623:650–665.

Kravtsov, A. V., Nagai, D., and Vikhlinin, A. A. (2005). Effects of Cooling and Star Formation on the Baryon Fractions in Clusters. *ApJ*, 625:588–598.

Krumholz, M. R. (2011). Star Formation in Molecular Clouds. *ArXiv e-prints*.

Krumholz, M. R. and McKee, C. F. (2005). A General Theory of Turbulence-regulated Star Formation, from Spirals to Ultraluminous Infrared Galaxies. *ApJ*, 630:250–268.

Krumholz, M. R., McKee, C. F., and Klein, R. I. (2006). Bondi-Hoyle Accretion in a Turbulent Medium. *ApJ*, 638:369–381.

Krumholz, M. R. and Tan, J. C. (2007). Slow Star Formation in Dense Gas: Evidence and Implications. *ApJ*, 654:304–315.

Kuijken, K. and Dubinski, J. (1995). Nearly Self-Consistent Disc / Bulge / Halo Models for Galaxies. *MNRAS*, 277:1341–1353.

Kurganov, A. and Tadmor, E. (2000). New High-Resolution Central Schemes for Nonlinear Conservation Laws and Convection-Diffusion Equations. *Journal of Computational Physics*, 160:241–282.

Kurosawa, R., Proga, D., and Nagamine, K. (2009). On the Feedback Efficiency of Active Galactic Nuclei. *ApJ*, 707:823–832.

Lacey, C. and Cole, S. (1993). Merger rates in hierarchical models of galaxy formation. *MNRAS*, 262:627–649.

Larson, R. B. (1974). Effects of supernovae on the early evolution of galaxies. *MNRAS*, 169:229–246.

Larson, R. B., Tinsley, B. M., and Caldwell, C. N. (1980). The evolution of disk galaxies and the origin of S0 galaxies. *ApJ*, 237:692–707.

Levine, R., Gnedin, N. Y., and Hamilton, A. J. S. (2010). Measuring Gas Accretion and Angular Momentum Near Simulated Supermassive Black Holes. *ApJ*, 716:1386–1396.

Li, Y., Haiman, Z., and Mac Low, M.-M. (2007a). Correlations between Central Massive Objects and Their Host Galaxies: From Bulgeless Spirals to Ellipticals. *ApJ*, 663:61–70.

Li, Y., Hernquist, L., Robertson, B., Cox, T. J., Hopkins, P. F., Springel, V., Gao, L., Di Matteo, T., Zentner, A. R., Jenkins, A., and Yoshida, N. (2007b). Formation of z˜6 Quasars from Hierarchical Galaxy Mergers. *ApJ*, 665:187–208.

Li, Y., Mac Low, M.-M., and Klessen, R. S. (2005). Star Formation in Isolated Disk Galaxies. I. Models and Characteristics of Nonlinear Gravitational Collapse. *ApJ*, 626:823–843.

Li, Z.-Y. and Nakamura, F. (2006). Cluster Formation in Protostellar Outflow-driven Turbulence. *ApJ*, 640:L187–L190.

Loeb, A. (2006). First Light. *ArXiv Astrophysics e-prints*.

Longair, M. S. (2008). *Galaxy Formation*.

Lucy, L. B. (1977). A numerical approach to the testing of the fission hypothesis. *AJ*, 82:1013–1024.

Magorrian, J., Tremaine, S., Richstone, D., Bender, R., Bower, G., Dressler, A., Faber, S. M., Gebhardt, K., Green, R., Grillmair, C., Kormendy, J., and Lauer, T. (1998). The Demography of Massive Dark Objects in Galaxy Centers. *AJ*, 115:2285–2305.

Marri, S. and White, S. D. M. (2003). Smoothed particle hydrodynamics for galaxy-formation simulations: improved treatments of multiphase gas, of star formation and of supernovae feedback. *MNRAS*, 345:561–574.

Martin, C. L. (2006). Mapping Large-Scale Gaseous Outflows in Ultraluminous Infrared Galaxies with Keck II ESI Spectra: Spatial Extent of the Outflow. *ApJ*, 647:222–243.

Mayer, L., Kazantzidis, S., Madau, P., Colpi, M., Quinn, T., and Wadsley, J. (2007). Rapid Formation of Supermassive Black Hole Binaries in Galaxy Mergers with Gas. *Science*, 316:1874–.

McKee, C. F. (1989). Photoionization-regulated star formation and the structure of molecular clouds. *ApJ*, 345:782–801.

McKee, C. F. and Ostriker, E. C. (2007). Theory of Star Formation. *ARA&A*, 45:565–687.

McKee, C. F. and Ostriker, J. P. (1977). A theory of the interstellar medium - Three components regulated by supernova explosions in an inhomogeneous substrate. *ApJ*, 218:148–169.

McKinney, J. C. and Blandford, R. D. (2009). Stability of relativistic jets from rotating, accreting black holes via fully three-dimensional magnetohydrodynamic simulations. *MNRAS*, 394:L126–L130.

McNamara, B. R. and Nulsen, P. E. J. (2007). Heating Hot Atmospheres with Active Galactic Nuclei. *ARA&A*, 45:117–175.

McNamara, B. R., Nulsen, P. E. J., Wise, M. W., Rafferty, D. A., Carilli, C., Sarazin, C. L., and Blanton, E. L. (2005). The heating of gas in a galaxy cluster by X-ray cavities and large-scale shock fronts. *Nature*, 433:45–47.

Merritt, D. and Ekers, R. D. (2002). Tracing Black Hole Mergers Through Radio Lobe Morphology. *Science*, 297:1310–1313.

Mihos, J. C. and Hernquist, L. (1994a). Dense stellar cores in merger remnants. *ApJ*, 437:L47–L50.

Mihos, J. C. and Hernquist, L. (1994b). Star-forming galaxy models: Blending star formation into TREESPH. *ApJ*, 437:611–624.

Mihos, J. C. and Hernquist, L. (1996). Gasdynamics and Starbursts in Major Mergers. *ApJ*, 464:641–+.

Mihos, J. C., Richstone, D. O., and Bothun, G. D. (1991). A numerical study of star formation in interacting disk galaxies. *ApJ*, 377:72–88.

Mo, H. J., Mao, S., and White, S. D. M. (1998). The formation of galactic discs. *MNRAS*, 295:319–336.

Monaghan, J. J. (1992). Smoothed particle hydrodynamics. *ARA&A*, 30:543–574.

Monaghan, J. J. and Lattanzio, J. C. (1985). A refined particle method for astrophysical problems. *A&A*, 149:135–143.

Murray, N., Quataert, E., and Thompson, T. A. (2005). On the Maximum Luminosity of Galaxies and Their Central Black Holes: Feedback from Momentum-driven Winds. *ApJ*, 618:569–585.

Murray, N., Quataert, E., and Thompson, T. A. (2010). The Disruption of Giant Molecular Clouds by Radiation Pressure and the Efficiency of Star Formation in Galaxies. *ApJ*, 709:191–209.

Nakamura, F. and Li, Z.-Y. (2008). Magnetically Regulated Star Formation in Three Dimensions: The Case of the Taurus Molecular Cloud Complex. *ApJ*, 687:354–375.

Navarro, J. F., Frenk, C. S., and White, S. D. M. (1996). The Structure of Cold Dark Matter Halos. *ApJ*, 462:563–+.

Navarro, J. F., Frenk, C. S., and White, S. D. M. (1997). A Universal Density Profile from Hierarchical Clustering. *ApJ*, 490:493–+.

Negroponte, J. and White, S. D. M. (1983). Simulations of mergers between disc-halo galaxies. *MNRAS*, 205:1009–1029.

Norman, M. L. and Bryan, G. L. (1999). Cosmological Adaptive Mesh Refinement. In *Numerical Astrophysics*, volume 240 of *Astrophysics and Space Science Library*, page 19.

Norman, M. L., Bryan, G. L., Harkness, R., Bordner, J., Reynolds, D., O'Shea, B., and Wagner, R. (2007). Simulating Cosmological Evolution with Enzo. *ArXiv e-prints*, 705:arXiv:0705.1556.

Ocvirk, P., Pichon, C., and Teyssier, R. (2008). Bimodal gas accretion in the Horizon-MareNostrum galaxy formation simulation. *ArXiv e-prints*, 803:arXiv:0803.4506.

Oey, M. S., Clarke, C. J., and Massey, P. (2001). Mechanical Feedback: From Stellar Wind Bubbles to Starbursts (Invited Talk). In de Boer, K. S., Dettmar, R.-J., and Klein, U., editors, *Dwarf galaxies and their environment*, page 181.

Omma, H., Binney, J., Bryan, G., and Slyz, A. (2004). Heating cooling flows with jets. *MNRAS*, 348:1105–1119.

Oppenheimer, B. D. and Davé, R. (2008). Mass, metal, and energy feedback in cosmological simulations. *MNRAS*, 387:577–600.

O'Shea, B. W., Bryan, G., Bordner, J., Norman, M. L., Abel, T., Harkness, R., and Kritsuk, A. (2004). Introducing Enzo, an AMR Cosmology Application. *ArXiv e-prints*, 403:arXiv:0403044.

O'Shea, B. W. and Norman, M. L. (2008). Population III Star Formation in a ΛCDM Universe. II. Effects of a Photodissociating Background. *ApJ*, 673:14–33.

Park, C. and Choi, Y.-Y. (2008). Combined Effects of Galaxy Interactions and Large-Scale Environment on Galaxy Properties. *ArXiv e-prints*, 809:arXiv:0809.2156.

Park, K. and Ricotti, M. (2010). Accretion onto Intermediate Mass Black Holes Regulated by Radiative Feedback I. Spherical Symmetric Accretion. *ArXiv e-prints*, 1006:arXiv:1006.1302.

Parkinson, H., Cole, S., and Helly, J. (2008). Generating dark matter halo merger trees. *MNRAS*, 383:557–564.

Peebles, P. J. E. (1969). Origin of the Angular Momentum of Galaxies. *ApJ*, 155:393–+.

Peebles, P. J. E. (1970). Structure of the Coma Cluster of Galaxies. *AJ*, 75:13–+.

Pelupessy, F. I., Schaap, W. E., and van de Weygaert, R. (2003). Density estimators in particle hydrodynamics. DTFE versus regular SPH. *A&A*, 403:389–398.

Peterson, J. R. and Fabian, A. C. (2006). X-ray spectroscopy of cooling clusters. *Phys. Rep.*, 427:1–39.

Pfleiderer, J. and Siedentopf, H. (1961). Spiralstrukturen durch Gezeiteneffekte bei der Begegnung zweier Galaxien. Mit 7 Textabbildungen. *ZAp*, 51:201–+.

Piontek, F. and Steinmetz, M. (2009a). The Angular Momentum Problem in Cosmological Simulations of Disk Galaxy Formation. *ArXiv e-prints*, 909:arXiv:0909.4156.

Piontek, F. and Steinmetz, M. (2009b). The Modelling of Feedback Processes in Cosmological Simulations of Disk Galaxy Formation. *ArXiv e-prints*, 909:arXiv:0909.4167.

Piontek, R. A. and Ostriker, E. C. (2007). Models of Vertically Stratified Two-Phase ISM Disks with MRI-Driven Turbulence. *ApJ*, 663:183–203.

Pounds, K. A., Reeves, J. N., King, A. R., Page, K. L., O'Brien, P. T., and Turner, M. J. L. (2003). A high-velocity ionized outflow and XUV photosphere in the narrow emission line quasar PG1211+143. *MNRAS*, 345:705–713.

Power, C., Nayakshin, S., and King, A. (2010). The Accretion Disc Particle Method for Simulations of Black Hole Feeding and Feedback. *ArXiv e-prints*, 1003:arXiv:1003.0605.

Press, W. H. and Schechter, P. (1974). Formation of Galaxies and Clusters of Galaxies by Self-Similar Gravitational Condensation. *ApJ*, 187:425–438.

Proga, D., Ostriker, J. P., and Kurosawa, R. (2008). Dynamics of Rotating Accretion Flows Irradiated by a Quasar. *ApJ*, 676:101–112.

Puchwein, E., Sijacki, D., and Springel, V. (2008). Simulations of AGN Feedback in Galaxy Clusters and Groups: Impact on Gas Fractions and the Lx-T Scaling Relation. *ApJ*, 687:L53–L56.

Reed, D., Gardner, J., Quinn, T., Stadel, J., Fardal, M., Lake, G., and Governato, F. (2003). Evolution of the mass function of dark matter haloes. *MNRAS*, 346:565–572.

Reed, D. S., Bower, R., Frenk, C. S., Jenkins, A., and Theuns, T. (2007). The halo mass function from the dark ages through the present day. *MNRAS*, 374:2–15.

Rees, M. J. and Ostriker, J. P. (1977). Cooling, dynamics and fragmentation of massive gas clouds - Clues to the masses and radii of galaxies and clusters. *MNRAS*, 179:541–559.

Richer, J. S., Shepherd, D. S., Cabrit, S., Bachiller, R., and Churchwell, E. (2000). Molecular Outflows from Young Stellar Objects. *Protostars and Planets IV*, pages 867–+.

Robertson, B., Yoshida, N., Springel, V., and Hernquist, L. (2004). Disk Galaxy Formation in a Λ Cold Dark Matter Universe. *ApJ*, 606:32–45.

Robertson, B. E. and Kravtsov, A. V. (2008). Molecular Hydrogen and Global Star Formation Relations in Galaxies. *ApJ*, 680:1083–1111.

Rocha, M., Jonsson, P., Primack, J. R., and Cox, T. J. (2008). Dust attenuation in hydrodynamic simulations of spiral galaxies. *MNRAS*, 383:1281–1291.

Roediger, E. and Brüggen, M. (2007). Ram pressure stripping of disc galaxies orbiting in clusters - I. Mass and radius of the remaining gas disc. *MNRAS*, 380:1399–1408.

Roediger, E. and Brüggen, M. (2008). Ram-pressure stripping of disc galaxies orbiting in clusters - II. Galactic wakes. *MNRAS*, 388:465–486.

Rood, H. J. (1987). The remarkable extragalactic research of Erik Holmberg. *PASP*, 99:921–951.

Rosen, A. and Bregman, J. N. (1995). Global Models of the Interstellar Medium in Disk Galaxies. *ApJ*, 440:634–+.

Rybicki, G. B. and Lightman, A. P. (1979). *Radiative processes in astrophysics*.

Saikia, D. J., Konar, C., and Kulkarni, V. K. (2006). J0041+3224: a new double-double radio galaxy. *MNRAS*, 366:1391–1398.

Saitoh, T. R., Daisaka, H., Kokubo, E., Makino, J., Okamoto, T., Tomisaka, K., Wada, K., and Yoshida, N. (2008). Toward First-Principle Simulations of Galaxy Formation: II. Shock-Induced Starburst at a Collision Interface During the First Encounter of Interacting Galaxies. *ArXiv e-prints*, 805:arXiv:0805.0167.

Salpeter, E. E. (1955). The Luminosity Function and Stellar Evolution. *ApJ*, 121:161–+.

Sarazin, C. L. and White, III, R. E. (1987). Steady state cooling flow models for normal elliptical galaxies. *ApJ*, 320:32–48.

Sazonov, S. Y., Ostriker, J. P., Ciotti, L., and Sunyaev, R. A. (2005). Radiative feedback from quasars and the growth of massive black holes in stellar spheroids. *MNRAS*, 358:168–180.

Sazonov, S. Y., Ostriker, J. P., and Sunyaev, R. A. (2004). Quasars: the characteristic spectrum and the induced radiative heating. *MNRAS*, 347:144–156.

Scannapieco, C., Tissera, P. B., White, S. D. M., and Springel, V. (2005). Feedback and metal enrichment in cosmological smoothed particle hydrodynamics simulations - I. A model for chemical enrichment. *MNRAS*, 364:552–564.

Scannapieco, C., Tissera, P. B., White, S. D. M., and Springel, V. (2006). Feedback and metal enrichment in cosmological SPH simulations - II. A multiphase model with supernova energy feedback. *MNRAS*, 371:1125–1139.

Scannapieco, C., Tissera, P. B., White, S. D. M., and Springel, V. (2008). Effects of Supernova Feedback on the Formation of Galaxy Disks. *ArXiv e-prints*, 804:arXiv:0804.3795.

Schaye, J. and Dalla Vecchia, C. (2008). On the relation between the Schmidt and Kennicutt-Schmidt star formation laws and its implications for numerical simulations. *MNRAS*, 383:1210–1222.

Schmidt, M. (1959). The Rate of Star Formation. *ApJ*, 129:243–+.

Schödel, R., Ott, T., Genzel, R., Hofmann, R., Lehnert, M., Eckart, A., Mouawad, N., Alexander, T., Reid, M. J., Lenzen, R., Hartung, M., Lacombe, F., Rouan, D., Gendron, E., Rousset, G., Lagrange, A., Brandner, W., Ageorges, N., Lidman, C., Moorwood, A. F. M., Spyromilio, J., Hubin, N., and Menten, K. M. (2002). A star in a 15.2-year orbit around the supermassive black hole at the centre of the Milky Way. *Nature*, 419:694–696.

Schweizer, F. (2006). Globular Cluster Formation in Mergers. *ArXiv e-prints*, 606:arXiv:0606036.

Shakura, N. I. and Sunyaev, R. A. (1973). Black holes in binary systems. Observational appearance. *A&A*, 24:337–355.

Sharma, P., Colella, P., and Martin, D. F. (2009). Numerical Implementation of Streaming Down the Gradient: Application to Fluid Modeling of Cosmic Rays and Saturated Conduction. *ArXiv e-prints*.

Shemmer, O., Brandt, W. N., Schneider, D. P., Fan, X., Strauss, M. A., Diamond-Stanic, A. M., Richards, G. T., Anderson, S. F., Gunn, J. E., and Brinkmann, J. (2006). Chandra Observations of the Highest Redshift Quasars from the Sloan Digital Sky Survey. *ApJ*, 644:86–99.

Sheth, R. K. and Tormen, G. (1999). Large-scale bias and the peak background split. *MNRAS*, 308:119–126.

Shin, M., Ostriker, J. P., and Ciotti, L. (2010). Feedback from Central Black Holes in Elliptical Galaxies. II. Can Purely Mechanical Energy Feedback Models Work? *ApJ*, 711:268–283.

Shu, C.-W. and Osher, S. (1988). Efficient implementation of essentially non-oscillatory shock-capturing schemes. *Journal of Computational Physics*, 77(2):439 – 471.

Shull, J. M. and van Steenberg, M. E. (1985). X-ray secondary heating and ionization in quasar emission-line clouds. *ApJ*, 298:268–274.

Sijacki, D., Pfrommer, C., Springel, V., and Enßlin, T. A. (2008). Simulations of cosmic-ray feedback by active galactic nuclei in galaxy clusters. *MNRAS*, 387:1403–1415.

Sijacki, D., Springel, V., Di Matteo, T., and Hernquist, L. (2007). A unified model for AGN feedback in cosmological simulations of structure formation. *MNRAS*, 380:877–900.

Sijacki, D., Springel, V., and Haehnelt, M. G. (2009). Growing the first bright quasars in cosmological simulations of structure formation. *MNRAS*, 400:100–122.

Silk, J. and Rees, M. J. (1998). Quasars and galaxy formation. *A&A*, 331:L1–L4.

Skillman, S. W., O'Shea, B. W., Hallman, E. J., Burns, J. O., and Norman, M. L. (2008). Cosmological Shocks in Adaptive Mesh Refinement Simulations and the Acceleration of Cosmic Rays. *ApJ*, 689:1063–1077.

Slyz, A. D., Devriendt, J. E. G., Bryan, G., and Silk, J. (2005). Towards simulating star formation in the interstellar medium. *MNRAS*, 356:737–752.

Somerville, R. S. and Primack, J. R. (1999). Semi-analytic modelling of galaxy formation: the local Universe. *MNRAS*, 310:1087–1110.

Sparke, L. S. and Gallagher, III, J. S. (2006). *Galaxies in the Universe - 2nd Edition*.

Spitzer, L. J. (1990). Theories of the hot interstellar gas. *ARA&A*, 28:71–101.

Springel, V. (2005). The cosmological simulation code GADGET-2. *MNRAS*, 364:1105–1134.

Springel, V. (2010). E pur si muove: Galilean-invariant cosmological hydrodynamical simulations on a moving mesh. *MNRAS*, 401:791–851.

Springel, V., Di Matteo, T., and Hernquist, L. (2005a). Black Holes in Galaxy Mergers: The Formation of Red Elliptical Galaxies. *ApJ*, 620:L79–L82.

Springel, V., Di Matteo, T., and Hernquist, L. (2005b). Modelling feedback from stars and black holes in galaxy mergers. *MNRAS*, 361:776–794.

Springel, V. and Hernquist, L. (2003a). Cosmological smoothed particle hydrodynamics simulations: a hybrid multiphase model for star formation. *MNRAS*, 339:289–311.

Springel, V. and Hernquist, L. (2003b). The history of star formation in a Λ cold dark matter universe. *MNRAS*, 339:312–334.

Springel, V., Wang, J., Vogelsberger, M., Ludlow, A., Jenkins, A., Helmi, A., Navarro, J. F., Frenk, C. S., and White, S. D. M. (2008). The Aquarius Project: the subhaloes of galactic haloes. *MNRAS*, 391:1685–1711.

Springel, V., White, S. D. M., Jenkins, A., Frenk, C. S., Yoshida, N., Gao, L., Navarro, J., Thacker, R., Croton, D., Helly, J., Peacock, J. A., Cole, S., Thomas, P., Couchman, H., Evrard, A., Colberg, J., and Pearce, F. (2005c). Simulations of the formation, evolution and clustering of galaxies and quasars. *Nature*, 435:629–636.

Springel, V., Yoshida, N., and White, S. D. M. (2001). GADGET: a code for collisionless and gasdynamical cosmological simulations. *New Astronomy*, 6:79–117.

Stawarz, Ł. (2004). On the Jet Activity in 3C 273. *ApJ*, 613:119–128.

Steinmetz, M. and Navarro, J. F. (1999). The Cosmological Origin of the Tully-Fisher Relation. *ApJ*, 513:555–560.

Steinmetz, M. and Navarro, J. F. (2002). The hierarchical origin of galaxy morphologies. *New Astronomy*, 7:155–160.

Stinson, G., Seth, A., Katz, N., Wadsley, J., Governato, F., and Quinn, T. (2006). Star formation and feedback in smoothed particle hydrodynamic simulations - I. Isolated galaxies. *MNRAS*, 373:1074–1090.

Stone, J. M. and Norman, M. L. (1992a). ZEUS-2D: A radiation magnetohydrodynamics code for astrophysical flows in two space dimensions. I - The hydrodynamic algorithms and tests. *ApJS*, 80:753–790.

Stone, J. M. and Norman, M. L. (1992b). ZEUS-2D: A Radiation Magnetohydrodynamics Code for Astrophysical Flows in Two Space Dimensions. II. The Magnetohydrodynamic Algorithms and Tests. *ApJS*, 80:791–+.

Stringer, M. J. and Benson, A. J. (2007). The formation of galaxy discs in a hierarchical universe. *MNRAS*, 382:641–651.

Strong, A. W., Moskalenko, I. V., and Ptuskin, V. S. (2007). Cosmic-Ray Propagation and Interactions in the Galaxy. *Annual Review of Nuclear and Particle Science*, 57:285–327.

Struck, C. (1999). Galaxy collisions. *Phys. Rep.*, 321:1–3.

Su, M., Slatyer, T. R., and Finkbeiner, D. P. (2010). Giant Gamma-ray Bubbles from Fermi-LAT: Active Galactic Nucleus Activity or Bipolar Galactic Wind? *ApJ*, 724:1044–1082.

Sutherland, R. S. and Dopita, M. A. (1993). Cooling functions for low-density astrophysical plasmas. *ApJS*, 88:253–327.

Tang, S., Wang, Q. D., Lu, Y., and Mo, H. J. (2008). Feedback from galactic stellar bulges and hot gaseous haloes of galaxies. *ArXiv e-prints*, 803:arXiv:0803.4215.

Tasker, E. J. (2011). Star Formation in Disk Galaxies. II. The Effect Of Star Formation and Photoelectric Heating on the Formation and Evolution of Giant Molecular Clouds. *ApJ*, 730:11–+.

Tasker, E. J., Brunino, R., Mitchell, N. L., Michielsen, D., Hopton, S., Pearce, F. R., Bryan, G. L., and Theuns, T. (2008). A test suite for quantitative comparison of hydrodynamic codes in astrophysics. *MNRAS*, 390:1267–1281.

Tasker, E. J. and Bryan, G. L. (2006). Simulating Star Formation and Feedback in Galactic Disk Models. *ApJ*, 641:878–890.

Tasker, E. J. and Bryan, G. L. (2008). The Effect of the Interstellar Model on Star Formation Properties in Galactic Disks. *ApJ*, 673:810–831.

Tassis, K., Abel, T., Bryan, G. L., and Norman, M. L. (2003). Numerical Simulations of High-Redshift Star Formation in Dwarf Galaxies. *ApJ*, 587:13–24.

Tassis, K., Kravtsov, A. V., and Gnedin, N. Y. (2008). Scaling Relations of Dwarf Galaxies without Supernova-driven Winds. *ApJ*, 672:888–903.

Teyssier, R., Chapon, D., and Bournaud, F. (2010a). The Driving Mechanism of Starbursts in Galaxy Mergers. *ApJ*, 720:L149–L154.

Teyssier, R., Moore, B., Martizzi, D., Dubois, Y., and Mayer, L. (2010b). Mass Distribution in Galaxy Clusters: the Role of AGN Feedback. *ArXiv e-prints*, 1003:arXiv:1003.4744.

Tonnesen, S. and Bryan, G. L. (2009). Gas Stripping in Simulated Galaxies with a Multiphase Interstellar Medium. *ApJ*, 694:789–804.

Tonnesen, S., Bryan, G. L., and van Gorkom, J. H. (2007). Environmentally Driven Evolution of Simulated Cluster Galaxies. *ApJ*, 671:1434–1445.

Toomre, A. (1977). Mergers and Some Consequences. In Tinsley, B. M. and Larson, R. B., editors, *Evolution of Galaxies and Stellar Populations*, page 401.

Toomre, A. (1978). Interacting systems. In Longair, M. S. and Einasto, J., editors, *Large Scale Structures in the Universe*, volume 79 of *IAU Symposium*, pages 109–116.

Toomre, A. and Toomre, J. (1972). Galactic Bridges and Tails. *ApJ*, 178:623–666.

Toth, G. (2000). The div*b = 0 constraint in shock-capturing magnetohydrodynamics codes. *J. Comput. Phys.*, 161(2):605–652.

Tremonti, C. A., Heckman, T. M., Kauffmann, G., Brinchmann, J., Charlot, S., White, S. D. M., Seibert, M., Peng, E. W., Schlegel, D. J., Uomoto, A., Fukugita, M., and Brinkmann, J. (2004). The Origin of the Mass-Metallicity Relation: Insights from 53,000 Star-forming Galaxies in the Sloan Digital Sky Survey. *ApJ*, 613:898–913.

Truelove, J. K., Klein, R. I., McKee, C. F., Holliman, II, J. H., Howell, L. H., and Greenough, J. A. (1997). The Jeans Condition: A New Constraint on Spatial Resolution in Simulations of Isothermal Self-gravitational Hydrodynamics. *ApJ*, 489:L179+.

Turk, M. J., Abel, T., and O'Shea, B. (2009). The Formation of Population III Binaries from Cosmological Initial Conditions. *Science*, 325:601–.

Valtonen, M. J., Lehto, H. J., Nilsson, K., Heidt, J., Takalo, L. O., Sillanpää, A., Villforth, C., Kidger, M., Poyner, G., Pursimo, T., Zola, S., Wu, J., Zhou, X., Sadakane, K., Drozdz, M., Koziel, D., Marchev, D., Ogloza, W., Porowski, C., Siwak, M., Stachowski, G., Winiarski, M., Hentunen, V., Nissinen, M., Liakos, A., and Dogru, S. (2008). A massive binary black-hole system in OJ287 and a test of general relativity. *Nature*, 452:851–853.

van de Voort, F., Schaye, J., Booth, C. M., and Dalla Vecchia, C. (2011). The drop in the cosmic star formation rate below redshift 2 is caused by a change in the mode of gas accretion and by AGN feedback. *ArXiv e-prints*.

van den Bosch, F. C. (2001). The origin of the density distribution of disc galaxies: a new problem for the standard model of disc formation. *MNRAS*, 327:1334–1352.

van Leer, B. (1979). Towards the ultimate conservative difference scheme. v. a second-order sequel to godunov's method. *Journal of Computational Physics*, 32(1):101 – 136.

Vázquez-Semadeni, E., Colín, P., Gómez, G. C., Ballesteros-Paredes, J., and Watson, A. W. (2010). Molecular Cloud Evolution. III. Accretion Versus Stellar Feedback. *ApJ*, 715:1302–1317.

Verner, D. A., Ferland, G. J., Korista, K. T., and Yakovlev, D. G. (1996). Atomic Data for Astrophysics. II. New Analytic FITS for Photoionization Cross Sections of Atoms and Ions. *ApJ*, 465:487–+.

Vlahakis, N. and Königl, A. (2003). Relativistic Magnetohydrodynamics with Application to Gamma-Ray Burst Outflows. I. Theory and Semianalytic Trans-Alfvénic Solutions. *ApJ*, 596:1080–1103.

Vlahakis, N. and Königl, A. (2004). Magnetic Driving of Relativistic Outflows in Active Galactic Nuclei. I. Interpretation of Parsec-Scale Accelerations. *ApJ*, 605:656–661.

von Hoerner, S. (1960). Die numerische Integration des n-Körper-Problemes für Sternhaufen. I. *ZAp*, 50:184–214.

Wada, K. and Norman, C. (2007). Density structure of the interstellar medium and the star formation rate in galactic disks. *ApJ*, 660(1):276–287.

Wang, P. and Abel, T. (2009). Magnetohydrodynamic Simulations of Disk Galaxy Formation: The Magnetization of the Cold and Warm Medium. *ApJ*, 696:96–109.

Wang, P., Abel, T., and Zhang, W. (2008). Relativistic Hydrodynamic Flows Using Spatial and Temporal Adaptive Structured Mesh Refinement. *ApJS*, 176:467–483.

Wang, P., Li, Z., Abel, T., and Nakamura, F. (2010). Outflow Feedback Regulated Massive Star Formation in Parsec-Scale Cluster-Forming Clumps. *ApJ*, 709:27–41.

White, S. D. M. and Frenk, C. S. (1991). Galaxy formation through hierarchical clustering. *ApJ*, 379:52–79.

White, S. D. M. and Rees, M. J. (1978). Core condensation in heavy halos - A two-stage theory for galaxy formation and clustering. *MNRAS*, 183:341–358.

Widrow, L. M. and Dubinski, J. (2005). Equilibrium Disk-Bulge-Halo Models for the Milky Way and Andromeda Galaxies. *ApJ*, 631:838–855.

Wise, J. H. and Abel, T. (2007). Resolving the Formation of Protogalaxies. I. Virialization. *ApJ*, 665:899–910.

Wise, J. H. and Abel, T. (2008). Resolving the Formation of Protogalaxies. III. Feedback from the First Stars. *ApJ*, 685:40–56.

Wise, J. H. and Abel, T. (2010). Enzo+Moray: Radiation Hydrodynamics Adaptive Mesh Refinement Simulations with Adaptive Ray Tracing. *ArXiv e-prints*, 1012:arXiv:1012.2865.

Wise, J. H., Turk, M. J., and Abel, T. (2008). Resolving the Formation of Protogalaxies. II. Central Gravitational Collapse. *ApJ*, 682:745–757.

Wise, J. H., Turk, M. J., Norman, M. L., and Abel, T. (2010). The Birth of a Galaxy: Primordial Metal Enrichment and Population II Stellar Populations. *ArXiv e-prints*, 1011:arXiv:1011.2632.

Wolfire, M. G., Hollenbach, D., McKee, C. F., Tielens, A. G. G. M., and Bakes, E. L. O. (1995). The neutral atomic phases of the interstellar medium. *ApJ*, 443:152–168.

Woo, J., Treu, T., Malkan, M. A., and Blandford, R. D. (2008). Cosmic Evolution of Black Holes and Spheroids. III. The $M_{BH} - \sigma_*$ Relation in the Last Six Billion Years. *ApJ*, 681:925–930.

Wyithe, J. S. B. and Loeb, A. (2003). Self-regulated Growth of Supermassive Black Holes in Galaxies as the Origin of the Optical and X-Ray Luminosity Functions of Quasars. *ApJ*, 595:614–623.

Xu, G. (1995). A New Parallel N-Body Gravity Solver: TPM. *ApJS*, 98:355–+.

Yoshida, N., Omukai, K., and Hernquist, L. (2008). Protostar Formation in the Early Universe. *Science*, 321:669–.

Zel'Dovich, Y. B. (1970). Gravitational instability: An approximate theory for large density perturbations. *A&A*, 5:84–89.

Zheng, X. Z., Bell, E. F., Somerville, R. S., Rix, H., Jahnke, K., Fontanot, F., Rieke, G. H., Schiminovich, D., and Meisenheimer, K. (2009). Observational Constraints on the Co-Evolution of Supermassive Black Holes and Galaxies. *ApJ*, 707:1566–1577.

Zwicky, F. (1956). Multiple Galaxies. *Ergebnisse der exakten Naturwissenschaften*, 29:344–385.